

# Disk Evolution in OB Associations - Deep *Spitzer*/IRAC Observations of IC 1795

Veronica Roccagliata<sup>1,2</sup>, Jeroen Bouwman<sup>1</sup>, Thomas Henning<sup>1</sup>, Mario Gennaro<sup>1</sup>, Eric Feigelson<sup>3,4</sup>, Jinyoung Serena Kim<sup>5</sup>, Aurora Sicilia-Aguilar<sup>1</sup>, Warrick A. Lawson<sup>6</sup>

## ABSTRACT

We present a deep *Spitzer*/IRAC survey of the OB association IC 1795 carried out to investigate the evolution of protoplanetary disks in regions of massive star formation.

Combining *Spitzer*/IRAC data with Chandra/ACIS observations, we find 289 cluster members. An additional 340 sources with an infrared excess, but without X-ray counterpart, are classified as cluster member candidates. Both surveys are complete down to stellar masses of about  $1 M_{\odot}$ . We present pre-main sequence isochrones computed for the first time in the *Spitzer*/IRAC colors. The age of the cluster, determined via the location of the Class III sources in the [3.6]-[4.5]/[3.6] color-magnitude diagram, is in the range of 3 - 5 Myr.

As theoretically expected, we do not find any systematic variation in the spatial distribution of disks within 0.6 pc of either O-type star in the association. However, the disk fraction in IC 1795 does depend on the stellar mass: sources with masses  $> 2 M_{\odot}$  have a disk fraction of  $\sim 20\%$ , while lower mass objects ( $2-0.8 M_{\odot}$ ) have a disk fraction of  $\sim 50\%$ . This implies that disks around massive stars have a shorter dissipation timescale.

*Subject headings:* ISM: individual (W3); open clusters and associations: individual (W3 IC1795); planetary systems: protoplanetary disks; stars: formation; stars: pre-main sequence; X-rays: stars

## 1. Introduction

Circumstellar (CS) disks have been found around all types of objects, ranging from Herbig Ae/Be stars to brown dwarfs, sharing similar dust composition, although differences between the disks of low-mass stars / brown dwarfs, solar type stars and more massive stars seem to exist

in the evolution of both the dust and gas components (e.g. Henning & Meeus 2009; Pascucci et al. 2009). Though the time-scales of disk evolution and dispersion are not well constrained, 90% of the PMS systems appear to disperse the dust and gas within the planet formation zone within  $\sim 10$  Myr (e.g. Mamajek et al. 2004; Bouwman et al. 2006; Fedele et al. 2010). Consequently, the formation of gas planets has to be completed within this time-scale.

Although most solar-type and low-mass stars form in OB associations, disks studies around PMS stars deal mostly with regions of low-mass star formation in the Gould Belt (e.g. Hartmann et al. 2005; Winston et al. 2007; Hatchell et al. 2007; Sicilia-Aguilar et al. 2008; Evans et al. 2009) and nearby moving groups (e.g. Lyo et al. 2003; Sicilia-Aguilar et al. 2009; Meeus et al. 2009).

An exception is the Orion Nebular Cluster (e.g. Hillenbrand 1997; Hillenbrand et al. 1998), the nearest ( $\sim 410$  pc; Jeffries 2007), young, dense and

<sup>1</sup>Max-Planck-Institut für Astronomie, Königstuhl 17, D-69117 Heidelberg, Germany

<sup>2</sup>Space Telescope Science Institute, Baltimore, MD 21218, USA

<sup>3</sup>Department of Astronomy and Astrophysics, Pennsylvania State University, University Park, PA 16802, USA

<sup>4</sup>Center for Exoplanets and Habitable Worlds, 525 Davey Laboratory, Pennsylvania State University, University Park, PA 16802, USA

<sup>5</sup>Steward Observatory, University of Arizona, 933 N. Cherry Ave. Tucson, AZ 85721-0065

<sup>6</sup>School of Physical, Environmental, and Mathematical Sciences, University of New South Wales, Australian Defence Force Academy, Canberra, ACT 2600, Australia

rich cluster with the O6 star,  $\theta^1$ Ori C, in the center. The disks are seen as dark silhouettes against the bright nebula background and they are called “proplyds” (e.g. O’dell & Wong 1996). Studies of the disk fraction in Orion (e.g. Hillenbrand et al. 1998) reveal a higher number of disks within 0.5 pc than at larger distances from the O6 star. This suggests that the central O star has had insufficient time to fully photoevaporate surrounding disks. However, Eisner et al. (2008) found that the percentage of disks more massive than  $\sim 0.01 M_{\odot}$  is lower than in Taurus.

There is compelling observational evidence that these disks have been influenced by the ultraviolet radiation from  $\theta^1$ Ori C (e.g. Johnstone et al. 1998; Clarke 2007; Gorti et al. 2009), in that the ionized gas surrounding these disks has a cometary-shape (McCullough et al. 1995; Bally et al. 1998), their mass distribution is truncated at  $0.03 M_{\odot}$  and the outer radii, in most of the cases, are smaller than 60 AU (Mann & Williams 2009). However, such a truncation in mass and radii distribution might be due to disk mass loss triggered by stellar encounters which are also responsible for the destruction of 10-15% disks in the Trapezium cluster (e.g Scally & Clarke 2001; Olczak et al. 2006).

Investigations of disk dissipation processes induced by massive stars, such as photoevaporation and dynamical destruction, must be made in rich, crowded young clusters. To properly carry out such a study, a disk-unbiased census of cluster members and a robust tracer of disks are needed. Chandra X-ray surveys provide member lists based on pre-main sequence magnetic activity; these are particularly effective in locating the disk-free (Class III) stellar population (Feigelson et al. 2007). Spitzer mid-infrared surveys provide sensitive member lists based on infrared excess; these are particularly effective in locating the disk (Class 0-I-II) stellar population. The X-ray and infrared approaches are complementary in other respects: the X-ray selected samples nicely discriminate young cluster members from older Galactic field stars that dominate infrared surveys, while the infrared samples detect the very low-mass population with magnetic activity too faint to be detected in most X-ray exposures.

The characterization of circumstellar material in the inner part of the disks can be pro-

vided by sensitive IRAC surveys, while a complete membership may be identified by an optical spectroscopy survey for low-mass members with spectral types K – M (via the Li emission at 6708Å, e.g. Jeffries et al. 2007; Mentuch et al. 2008) or accreting objects (via H $\alpha$  and UV-excess emission, Fedele et al. 2010; Sicilia-Aguilar et al. 2010; Fang et al. 2009). The solar-type mass population can be identified via an X-ray survey.

### 1.1. Past work

This approach has been used by, e.g., Damiani et al. (2006), who combined a deep X-ray Chandra survey with an optical spectroscopic survey to study the population properties of the 5 Myr old cluster NGC 2363, which hosts an O9.5I star. They found that only 5-9% of the cluster members are still accreting.

Recently Balog et al. (2007) studied disk evolution and the influence of the O stars in the high-mass star-forming region NGC 2244. Using IRAC observations, they found an overall disk fraction of 44.5%, but that the fraction of sources with disks was lower ( $\sim 27\%$ ) within 0.5 pc of the O stars. Guarcello et al. (2009, 2007) analyzed the disk fraction in the high-mass OB association NGC 6611, which hosts 56 stars with spectral type earlier than B5. The cluster membership and the disk-fraction were defined combining optical, near- and mid-infrared and X-ray studies. The disk fraction for the O and B stars was found varying between 31% and 16% across a complete range of incident fluxes up to  $800 \text{ erg cm}^{-2} \text{s}^{-1}$ . In a smaller region compared to the Guarcello et al. (2009, 2007) studies, Oliveira et al. (2005) computed a much higher disk fraction ( $\sim 58\%$ ) probably due to the lower sensitivity of their survey.

Getman et al. (2009) studied a portion of the Cep OB3b cluster and the triggered population in the adjacent Cep B molecular cloud. Using a combined *Chandra* – *Spitzer* sample, they found that the disk fraction showed a spatial gradient from 75% in the cloud core to 25% in the unobscured cluster. They attributed the gradient to stellar ages rather than photoevaporation.

Hernández et al. (2008) computed the disk fraction in the 5 Myr old  $\gamma$ Velorum cluster, with a central binary consisting of an O7.5 star and a Wolf-Rayet star. Only 5% of cluster members

showed an infrared excess.

Despite these studies, the number of investigations concerning the presence of disks around stars in OB associations has been limited.

## 1.2. This work

In this paper, we present the analysis of protoplanetary disks around young stars in the IC 1795 OB association. We obtained infrared imaging data of the IC 1795 OB association with the Infrared Array Camera (IRAC; Fazio et al. 2004) on board the *Spitzer Space Telescope* (Werner et al. 2004). To define the cluster membership of IC 1795 we carried out a deep survey with the Advanced CCD Imaging Spectrometer (ACIS) detector on board the *Chandra X-ray Observatory* (Weisskopf et al. 2002).

The IC 1795 cluster ionizes the diffuse HII region in the W3 giant molecular cloud complex. This region is located in the Perseus arm, which contains several spectacular regions of high- and low-mass star formation: W3-North, W3-Main and W3-OH. IC 1795 hosts a bright O6.5V star, BD +61°411, originally spectrally classified by Mathys (1989), a O9.7I star and two B stars which have been spectrally classified in the optical by Oey et al. (2005). The cluster is assumed to lie at the same distance as W3-OH. From maser kinematics this has been accurately measured to be 2.0 kpc (Xu et al. 2006; Hachisuka et al. 2006).

Oey et al. (2005) derived an approximate age of 3 - 5 Myr and they propose that this OB association, triggered by the neighboring W4 superbubble, is triggering new star formation in the young massive regions W3-North, W3-Main and W3-OH. The X-rays morphology of these regions suggests, however, that only the W3-OH structures are consistent with the collect-and-collapse triggering process caused by shocks from the older IC 1795 cluster (Feigelson & Townsley 2008). In the X-ray maps, the embedded W3-Main cluster does not show the elongated and patchy structure of a recently triggered star cluster, and instead it appears to have formed in an earlier episode.

Previous IRAC observations of the entire W3 region, presented by Ruch et al. (2007), revealed that a large fraction of Class II sources lie within the central cluster IC 1795. No analysis of the spatial distribution and disk fraction of the clus-

ter has been performed so far. The photometric observations presented in this paper concentrate on the lightly obscured IC 1795 OB association, and they have one order of magnitude better sensitivity compared with the Ruch et al. (2007) observations. A new deeper X-ray *Chandra* survey of IC 1795 is also presented in this work to accurately define the cluster membership.

This paper is organized as follows: in section 2 we present our *Spitzer* and *Chandra* observations, along with the data reduction. Results are shown in section 3. Sections 4 and 5 include the analysis of the cluster (membership, age, infrared properties of the stars). In section 6 we discuss our results in terms of disk evolution. Conclusions are drawn in section 7.

## 2. Observations and data reduction

### 2.1. IRAC observations

IC 1795 was observed in 2007 September <sup>1</sup> with all 4 channels centered at  $3.6 \mu\text{m}$ ,  $4.5 \mu\text{m}$ ,  $5.8 \mu\text{m}$ ,  $8.0 \mu\text{m}$  respectively, using a 3x4 mosaic pattern, with pointings separated by  $220''$  and aligned with the array axes. The resulting images provide full coverage over a  $14' \times 12'$  area in all four IRAC channels.

The images have been obtained in High Dynamical Range Mode in order to obtain unsaturated measurements for all observed cluster members. The maps are obtained in 144 cycles organized in 12-point dither patterns. In each channel, a short exposure of 144 frames of  $0.4 \text{ s}$  each and a long exposure of  $10.4 \text{ s}$  per 144 frames have been carried out. In each channel, the average short and long exposures over the entire mosaic are 58 and 1497 sec, respectively. The long and the short exposures are analyzed separately to avoid saturation of bright sources in the long exposures.

The raw data were processed and calibrated with the IRAC pipeline (version S16.1.0) and the Basic Calibrated Data (BCD) were downloaded from the *Spitzer* archive<sup>2</sup>. The final mosaics were created using the MOPEX pipeline (version 18.2.2)<sup>3</sup>: the software takes the individual BCD frames

<sup>1</sup>Spitzer program ID 30726, PI J. Bouwman

<sup>2</sup><http://archive.spitzer.caltech.edu/>

<sup>3</sup><http://ssc.spitzer.caltech.edu/postbcd/download-mopex.html>

and combines them to create a mosaic of the observed region, removing cosmic rays and bad pixels from the single frames. The combined mosaic of the long exposures at  $3.6\text{ }\mu\text{m}/4.5\text{ }\mu\text{m}/8.0\text{ }\mu\text{m}$  of IC 1795 is shown in Fig. 1, together with the positions of the center and the edge of the cluster. Due to the mosaic configuration, the exposures of ch1 and ch3 cover part of W3-Main, while ch2 and ch4 cover part of W3-OH.

## 2.2. IRAC photometry

We used the APEX/MOPEX package to perform PSF-photometry for every detection. In particular, we used the APEX MultiFrame pipeline, where the detection of the point sources is done on the final mosaic in order to recover also the fainter objects, while the PSF photometry is carried out on each frame separately.

Over the cluster region, the background was highly variable. We estimated the background variability by considering six different regions of the cluster of  $25\times 25$  pixels each, corresponding to an area of  $\sim 30'' \times 30''$ . The mean background flux at  $3.6\text{ }\mu\text{m}$  was about 0.07 Jy with an average standard deviation of 0.05 Jy. At the edge of IC 1795, where it borders on the younger regions W3-OH on the south-west direction and on W3-Main on the North-East direction, the background increases up to 0.08 Jy and 1.6 Jy at  $3.6$  and  $8\text{ }\mu\text{m}$ , respectively. Here the background is most likely associated to the molecular clouds of the younger W3-OH and W3-Main regions. Over the cluster region it is instead associated with the PAH emission which peaks at  $3.3, 6.3, 7.7$  and  $8.6\text{ }\mu\text{m}$ .

As the background was highly variable, PSF photometry was computed in a small area of  $8\times 8$  pixels and subtracted before performing PSF-photometry. Instead of PSF fitting, APEX uses the point-response function (PRF) fitting method. The PRF is the response of the detector array pixels to a point source and combines information on the PSF, the detector sampling and the intra-pixel sensitivity variation. We used the standard PRFs provided in APEX. The point-source positional uncertainties and the flux uncertainty ( $\Delta_{PRF}$ ) are computed from the covariance matrix calculated from the “best-fit” to the data.

The calibration uncertainties (Reach et al. 2005) are dominated by the array-location-dependent photometric correction and the pixel phase effect

which might introduce an uncertainty of up to 10% of the flux. However, since the pixel phase effect decreases as the square root of the number of dithers (12 in our case), we conservatively adopt a value of 5%. The color correction and the absolute calibration error are of on the order of a few %. Overall the final flux calibration error ( $\Delta_{cal}$ ) is smaller than 10% of the flux. The total flux uncertainty is:

$$\Delta_{flux} = \sqrt{\Delta_{PRF}^2 + \Delta_{cal}^2}.$$

Only sources with a signal-to-noise (S/N) flux measurement greater than 6 in each IRAC channel have been considered in our final catalog. The final photometric catalog was created, combining the results of the analysis of the short and long exposures separately. For objects detected in both exposures (and not saturated), we adopt the photometry measured in the long exposure. The detection limit of our IRAC survey in the  $3.6\text{ }\mu\text{m}$  band is 16.5 mag. However, we have cases where the high variability of the background did not enable us to detect all the sources with brightness between 15.5–16.5 mag at  $3.6\text{ }\mu\text{m}$ . At  $4.5\text{ }\mu\text{m}$  we detected sources down to 16 mag, at  $5.8\text{ }\mu\text{m}$  13.3 mag, and at  $8.0\text{ }\mu\text{m}$  11.5 mag.

## 2.3. ACIS observations

Our X-ray catalog was generated from a mosaic of *Chandra* observations consisting of the 7 exposures of W3 presented by Feigelson & Townsley (2008) and an additional exposure of IC 1795. This is a 50.0 ks exposure obtained on 2007 December 4 centered on  $(\alpha_{J2000}, \delta_{J2000}) = (02h:26m:33.6s, +62^\circ:00':35.9'')$  with the 4-CCD ACIS Imaging Array subtending  $17' \times 17'$ . The data were reduced using procedures implemented in the IDL-based *Tools for ACIS Review and Analysis (TARA)* and *ACIS Extract* software packages. The algorithms are described in Broos et al. (2010) and are available online<sup>4</sup>. Their application to stellar populations in other star-forming regions include M 17 (Broos et al. 2007), the Rosette Nebula (Wang et al. 2008, 2009), and NGC 6334 (Feigelson et al. 2009).

Summarizing briefly here, the *Chandra* satellite telemetry data are subject to various cleaning operations, and the image is aligned to the 2MASS/*Hipparcos* astrometric frame. A superset

---

<sup>4</sup><http://www.astro.psu.edu/xray/docs/TARA>

of tentative sources is identified by a combination of wavelet-based source detection, peaks in image tiles with point spread function removed by a maximum-likelihood image reconstruction, and visual inspection for close multiple sources. Photons are extracted from each tentative source in the broad soft, hard and total X-ray bands, and photon counts are compared to the locally measured background. Local backgrounds are essential due to the different exposures from overlapping ACIS exposures. Source significance is evaluated statistically by the quantity  $P_B$ , the probability based on Poisson statistics that the observed source counts would be present given the observed local background rate.

Choosing a source significance limit  $P_B < 1\%$  in at least one broad band, we find 2192 X-ray sources in the *Chandra* mosaic covering the W3-North, W3-Main, W3-OH, and IC 1795 regions. Source properties including X-ray spectra, absorptions, luminosities, and variability, will be presented in a forthcoming paper (Townsley et al., in preparation). For the present study, we consider only the X-ray source positions and error circles. Typical estimated  $1\sigma$  error circle radii are  $0.2'' - 0.5''$  but can exceed  $1''$  for sources far off-axis. Note that the *Chandra* positional errors are often considerably smaller than IRAC positional errors shown in Fig. 2 (panels A and B).

#### 2.4. Near-infrared survey of IC 1795

Near-infrared photometry of IC 1795 has been also analyzed. Near-infrared photometry in  $J$  ( $1.25\mu\text{m}$ ),  $H$  ( $1.65\mu\text{m}$ ) and  $K_s$  ( $2.17\mu\text{m}$ ) bands is taken from the Two Micron All Sky Survey (2MASS Skrutskie et al. 2006)<sup>5</sup>. The  $3\sigma$  limiting sensitivity of this survey is 17.1, 16.4 and 15.3 mag for the three bands, respectively.

### 3. The IRAC point source catalog

#### 3.1. Positions of the IRAC sources

The final photometric catalogs have been filtered for position errors, rejecting sources with positional errors in RA and DEC larger than  $3.6''$  (2 times the FWHM of the PSF in all IRAC channels). The distribution of source positions as a

<sup>5</sup>only good photometry denoted by the flag *AAA* has been considered.

function of their error shows that sources with a larger position error are the fainter targets with a larger uncertainty in the flux (see Fig. 2 for channel 1).

The histograms of the source positions in panels C-D of Fig. 2 show a bimodal structure which reflects the distribution of stars in IC 1795 and W3-Main (ch1-ch3), and of stars in IC 1795 and W3-OH (ch2-ch4). From the peak of the histogram centered on IC 1795, the center of the cluster is found to be  $(\alpha_{J2000}, \delta_{J2000}) = (02h:26m:39s, +62^\circ:00':41'')$ . This is  $\sim 4'$  southeast of the cluster center chosen by Oey et al. (2005).

In panels A-B of Fig. 3, the density distribution of all infrared sources ( $D_{star}$ ) is analyzed.  $D_{star}$  is computed as the total number of sources in a ring ( $N$ ), defined between two consecutive radii from the cluster center, divided by the ring area ( $A_{ring}$ ). The annuli start at  $60''$  from the center of the cluster and end at  $330''$ . The width of each annulus is  $30''$ . The errors in the density distribution are computed as  $\sqrt{N}/A_{ring}$ . The density distribution of sources detected at least in one IRAC channel has been analyzed as a function of the distance from the cluster center (panel A of Fig. 5).  $D_{star}$  peaks at  $90''$  from the center of the cluster and smoothly declines until  $330''$  with the exception of a second minor peak at  $\sim 270''$  (panel B of Fig. 3). The density distribution is consistent with a cluster extension of  $\sim 3.2$  pc. The first peak in density distribution at  $\sim 0.9$  pc from the cluster center originates from a small clump of stars in the North West direction and by an asymmetric distribution of the stars in IC 1795.

#### 3.2. Photometry of the IRAC sources

The four *Spitzer* channels were matched using the IDL procedure *match\_xy.pro* in the IDL-based *Tools for ACIS Review and Analysis (TARA)* package<sup>6</sup> (Broos et al. 2010). The source matching is based on agreement of positions assuming that positional errors are 2-dimensional Gaussians at the 99% confidence level.

The total number of point sources detected decreases as the IRAC wavelength increases due to a decrease in sensitivity. In particular, within  $330''$  from the cluster center, we detect 918, 841, 303 and 243 sources at  $3.6\mu\text{m}$ ,  $4.5\mu\text{m}$ ,  $5.8\mu\text{m}$  and

<sup>6</sup><http://www.astro.psu.edu/xray/docs/TARA>

$8.0\text{ }\mu\text{m}$  respectively. 143 objects were detected in all four IRAC channels.

The color-color diagram (CCD) of the sources detected in all four IRAC channels and the color-magnitude diagram (CMD) of the sources detected at  $3.6\text{ }\mu\text{m}$  and  $4.5\text{ }\mu\text{m}$  (the most sensitive) are shown in panels C-D of Fig. 3 (including the sources detected in all four bands). Megeath et al. (2004) and Allen et al. (2004) proposed a conversion scheme from IRAC colors to source classification (Class 0,I,II,III sources), which has been later improved by Gutermuth et al. (2008, 2009).

The results of this classification for our sources are summarized in Table 1. Using the CMD in panel C of Fig. 3, we distinguish between sources with infrared excess (characteristic of circumstellar disks around young star;  $[3.6]-[4.5]\geq 0.2$  mag) and “photospheric sources” without infrared excess ( $[3.6]-[4.5]<0.2$  mag). The *excess-threshold* adopted here ( $[3.6]-[4.5] = 0.2$  mag) takes into account two factors: 1) model isochrones computed in the IRAC bands do not predict  $[3.6]-[4.5]$  colors exceeding 0.1 mag; see section 5.1 and Appendix A for details; 2) the maximum uncertainty of our photometry (0.07 mag). Out of 592 sources detected at  $3.6\text{ }\mu\text{m}$  and  $4.5\text{ }\mu\text{m}$ , 327 show an infrared excess and 265 are classified as “photospheric” sources. In the following sections we will call “infrared sources” objects detected at least in one *Spitzer* channel, and “excess sources” objects with  $[3.6]-[4.5]\geq 0.2$  mag.

Out of 66 Class I and Class II sources previously classified using the definitions of Megeath et al. (2004) and Allen et al. (2004), all sources have a  $[3.6]-[4.5]\geq 0.2$ . Out of 57 ClassI+II sources, 60% have  $[3.6]-[4.5]\geq 0.2$ . This ensures the reliability of the new scheme adopted to determine a Class I and Class II sources. It is important to notice that the effect of the visual extinction is negligible at these wavelengths: following the extinction relations of Cardelli et al. (1989)  $A_V=2$  mag (typical of a cluster at 2 kpc), corresponds to  $A_{[3.6]}=5.9\cdot 10^{-2}$  mag.

Ruch et al. (2007) analyzed the IRAC observations of the entire W3 region available in the *Spitzer* archive (GTO PID 127) and obtained with a total exposure time of 63.6 s in all IRAC channels. This corresponds to our short exposure, and it is almost one order of magnitude shorter than our long exposure time. They performed PSF

photometry, using a version of DAOPHOT modified by the Galactic Legacy Infrared Mid-Plane Survey Extraordinaire (GLIMPSE) team.

Within  $330''$  from the center of the cluster, they identified 77 sources visible in all four IRAC channels. With our deeper infrared survey we detected 143 sources. There are however some differences between the two surveys: At  $3.6\mu\text{m}$  and  $4.5\mu\text{m}$  we do confirm 76/77 sources previously identified by Ruch et al. (2007), while 1 source has a position error larger than  $3.6''$  and it is not included in our analysis. At  $5.8\mu\text{m}$  we confirmed the detection of 60 sources. Of the remaining 17 sources, 3 have position errors larger than  $3.6''$ , while 14 have not been detected by the PRF fitting method performed in APEX. At  $8.0\mu\text{m}$  we identified 32 sources. Of the remaining 45 sources, 26 have position errors larger than  $3.6''$ , while 19 have not been detected with APEX. We inspected all the non-matched detections (14 at  $5.8\mu\text{m}$  and 19 at  $8.0\mu\text{m}$ ) in our deeper survey: In all cases we find that the local background is highly variable compared to the source brightness and for this reason we did not detect any point-source with our PRF fitting method.

In summary we confirm 76 sources out of 77 sources detected by Ruch et al. (2007) in the ch1 of IRAC and 32 sources in all four IRAC channels. In addition to these sources we identified 111 new sources in all four channels.

### 3.3. Extragalactic contamination of the IR catalog

The extragalactic contamination of the infrared source catalog is estimated using the  $3.6\text{ }\mu\text{m}$  cumulative extragalactic counts from the IRAC/GOODS sample together with the incompleteness correction from Franceschini et al. (2006). About 10 galaxies brighter than 1 mJy ( $\sim 13.6$  mag) at  $3.6\text{ }\mu\text{m}$  are expected in an area of  $1^\circ \times 1^\circ$ . The number of galaxies increases to about one order of magnitude up to  $\sim 300$  sources with fluxes higher than 0.1 mJy. Scaling these values for the IC 1795 area of about  $0.26^\circ \times 0.26^\circ$  the contamination of extragalactic sources is negligible (about 2.6 sources) down to 13.6 mag. In the 13.6 - 15.5 magnitude range, about 70 sources ( $\sim 8\%$  of the total sources detected at  $3.6\text{ }\mu\text{m}$ ) might contaminate the IR source catalog of IC 1795.

## 4. Cluster membership

As outlined in the Introduction, a full understanding of protoplanetary disk evolution in rich stellar clusters requires a cluster membership sample identified in a disk-unbiased way. Many photometric surveys of protoplanetary disks have been pursued with *Spitzer*, but *Spitzer* data alone suffers an important limitation: despite the excellent characterization of disks, sensitive IRAC surveys have biased the ratio of disked systems to non-disked systems in favor of the disk sources.

Optical spectroscopy is widely used to identify cluster members in star-forming regions. This is mainly based on two spectral features: the presence of H $\alpha$  emission at 6563Å and strong absorption of the Li line at 6708Å. These diagnostics are powerful tools for identifying young high accreting objects (H $\alpha$ ), or young low-mass stars with spectral type of K – M (Li). However, this method is not effective at identifying earlier spectral type members: G-type stars, e.g., do not show a strong, age dependent Li I absorption and if they are non-accreting they show only tiny or zero H $\alpha$  emission. An alternative, robust, approach to study the complete population of a young stellar cluster is to combine sensitive X-ray and infrared observations (e.g. Mercer et al. 2009; Stelzer & Scholz 2009; Wang et al. 2008; Getman et al. 2009).

Sensitive X-ray surveys are effective in identifying pre-main sequence stellar populations due to their enhanced magnetic flaring compared to older stars (e.g. Feigelson et al. 2007). Flux-limited X-ray samples have the advantage of selecting young stars both with and without disks, but have the disadvantage of missing stars with fainter bolometric luminosities and lower masses. X-ray selected samples are complementary to *Spitzer* samples because they suffer less contamination from Galactic field stars or from diffuse nebular emission than infrared surveys. Getman et al. (2009) provide details on the relationships between stellar samples selected in *Chandra* and *Spitzer* surveys of a star-forming region. The high-spatial resolution telescope on the *Chandra X-ray Observatory* is essential to resolve crowded regions such as the IC 1795 and the W3 complex.

For IC 1795 we classified as cluster members sources detected in both, our infrared and X-ray, surveys, recognizing that extragalactic contamination may still be present (see discussion

in section 4.2). We also considered as potential members sources detected by *Spitzer* which show an infrared excess at 4.5μm but lack an X-ray counterpart. This approach is fundamental when studying distant young clusters (>1kpc), that can be strongly contaminated by background and foreground stars.

### 4.1. Cluster membership based on X-ray detection

*Chandra* source locations are matched to IRAC source locations using the IDL procedure *match\_xy.pro* in the TARA package<sup>7</sup> (Broos et al. 2010). Associations between *Chandra* and *Spitzer* sources are assumed to be real when the probability that the X-ray and infrared sources are coincident exceeds 99%, assuming bivariate Gaussian error distributions for the two source positions. Within 330'' from the cluster center, we find 280 associations between X-ray and infrared sources, and 9 cases where a single IRAC source has two or more possible *Chandra* counterparts. The *Chandra-Spitzer* matched positions are listed in Table 3. The corresponding optical, 2MASS, and IRAC photometry is compiled in Table 4.

We analyzed the distribution of infrared sources with X-ray counterpart as a function of the distance from the cluster center (panels A-B of Fig. 5). The distribution peaks at ∼90'' from the center, declines down to 200'' and then remains constant to 330'' (except for a second peak at ∼270''). The positions of these two peaks are also found in the distribution of infrared source positions (section 3.1, panel B of Fig. 3).

The number of X-ray sources alone, with and without infrared counterpart, and infrared sources (e.g. detected at least in one *Spitzer* channel) without X-ray counterpart are summarized in Table 1. The final catalog of the IC 1795 cluster members is in Table 4.

### 4.2. Contaminants in the X-ray catalog

The sensitivity limit to X-ray sources in the IC 1795 cluster using the *ACIS Extract* methods is approximately  $L_x \sim 5 \times 10^{29}$  erg s $^{-1}$  in the *Chandra* total band, 0.5 – 8 keV, assuming moderate absorption around  $N_H \sim 10^{21} - 10^{22}$  cm $^{-2}$  ( $A_V \sim 0.5 - 5$  mag) and source spectra typical of

<sup>7</sup><http://www.astro.psu.edu/xray/docs/TARA>

PMS stars. This is not a well-established value due to differences in source spectra, spatial variations in extinction, loss of sensitivity off-axis due to degradation of the *Chandra* point spread function, and gain of sensitivity in some regions due to overlapping exposures in the W3 ACIS mosaic. In this paper we use only the X-ray positions. A more detailed analysis of the X-ray observations will be presented in a forthcoming paper (Townsley et al. in preparation). We estimate the completeness limit to be around  $L_x \sim 1 \times 10^{30}$  erg s $^{-1}$ . Based on the well-established empirical correlation between X-ray luminosity and stellar mass (Telleschi et al. 2007), this X-ray limit corresponds to a mass completeness limit of about  $1 M_\odot$ , although a considerable number of lower mass stars will be included in the *Chandra* sample.

A fraction of the X-ray sources should be contaminants, uniformly distributed, unrelated to the IC 1795 cluster (see discussion in Getman et al. 2006). About  $\sim 30 - 40$  faint and heavily-absorbed X-ray sources in a 100 arcmin $^2$  region (which is of the order of the cluster size) will be background extragalactic objects, mainly quasars and AGNs, seen through the molecular material in the W3 complex and Galaxy along the line-of-sight. At least 20-30 lightly absorbed X-ray sources in a 100 arcmin $^2$  region should be foreground Galactic field stars, and  $\sim 10$  sources should be background stars. The value depends on the amount of recent star formation along the line-of-sight to the W3 complex.

We expect that most of these contaminants, except for foreground stars, will not have an infrared counterpart and so will not contribute to our source list. These extragalactic and Galactic contaminants in the X-ray sample will exhibit a random spatial distribution, as is clearly shown for X-ray sources without infrared counterpart in panels E-F of Fig. 5. However a few quasars can have IRAC colors and X-ray fluxes similar to CTTS (e.g. Richards et al. 2009). This last source of contamination can only be removed via optical spectroscopy.

#### 4.3. Cluster member IR properties

In section 4.1 the cluster members have been defined as an infrared source with a X-ray counterpart. In panels A-B of Fig. 4 the CCD and CMD of the cluster members (i.e. infrared sources with

X-ray counterpart) detected within 330'' from the center of the cluster are shown. We distinguish between cluster members with infrared excess ( $[3.6] - [4.5] \geq 0.2$ ) and “photospheric” sources without infrared excess ( $[3.6] - [4.5] < 0.2$ ).

In panel A of Fig. 4 the 145 sources detected in all IRAC channels are shown. In Table 1 we summarized the classification of the disks using the IRAC colors from Megeath et al. (2004) and Allen et al. (2004).

For comparison in panels C-D of Fig. 4 we plot the IRAC detections with no X-ray counterpart: we notice that sources with and without infrared excess in the CMD of panel D reach  $[3.6] \sim 16$  mag, while in the CMD of panel B sources without excess have  $3.6\mu\text{m}$  magnitudes down to 15.5 mag, and only few sources with excess have  $3.6\mu\text{m}$  magnitudes larger than 14 mag. The density distribution<sup>8</sup> of the cluster members is shown in panels A-B of Fig. 5. The distribution peaks within 100'' from the center of the cluster. In panels C-D of Fig. 5 the density distribution of infrared sources without a X-ray counterpart is shown. Out of 593 sources detected in ch1 and ch2 without a X-ray counterpart, we find 248 IRAC excess sources<sup>9</sup>. The distribution of sources with excess is similar to the distribution of the cluster members, while the flat distribution of sources without excess suggests that most of them are not related to the cluster. For this reason, infrared sources without X-ray counterpart but with excess emission have been classified as *cluster member candidates*<sup>10</sup>. Table 5-6 give positions and IRAC fluxes of the cluster member candidates (i.e. infrared sources with excess without X-ray counterpart).

#### 5. Age and Mass Distribution of the cluster members

In this section we estimate the age, the mass distribution and the completeness of the cluster members of IC 1795, defined in section 4 as infrared sources with an X-ray counterpart.

<sup>8</sup>defined as in section 3.1

<sup>9</sup>defined as  $[3.6] - [4.5] \geq 0.2$

<sup>10</sup>see section 3.3 for a possible extragalactic contamination

### 5.1. Age of the cluster

The ages of PMS associations are usually estimated by comparing the location of the association members in a CMD or Hertzsprung-Russell diagram, to isochrones resulting from the predictions of PMS evolutionary model grids. This comparison usually makes use of dereddened optical or near-infrared photometry unaffected by the presence of a protoplanetary disk, but optical spectroscopy of most of the cluster members, to quantify the differential reddening to each source, is not available. The positions of the sources in these CMDs can thus be either affected by differential extinction, or by a spread in age, as well as by undetected binarity.

However, for IC 1795 members we do have extensive 2MASS J-band and IRAC infrared [3.6] and [4.5] photometry. Thus to optimize the isochronal fitting of IC 1795 members, we first look for the best magnitude and color to distinguish between sources with and without infrared excess. This is needed to clean the CMD of the infrared-excess sources.

The  $J$  magnitude is not affected by infrared excess (which in the different classes of disks would usually start, at least, from the  $H$ -band), and is sensitive to the stellar mass. The first CMD analyzed used the  $J$  vs.  $J - H$  magnitudes (Fig. 6A). However the disadvantage is that the  $J$  and  $H$  magnitudes are strongly affected by extinction along the line of sight. This represents a serious problem in particular working on a cluster at more than 1 kpc in distance such as IC 1795. Overlaid on the CMD in Fig. 6A are the 3 Myr and the 5 Myr isochrones obtained using the FRANEC evolutionary code (see Appendix A). The isochrones are reddened with  $A_V = 2$  mag which is the minimum extinction expected for a cluster at distance of 2 kpc. Without any information on a possible differential extinction within the cluster, from this CMD it is not possible to distinguish between the different isochrones. The positions of the sources can be either affected by additional extinction, or by a spread in age, as well as by undetected binarity. Different CMDs, combining in different ways the  $J$ ,  $3.6\mu\text{m}$  and  $4.5\mu\text{m}$  magnitudes, have been further compiled. The advantage of using the  $J$ -[3.6] or  $J$ -[4.5] combinations is that photospheric and infrared excess sources are clearly separated in color. The advantage of using the [3.6]-[4.5] combination

instead, is that at these wavelengths the effect of interstellar extinction is lower (see the module of the extinction  $A_V$  in Fig. 6). We thus use the [3.6] vs. [3.6]-[4.5] CMD to distinguish between objects with and without infrared excess, taking advantage of the negligible extinction at these wavelengths.

In Fig. 6 panel B we show the [3.6] - [3.6]-[4.5] CMD of the Class III cluster members, together with the 1 Myr, 3 Myr and 5 Myr isochrones. In this CMD, the only parameters that determine the vertical position of the Main-Sequence Turn-On (*MSTON*; see appendix A) are the age and the distance of the cluster. We notice that at these wavelengths an error of 10% in distance corresponds to an uncertainty of less than 1 Myr in age and the reddening is unimportant because the reddening vector (see Fig. 6 panel B) runs parallel to the low-mass population. We also investigate whether an additional extinction of 2 mag in  $V$  would change the position of *MSTON*, and hence the conclusions about the upper limit on the age of the system. In Fig. 14B the 5 Myr isochrone is reddened by  $A_V = 2$  mag and  $A_V = 4$  mag. Taking into account the errors on the distance of the cluster (shown also in Fig. 14B) and on the photometry of the single sources (the maximum error was 0.07 mag; see section 3.2), we conclude that, within the errors, all the stars still lie close or above the 5 Myr isochrone. For these reasons the apparent age of the cluster can be determined using reddened photometry. From the *MSTON* we can conclude that the cluster is younger than 5 Myr and it likely has an age between 3 and 5 Myr. This is consistent with an earlier estimate (Oey et al. 2005) which was obtained from the position in the H-R diagram of the early type sources of IC 1795.

Due to the presence of other stars with a  $3.6\mu\text{m}$  magnitude in the range of 12.5 - 14 mag which do not follow the shape of the isochrones, we investigate the possibility of a spread in age of the cluster members. We first notice that the 1 Myr isochrone does not reproduce the distribution of the observed sources on the CMD (Fig. 6). If we presume that the cluster has a spread in age between 1 and 5 Myr due to different episodes of star formation, sources with a  $3.6\mu\text{m}$  magnitude in the range of 12.5 - 14 mag would represent the younger population of the cluster, since for the 1 Myr isochrone all stellar masses reside

within this magnitude range (Fig. 6). In this case, they would also have a different spatial distribution in respect to the older population with  $3.6\mu\text{m} > 14\text{mag}$ . However, the random spatial distribution of the photospheric sources with different [3.6] mag argues against a significant spread in age in the cluster population caused by triggered episodes of star formation. A second argument against a young population present in the cluster regards the CMD using the 2MASS magnitudes (Fig. 6 panel A). The overlaid isochrones are shifted assuming a distance to the cluster of 2 kpc and  $\text{Av} = 2$  mag, which is the minimum extinction for a cluster at that distance. In this CMD the bulk of the sources are bluer and fainter than the 1 Myr isochrone.

These arguments, however, do not exclude that a younger population might be present in the cluster and is viewed in projection over the older one. A possibility is that stars with  $[3.6] = 12 - 14$  are binaries. In section 5.2 we test this hypothesis by including the binarity in a simulation of the theoretical luminosity function of the cluster.

## 5.2. Luminosity and Mass Functions of IC 1795

The comparison of the observed and theoretical luminosity function enables to estimate the completeness limit of our *Spitzer-Chandra* survey. The observed luminosity function is compiled using the  $3.6\mu\text{m}$  magnitude as a tracer of the stellar photosphere. To have a description of the entire stellar population of IC 1795, the observed luminosity function includes cluster members with and without infrared excess and cluster member candidates (defined in section 4.3). This approach is necessary because the disk fraction may be mass dependent (section 6). We used the method described in Appendix B to determine the “photospheric”  $3.6\mu\text{m}$  magnitude of the sources with infrared excess. The same has been done for the cluster member candidates.

We computed the theoretical luminosity function using a galactic initial mass function (IMF) (Kroupa 2002) and the 4 Myr and 5 Myr isochrones respectively. The simulated population is normalized to the observed stellar sample down to a certain completeness magnitude limit. We compare the simulations obtained using a completeness value of 13.5 mag, 13.75 mag, 14 mag, 14.25 mag,

14.5 mag and 15 mag at  $3.6\mu\text{m}$ . We conclude that the completeness of our survey at  $3.6\mu\text{m}$  is 14 mag.

We notice, however, that for both ages of 4 Myr and 5 Myr, the simulations do not well-reproduce the number of sources in the  $3.6\mu\text{m}$  magnitude range of 13–14. This might be an effect of a binary population unresolved in the cluster. To test this, we ran simulations with 30% and 50% binary fractions, with primary and secondary masses drawn independently from the same IMF. The outcomes are only slightly different from our original calculations. This implies that the luminosity function is only marginally affected by binarity.

In order to convert the completeness expressed in magnitude into the corresponding stellar mass value, the mass function of IC 1795 is now extracted.

Using the 4 Myr and 5 Myr isochrones, from the observed luminosity function we derived the stellar masses and hence construct the mass function for the cluster. We used the method described in Appendix C to assign a stellar mass to each source. The resulting observed total mass function is shown in Fig. 7 together with the mass functions of the single sub-groups considered for the total mass function: the cluster members<sup>11</sup> without and with infrared excess and the cluster candidates<sup>12</sup>. The theoretical IMF (Kroupa 2002) is normalized to the total number of stars down to 14 mag. We notice that all the distributions peak at the same mass. This ensures that both the *Spitzer* and *Chandra* surveys have the same completeness. There is a large population of low mass cluster candidates, down to  $0.4 M_{\odot}$  which lack a X-ray counterpart. The observed mass function falls below the theoretical IMF below  $\sim 1.0 M_{\odot}$ . This mass corresponds to the estimated completeness at  $3.6\mu\text{m}$  of 14.0 mag.

Extrapolating the total population of IC 1795 down to a mass of  $0.08 M_{\odot}$ , the total cluster membership numbers  $\sim 2000$  stars. This corresponds to a stellar density of  $\sim 15$  stars  $\text{pc}^{-3}$ , which is several thousands lower than the density in the Trapezium cluster.

In summary:

- IC 1795 has an age between 3 and 5 Myr

---

<sup>11</sup>Spitzer sources with X-ray counterpart

<sup>12</sup>Spitzer sources with excess without X-ray counterpart

consistent with the previous estimate of Oey et al. (2005),

- the mass function is well-reproduced by a standard IMF to a mass limit of  $1 M_{\odot}$ - $1.2 M_{\odot}$ ,
- the cluster population is estimated to be 2000 sources at a mass limit of  $0.08 M_{\odot}$ .

## 6. Disk evolution: effect of the stellar mass and the environment

In this section the analysis of the disk fraction as a function of the stellar mass and distance from the center of the cluster is presented for the cluster members<sup>13</sup> of IC 1795.

### 6.1. Disk fraction vs stellar mass and spatial distribution

We examine the mass dependence of disk emission of the 3 - 5 Myr old cluster IC 1795. Since only few stars have been spectrally classified so far (Oey et al. 2005), and a detailed spectral classification of the cluster members is in preparation (Kim et al. 2010, in preparation), the disk fraction is computed using the  $3.6\mu m$  and the  $J$  magnitudes as a tracer of stellar photosphere (Fig. 8 and 10, details in section 5.2).

In order to calculate the fraction of sources with and without infrared excess, we follow the method described in Appendix B. We notice that, between  $[3.6] = 10 - 12$ , the disk fraction rapidly increases from 20% to 50%, and then it remains constant at 60-40% between 12 and 14.5 mag. Constructing a  $2 \times 2$  contingency table of IR excess for the  $[3.6] = 10 - 12$  and  $12 - 14$  magnitude ranges, we formulate a hypothesis test with null hypothesis that IR excess does not depend on  $[3.6]$  or, equivalently, on stellar mass. A Fisher's exact test applied to the contingency table indicates the probability of this null hypothesis is  $P = 0.005$ . The test is implemented by the *R* statistical software package (R Development Core Team 2009). We conclude that the effect is statistically reliable. Since  $\sim 80\%$  of our IRAC sources have a near infrared counterpart, we used the  $J$  magnitude as a proxy for stellar mass (see, e.g. Hernández et al.

2007). These bands have the advantage of being relatively unaffected by disk excess emission. However, they are strongly affected by extinction. The 4 Myr isochrone (see section 6) has been used to infer masses from the  $J$  magnitudes. In this band the relation between mass and magnitude is almost unique (see Fig. 9).

In Fig. 10 (panel A) we show the CMD using the  $J$  magnitude as a photospheric tracer and the  $[3.6]-[4.5]$  IRAC colors to define the sources with and without infrared excess. After the histograms of sources with and without excess (panel B of Fig. 10), the disk fraction is shown in panel C. This is computed as the ratio of sources with and without excess in bins of one magnitude. The errors are computed as the square root of the number of sources in each bin. The corresponding mass is reported in the upper x-axis.

The disk fraction is found to increase from 20% to 60% for  $J$  magnitudes from 11 to 15. This corresponds approximately to masses between  $8.4$  and  $0.8 M_{\odot}$ . The disk fraction remains constant around 50% toward lower masses. An increasing frequency of disks is obvious down to 15 magnitudes even after taking into account the uncertainty in the disk fraction.

Taking into account solar-type stars only with masses  $\sim 1 M_{\odot}$  (our completeness level, section 5.2), the disk fraction is 50%.

This value is consistent with the disk fraction of solar-type stars previously computed with the  $3.6\mu m$  magnitude. A dependency of the disk fraction on the stellar mass was found in *Spitzer* surveys of young clusters with low and high-mass members (e.g. Hernández et al. 2007; Carpenter et al. 2006; Currie et al. 2007; Lada et al. 2006; Luhman et al. 2010). The general finding is that massive stars seem to loose their disk earlier than lower mass stars. This was also found in clusters older than 3 Myr by Kennedy & Kenyon (2009), using published optical spectra and infrared excess data.

In young clusters the disk fraction may depend also on the spatial position. If triggered star-formation took place in IC 1795 itself, a different spatial distribution of sources with and without disks and with an age gradient is expected (e.g. Cepheus B, Tr 37, Getman et al. 2009; Sicilia-Aguilar et al. 2005, 2006). In Fig. 11 we show the spatial density distribution of sources

<sup>13</sup>defined in section 4 as infrared sources with an X-ray counterpart.

with and without infrared excess.

The disk fraction ( $f_d$ ) is defined as the ratio between the number of sources with disks ( $N_{\text{disk}}$ ) and the total number of sources (with and without disks;  $N_{\text{tot}}$ ). The fraction  $f_d$  was computed in consecutive rings. Within the uncertainties, the disk fraction remains constant across the IC 1795 region at about 50%.

This result argues against a triggered star formation scenario for IC1795. A constant disk fraction as a function of the distance from the center of the cluster was also found e.g. in  $\sigma$  Ori (Oliveira et al. 2006) using  $K$  and  $L$ -band observations. This result is however in contrast with Hernández et al. (2007) who instead found an evidence for a higher disk fraction near the cluster center for  $\sigma$  Ori.

## 6.2. Influence of the O star in the cluster: disk photoevaporation and cluster dynamics

In Fig. 1, we notice that the O6.5V and the O9.7I stars lie at  $39''$  west and  $120''$  north respectively, from the projected spatial center of the cluster defined in sec. 3.1. In order to study the influence of the O stars in the cluster we have re-centered the cluster on each O star. In both cases, the spatial distribution of the disk fraction observed is almost constant with distances from each O star including within the first  $60''$  (which corresponds to 0.58 pc at the cluster distance). This result is not in agreement with previous works of Balog et al. (2007) and Mercer et al. (2009). From the analysis of the 2-3 Myr NGC 2244 cluster Balog et al. (2007) found a smaller disk fraction within 0.5 pc from the O stars, including the two highest-mass O stars, HD 46223 (O5) and HD 46150 (O6) of the cluster. Johnstone et al. (1998) predicted an absence of disks in systems proximate to O-stars, a prediction supported observationally by Hernandez et al. (2008) who found no evidence for primordial disks within 0.75 pc of an high-mass binary (consisting of an O 7.5 star and a Wolf-Rayet star) in the  $\gamma$  Velorum star-forming region. However, theoretical expectations predict the photoevaporation of the outer part of the disk ( $> 5$  AU), while in the inner regions (traced by *Spitzer/IRAC*), where the escape velocity exceeds the sound speed of the ionized gas, cannot be evaporated. The dissipation of such a part of the disk

proceeds via viscous transport of material from the inner to the outer disk (e.g. Adams et al. 2004). Models predict that a high-mass star introduces an external UV radiation which can photoevaporated disks only within 0.3-0.7 pc (e.g. Johnstone et al. 1998; Adams et al. 2004; Clarke 2007; Gorti et al. 2009). Finally, we investigate whether mass segregation acted on the dynamics of the cluster.

In IC 1795 the high-mass stars are not in the center of the cluster, nor are they preferentially concentrated in a particular region compared to lower mass members (see Fig. 1). The exception is represented by the O6.5V star which is only  $38''$  away from cluster center. Since the spatial distribution of high-mass stars does not allow to conclude if mass segregation has taken place in IC 1795, we check whether the cluster is in dynamical relaxation. The time scale of mass segregation can be approximated by the relaxation time ( $t_{\text{relax}}$ <sup>14</sup>). Adopting a radius of the cluster  $R \sim 3.2\text{pc}$  (see section 3.1) and using a rough estimate for the unmeasured velocity dispersion  $v_{\text{disp}} \sim 3\text{km}\text{s}^{-1}$  (Binney & Tremaine 1987), and  $N \sim 2000$  stars (see section 5.2), we obtain  $t_{\text{relax}} \sim 68$  Myr for IC 1795. As the cluster age is  $\sim 17$  times less than its relaxation time, this calculation supports the observational evidence that mass segregation has not occurred in IC 1795. A similar result has been found in the 2-3 Myr old cluster NGC 2244 by Wang et al. (2008, 2009). However, in young rich clusters, massive stars are usually concentrated in the center (e.g. ONC, Hillenbrand et al. 1998).

## 6.3. Disk evolution in low and high-mass environments

In this section the disk fraction of IC 1795 is compared with the results obtained in other low and high-mass star-forming regions with the aim of investigating the influence of high-mass stars on the disk dissipation timescale. In particular, using the mid-infrared wavelength range, which traces the circumstellar dust at a few AU from the star, it is possible to constrain the dissipation timescale of the region of the circumstellar disks

---

<sup>14</sup>  $t_{\text{relax}} \approx (N/8\ln N)t_{\text{cross}}$ , where  $t_{\text{cross}} = 2R/v_{\text{disp}}$  is the crossing timescale and  $v_{\text{disp}}$  the velocity dispersion, (Bonatto et al. 2006). ) in which a cluster reaches some level of kinetic energy equipartition, with the massive stars sinking to the core and low-mass stars moving to the cluster halo (e.g. Bonatto et al. 2006).

where planets form.

The disk fractions computed using the IRAC/*Spitzer* colors have been compiled from the literature and compared with the result obtained on IC 1795. The clusters considered are listed in Table 2. The total disk fraction from the individual studies is presented highlighting the completeness mass range of their work. When available, the disk fraction only in the intermediate-high-mass range is also reported. When the errors on the disk fractions ( $\Delta f$ ) are not available in the literature, we used  $\Delta f = \frac{1}{\sqrt{N_{TOT}}}$ , where  $N_{TOT}$  is the total number of cluster members.

The general trend of disk dissipation in low-mass and high mass environments (see Fig. 12) suggests that in young clusters (1 Myr) the fraction of disks is about 90%-80%. By about 3-4 Myr the fraction of disks is reduced to 50%-40%. At 5 Myr the disk fraction drops to 20% while after 10 Myr almost all disks are dissipated.

Apart from the general trend previously described, the disk fraction of clusters containing more than 5 O/B stars shows mass dependent effects. For the O and B stars, the disk fraction decreases to 30% in the first 3 Myr, while in the low-mass environment it is still 60%-85%.

Our result is consistent with the disk fraction found in cluster Tr 37 (Sicilia-Aguilar et al. 2006), an OB association with an age similar to that of IC 1795.

Most of the disk fractions from the literature are computed for clusters within 1kpc. IC 1795 is at  $\sim 2$  kpc and our study is complete to  $\sim 1 M_\odot$ , which corresponds to early-K spectral types. Therefore a comparison between the disk fraction of  $50\% \pm 10\%$  found for IC 1795 and that of other clusters might be misleading, e.g. for lower masses where our survey is incomplete, we expect to miss a significant fraction of the photospheric population.

A number of bias effects in compiling disk fractions from the literature, (e.g. the completeness of the cluster memberships, the uncertainty on the age and the disk fractions not specified in different mass range), have been carefully highlighted, since they can affect our conclusions. Given all uncertainties, we find that IC 1795 follows the smooth decline of the disk fraction with age observed for other clusters.

## 7. Summary

In this paper we presented a deep *Spitzer*/IRAC survey of the OB association IC 1795. Combining the infrared *Spitzer*/IRAC observations with a deep X-ray *Chandra*/ACIS survey we carefully establish the cluster membership of the cluster. Compared to previous optical based studies on young clusters, this is the only method which allows for a determination of the disk fraction for cluster members with masses  $\gtrsim 1.0 M_\odot$ . The IR/X-ray surveys are complete down to  $1 M_\odot$  or  $1.2 M_\odot$  computed with the 4 Myr or 5 Myr isochrones, respectively. The age of the cluster is determined via the position of the Class III stars (stars with no disks) on the [3.6] – [3.6]-[4.5] color-magnitude diagram. For IC 1795 we determine an age of 3 – 5 Myr.

The spatial distribution of the cluster was found to be asymmetric around the cluster center and no mass segregation is present.

The disk fraction was analyzed as a function of the distance from the cluster center as well as a function of the stellar mass. The objects with disks represent the 50% of the total source number. No spatial dependence of the disk frequency was found.

Using the [3.6] IRAC magnitude as a tracer for the stellar mass we find that the disk fraction is  $\sim 20\%$  for masses  $> 2 M_\odot$  and  $\sim 50\%$  for masses  $< 2 M_\odot$ . We confirm that the dissipation of disks around high-mass stars ( $> 2 M_\odot$ ) is faster compared to the dissipation around stars of  $1-2 M_\odot$ .

We found no variation in the disk fraction within 0.6 pc of the O-type stars in the association.

Measurements of the disk fractions in low-mass and high-mass environments have been collected from the literature. We found that, in general, the disk dissipation timescale is comparable in high-mass and low-mass clusters.

We are grateful to the *Spitzer Science Center* for their support during the data reduction. We acknowledge Leisa Townsley for supplying the *Chandra*/ACIS sourcelist for W3 and thank Patrick Broos for assistance with matching those X-ray sources to the IRAC sources. We acknowledge G. Rodighiero for the helpful discussion about the extragalactic contamination in the mid-infrared. This publication makes use

of data products from the Two Micron All Sky Survey, which is a joint project of the University of Massachusetts and the Infrared Processing and Analysis Center/California Institute of Technology, funded by the National Aeronautics and Space Administration and the National Science Foundation. E.D.F. was supported by Chandra grant SV4- 74018, NASA grant NNX09AC74G and NSF grant AST-0908038. ASA is supported by the Deutsche Forschungsgemeinschaft (DFG) grant number SI 1486/1-1.

## A. Evolutionary model

The isochrones adopted for the analysis have been computed using the FRANEC evolutionary code. We briefly describe here the physical inputs in the code. For detailed explanation the reader can refer to Chieffi & Straniero (1989); Degl'Innocenti et al. (2008). The opacity tables are from Ferguson et al. (2005) for  $\log T[K] < 4.5$  and from Iglesias & Rogers (1996) for higher temperatures. The equation of state (EOS) is described in Rogers et al. (1996). Both opacity tables and EOS are calculated for a heavy elements mixture equal to the solar mixture of Asplund et al. (2005). Our models are completely self-consistent, with a *unique* solar chemical composition,  $(Y, Z) = (0.27, 0.02)$ . The value of the mixing length parameter adopted in the models is  $\alpha_{MLT} = 1.6$ .

Transformations from the theoretical ( $\log(T_{eff}[K]), \log(L/L_\odot)$ ) to the observational planes have been performed via synthetic photometry. In particular we have computed the isochrones in the 2MASS and  $VI_{\text{Bessell}}$  photometric systems and for the first time in the IRAC photometric system. The optical and near-IR isochrones are consistent with the PMS isochrones computed by Siess et al. (2000). The filter throughputs and zero points of the IRAC photometric system are defined in Reach et al. (2005). We used stellar spectra generated with both the ATLAS9 (see Castelli & Kurucz (2003)) and PHOENIX (Brott & Hauschildt (2005)) model atmospheres codes.

The ATLAS9 grid of models is limited to temperatures higher than 3500 K; corresponding isochrones have then a lower cut in mass at values of  $0.36 M_\odot$  and  $0.38 M_\odot$  for 3 and 5 Myr respectively. The PHOENIX grid can cover a region of lower temperatures ( $T > 2000$  K) but has an upper limit in temperature of 10000 K. This corresponds to  $2.96 M_\odot$  and  $2.56 M_\odot$  for 3 and 5 Myr respectively.

### A.1. Mid-infrared isochrones

In the mid-infrared (MIR) CMDs, the part of the isochrone for intermediate-to-high-mass stars that have reached already the Main Sequence (MS) is almost vertical. Lower mass stars are still in the PMS phase. The PMS objects are cooler and with lower surface gravities; their spectra at the MIR wavelengths are no longer described by an (approximate) black body exponential tail, as in the MS phase. Due to the presence of spectral features the PMS isochrones show tendency towards redder colors.

PMS stars have larger radii when they are at the top of their Hayashi track, and the radii become smaller as the stars evolve and contract. In the totally-convective phase the effective temperature changes little, leaving the observed color almost unchanged, even though the change in surface gravity slightly affects the shape of the emerging spectrum. But with decreasing age, the change in radius heavily affects the total luminosity. For this reason mid-infrared PMS isochrones are no longer age-degenerate as they are in the MS phase. On the contrary different PMS isochrones are well separated in the MIR CMDs and can be used for age-dating the cluster, or, at least, setting some constraint on its age. In particular, the transition phase between PMS to MS is characterized by a hook-shaped bending in the isochrone. As the age increases, the hook and the red PMS branch move towards larger magnitudes (lower luminosities). When an independent estimate of the distance and the extinction is available, as in our case, the Main-Sequence Turn-On (MSTON) can be used as upper limit for the age of a cluster. After placing an isochrone in the CMD, if no star is observed below the MSTON, at color equal zero, then the cluster must be younger than the given isochrone.

For this reason the position of the MSTON is used to infer the age of the cluster.

## B. Disk fraction in the [[3.6],[3.6]-[4.5]] CMD

Fig. 13A shows the [[3.6]-[4.5], V] CMD. In this diagram the presence of the circumstellar disk causes the object to move horizontally towards red colors. This is because the disk emission affects only slightly the V magnitude (e.g. through optical veiling produced by mass accretion).

In the [[3.6]-[4.5],[3.6]] CMD shown in Fig. 13B, disk emission also affects the stellar luminosity ([3.6] mag). As a consequence the presence of the disk will move the object towards red colors obliquely.

To properly compute the disk fraction as a function of the [3.6] magnitude (and hence stellar mass) it is

necessary to take into account this effect. We calculate the isomass in the [3.6] magnitude in the [[3.6]-[4.5],[3.6]] CMD. This was computed in the following way: we select all stars in a series of horizontal slices in the [[3.6]-[4.5], V] CMD (central V = 20.5; 21.5 mag and bin = 0.5 mag). We look for the position of the same objects (highlighted with the same symbols) in the [[3.6],[3.6]-[4.5]] CMD. We extrapolate the median inclination of the position of these sources in this CMD for each magnitude bin. Finally, we computed the disk fraction in a series of bins counting the sources in the oblique slices.

### C. Relation between $3.6\mu\text{m}$ IRAC magnitude and stellar mass

Due to the spread of the sources along the isochrone, we assign the most probable mass by taking into account the photometric uncertainty via a maximum-likelihood method. We define the Likelihood function for the i-th observed star as:

$$\mathcal{L}^i(m_j) = \frac{1}{2\pi \sigma_{3.6}^i \sigma_{4.5}^i} \times \exp(-\chi^2/2) ; \quad (\text{C1})$$

where:

$$\chi^2 = \left( \frac{[3.6]_{obs}^i - [3.6]_{th}^j}{\sigma_{3.6}^i} \right)^2 + \left( \frac{[4.5]_{obs}^i - [4.5]_{th}^j}{\sigma_{4.5}^i} \right)^2 ; \quad (\text{C2})$$

here the j index runs on the masses along the isochrone and  $\sigma^i$  are the photometric uncertainties for the i-th star and subscripts *obs* and *th* stand for observed and predicted quantities respectively. Since we use the magnitude-magnitude space the uncertainties can be considered uncorrelated and the  $\chi^2$  assumes the form of eq. (C2). We assign to the i-th data point the mass value  $m_{j*}$  for which  $\mathcal{L}(m_j)$  has its maximum.

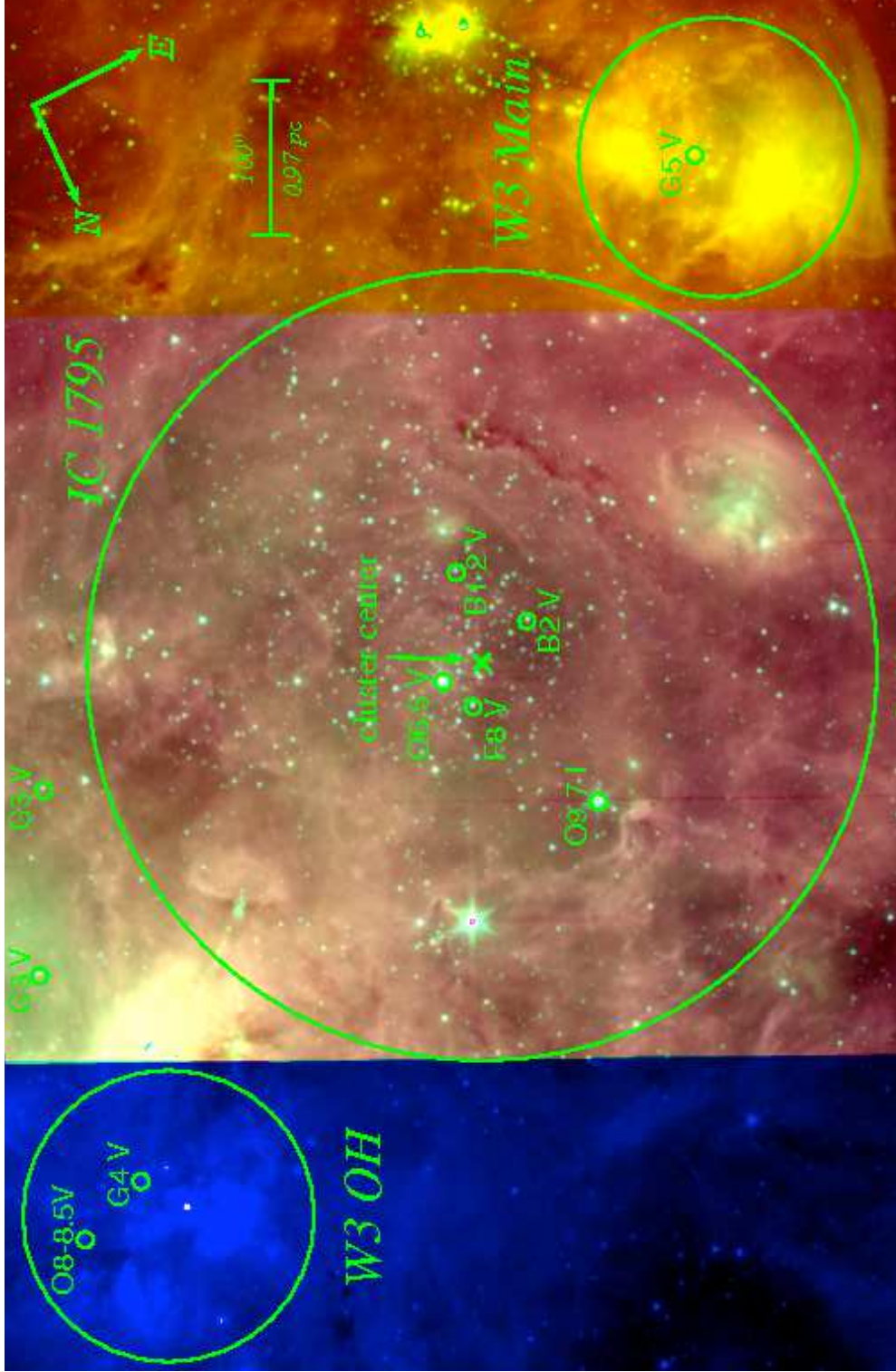


Fig. 1.— Combined image of the mosaics obtained with the long exposures of IRAC/ch1, IRAC/ch2 and IRAC/ch4. Highlighted are the edge and center of IC 1795 together with the positions of the high- and intermediate-mass stars in the region spectrally classified by Oey et al. (2005). W3-Main and W3-OH are not covered by all IRAC channels.

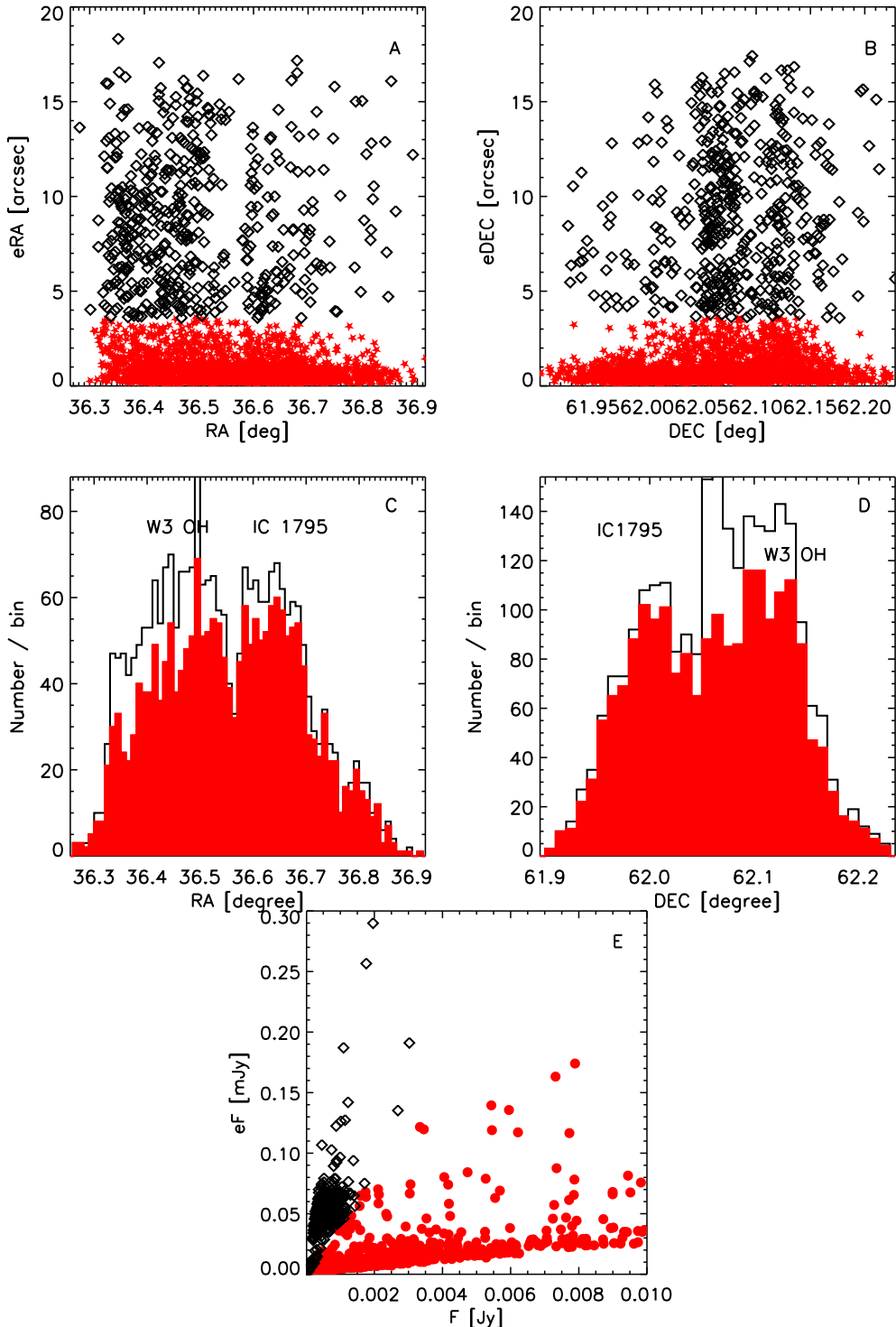


Fig. 2.— *A-B*: RA and DEC errors versus RA and DEC coordinates of all the sources detected in IRAC/ch1. The empty diamonds represent sources with coordinates errors larger than  $3.6''$ . Sources with positional errors less than  $3.6''$  are highlighted with filled red stars. *C-D*: Black empty histograms represent the RA and DEC coordinates of all sources shown in panels A-B with empty diamonds. The red filled histograms represent RA and DEC coordinates of sources of our final lists (filled red stars in panels A-B). *E*: Flux error versus the flux of the sources shown in the upper panels. The red filled stars represent the sources of our final lists selected with position errors in RA and DEC  $\leq 3.6''$ . Positional errors  $> 3.6''$  (black empty diamonds) correspond to the fainter sources with larger positional errors.

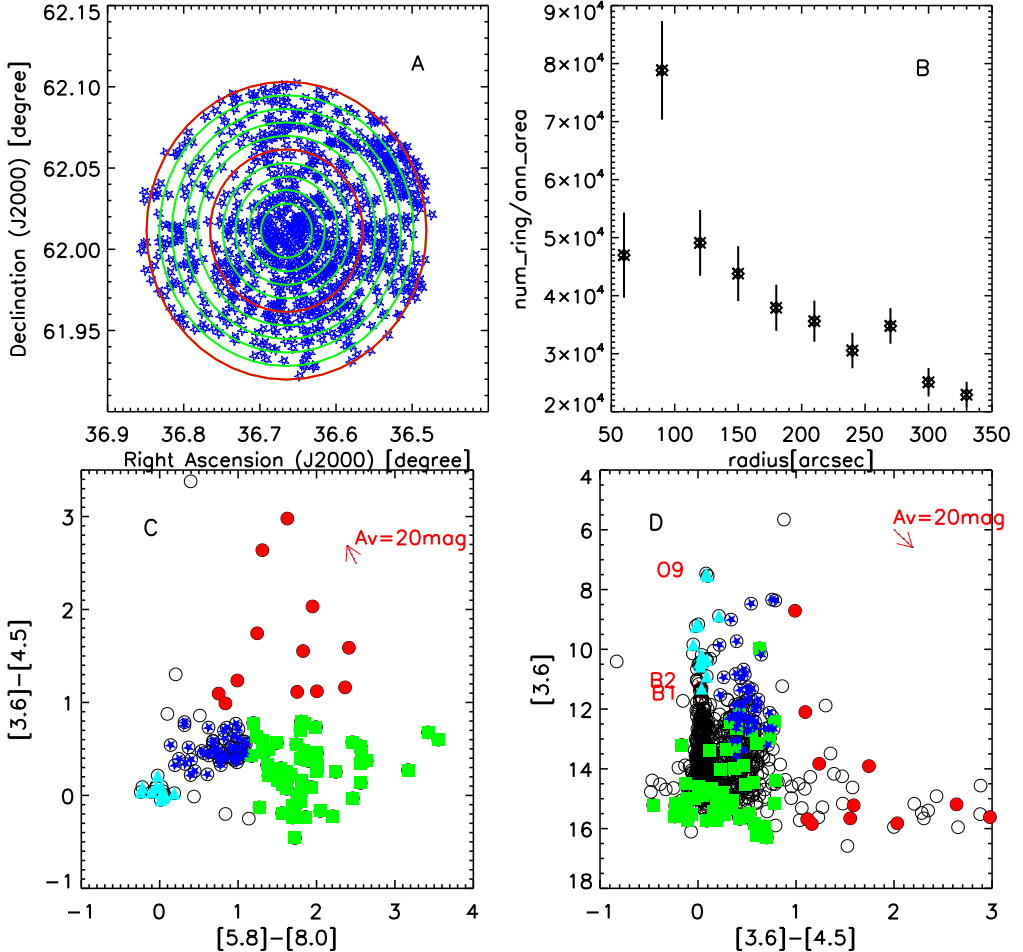


Fig. 3.— Spatial density distribution of all IR sources (A), and their spatial density distribution as a function of the distance from the center of the cluster (B). The green circles represent radii from  $60''$  from the center of the cluster to  $330''$  with  $30''$  spacing. C: Color-Color Diagram (CCD) of the IRAC/*Spitzer* sources detected within  $330''$  from the center of the cluster. The different symbols and colors represent the disk classification from Megeath et al. (2004) and Allen et al. (2004): filled (cyan) triangles: photosphere/Class III ; filled (green) squares: Class I/II; filled (blue) stars: Class II; filled (red) circles: Class O/I; D: Color-Magnitude Diagram (CMD) of all the sources identified at  $3.6\mu\text{m}$  and  $4.5\mu\text{m}$ . The different symbols represent the sources detected in four IRAC channels classified in the CCD on the right. Empty (black) circles: sources with magnitudes that do not follow the previous classification. The arrows represent an extinction  $A_V = 20$  mag.

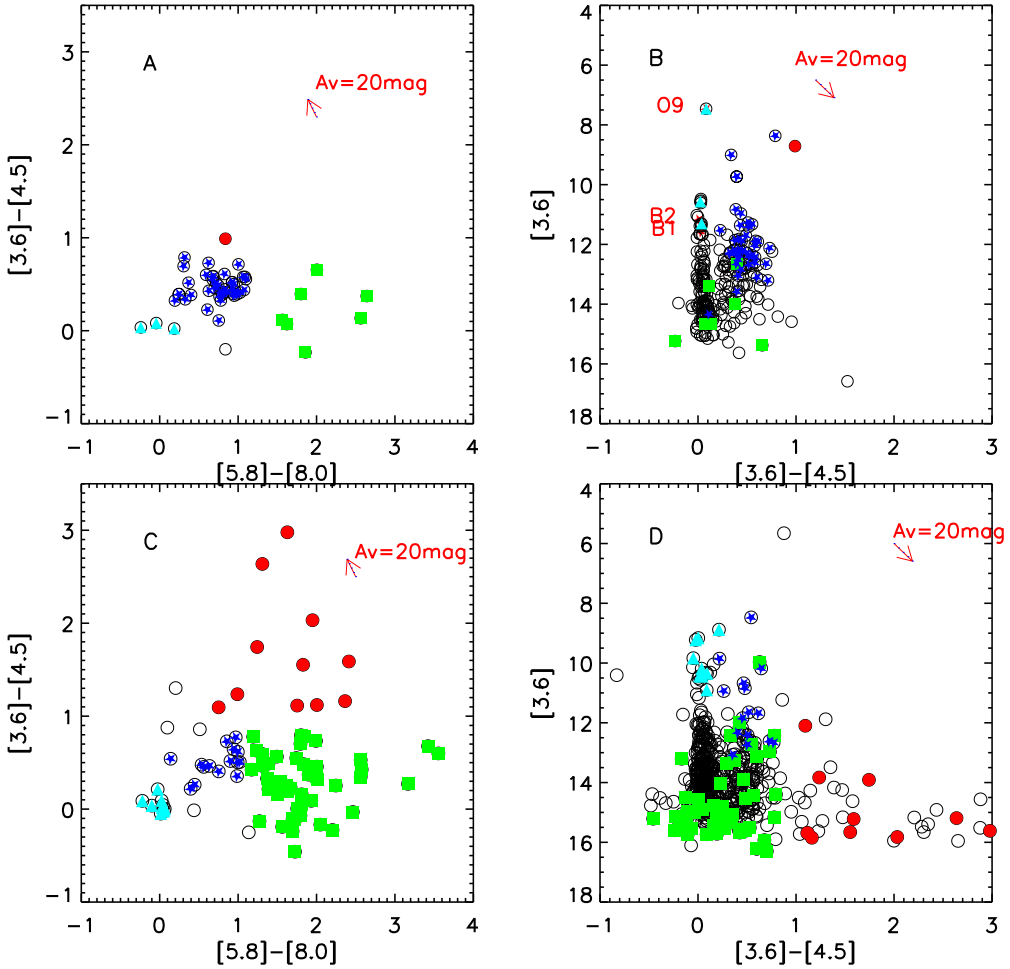


Fig. 4.— *Left:* CCD of the IRAC/Spitzer sources detected within  $330''$  from the center of the cluster (empty black circles). The different symbols and colors represent the disk classification from Megeath et al. (2004) and Allen et al. (2004): *filled (cyan) triangles*: photosphere/Class III ; *filled (blue) stars*: Class II; *filled (green) squares*: Class I/II; *filled (red) circles*: Class 0/I; *Right:* CMD of all sources identified in IRAC/ch1 and IRAC/ch2. The different symbols represent the sources detected in the 4 IRAC channels classified in the CCD on the right. The arrows represent an extinction  $A_V = 20$  mag. *A-B:* infrared sources with an X-ray counterpart. *C-D:* infrared sources without an X-ray counterpart.

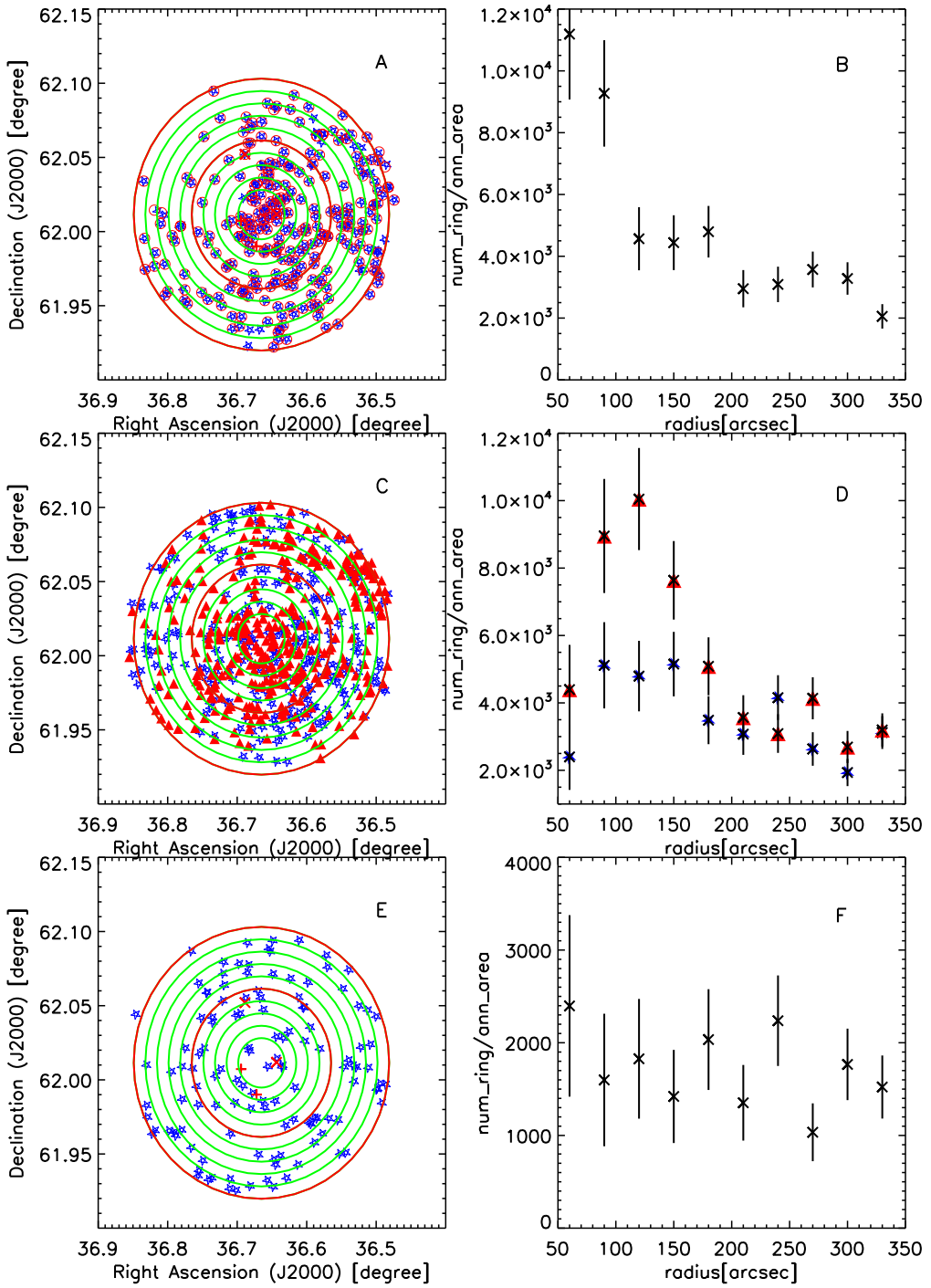


Fig. 5.— Spatial density distribution of all the IR sources (*left column - A, C, E*), and their spatial density distribution as a function of the distance from the center of the cluster (*right column - B, D, F*). The green circles represent annuli from  $60''$  from the center of the cluster to  $330''$  with a spacing of  $30''$ . The 'x' and '+' symbols represent the positions of the O and B stars in the cluster. *A-B*: infrared sources with an X-ray counterpart. *C-D*: infrared sources without an X-ray counterpart: the triangles represent sources with excess and the stars sources without excess. *E-F*: X-ray sources without infrared counterpart.

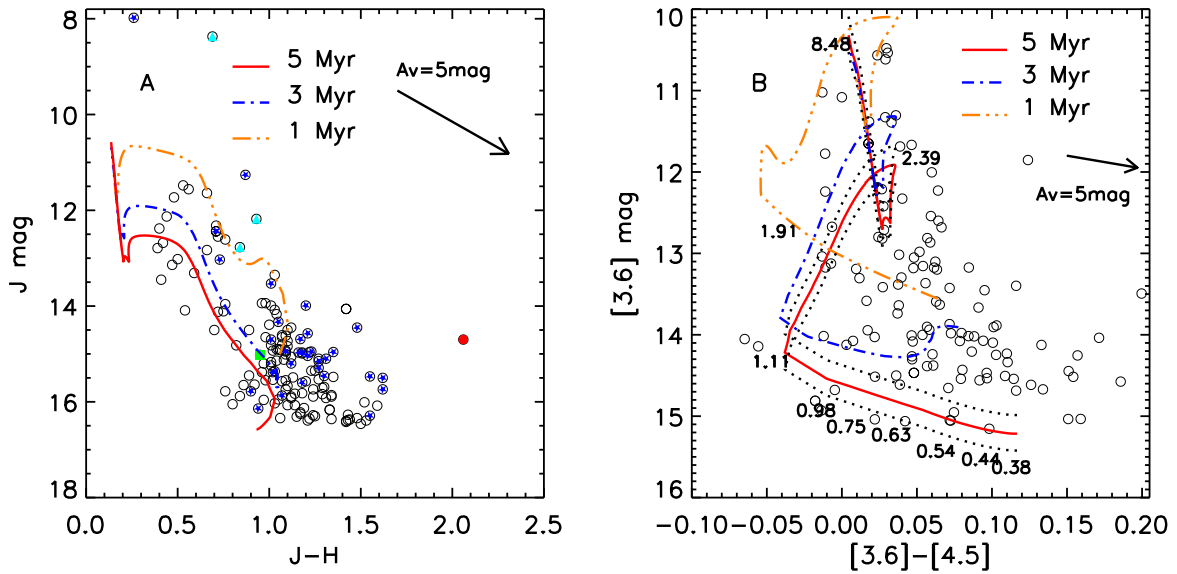


Fig. 6.— *A*: CMD of the cluster members using the 2MASS magnitudes. Overlaid are the 1 Myr, 3 Myr and 5 Myr isochrones (shifted at a distance of the cluster of 2 kpc and  $A_V = 2 \text{ mag}$ ). The different symbols and colors are like in Fig. 4. *B*: Close up of CMD in panel B in Fig. 4 around sources without infrared excess (empty circles) in the IRAC CMD (panel B in Fig. 4). Overlaid are the 1 Myr, 3 Myr and 5 Myr isochrones (shifted at a distance of the cluster of 2 kpc and  $A_V = 2 \text{ mag}$ ). The dotted lines represent the 5 Myr isochrones but shifted at a maximum and minimum distance of 2.2 and 1.8 kpc. The numbers along the 5 Myr isochrone represent the corresponding masses (in  $M_\odot$ ). The arrow in panels *A* and *B* represents an extinction  $A_V = 5 \text{ mag}$ .

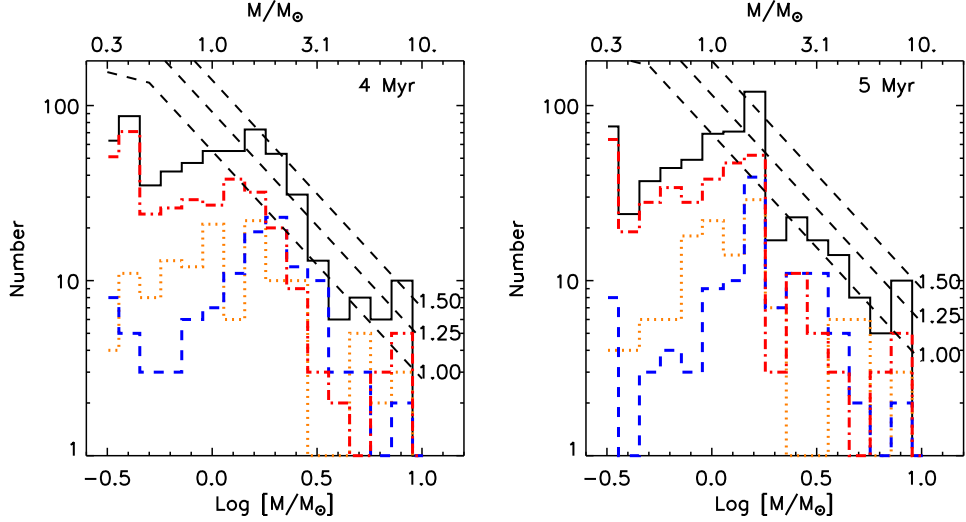


Fig. 7.— Mass function computed at [3.6]  $\mu\text{m}$  of the cluster members (infrared sources with X-ray counterpart) and candidates (infrared sources with excess without X-ray counterpart) using isochrones at 4 and 5 Myr. Overplotted are the galactic IMFs (Kroupa 2002) normalized at different completeness masses:  $1 M_{\odot}, 1.25 M_{\odot}, 1.5 M_{\odot}$ . The mass function at [3.6]  $\mu\text{m}$  of the different subgroups are overplotted in different line-styles and colors: the *red dashed-dotted* line represents the candidates members alone (i.e. Spitzer sources with excess); the *blue dashed* line represents the cluster members with excess (i.e. Spitzer sources with excess with X-ray counterpart); the *orange dotted* line represents the cluster members without excess.

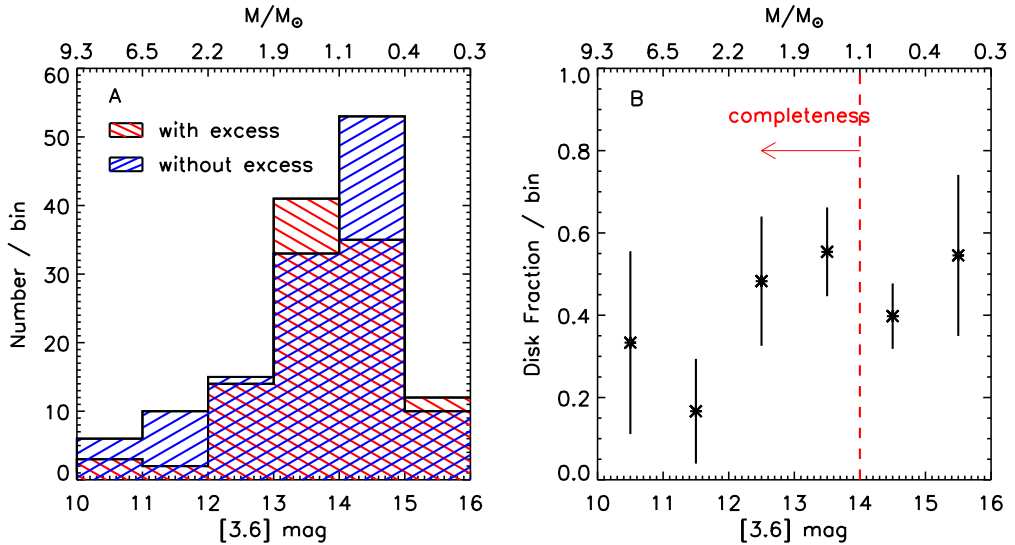


Fig. 8.— *A*: Histogram of cluster members (e.g. IRAC sources with an X ray counterpart) sources with excess (i.e. with  $[3.6]-[4.5]>0.2$ ) and without excess with a bin of 1 magnitude. *B*: Disk fraction computed as ratio of the sources with excess per [3.6] bin and the total number of sources per bin. The corresponding masses are computed using the 4 Myr isochrone.

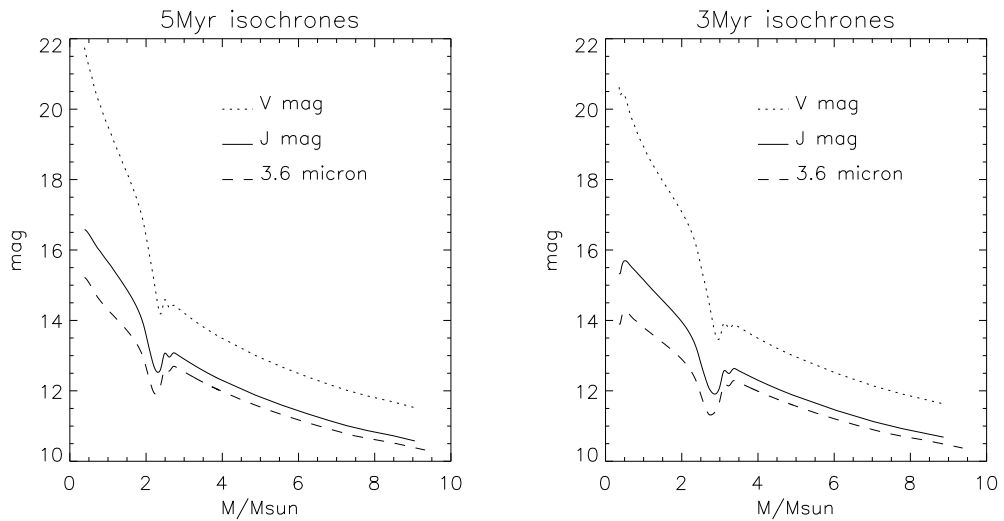


Fig. 9.— Relation between the V, J and  $3.6\mu\text{m}$  magnitudes and the stellar masses computed by the 5 Myr (left) and 3 Myr (right) isochrones.

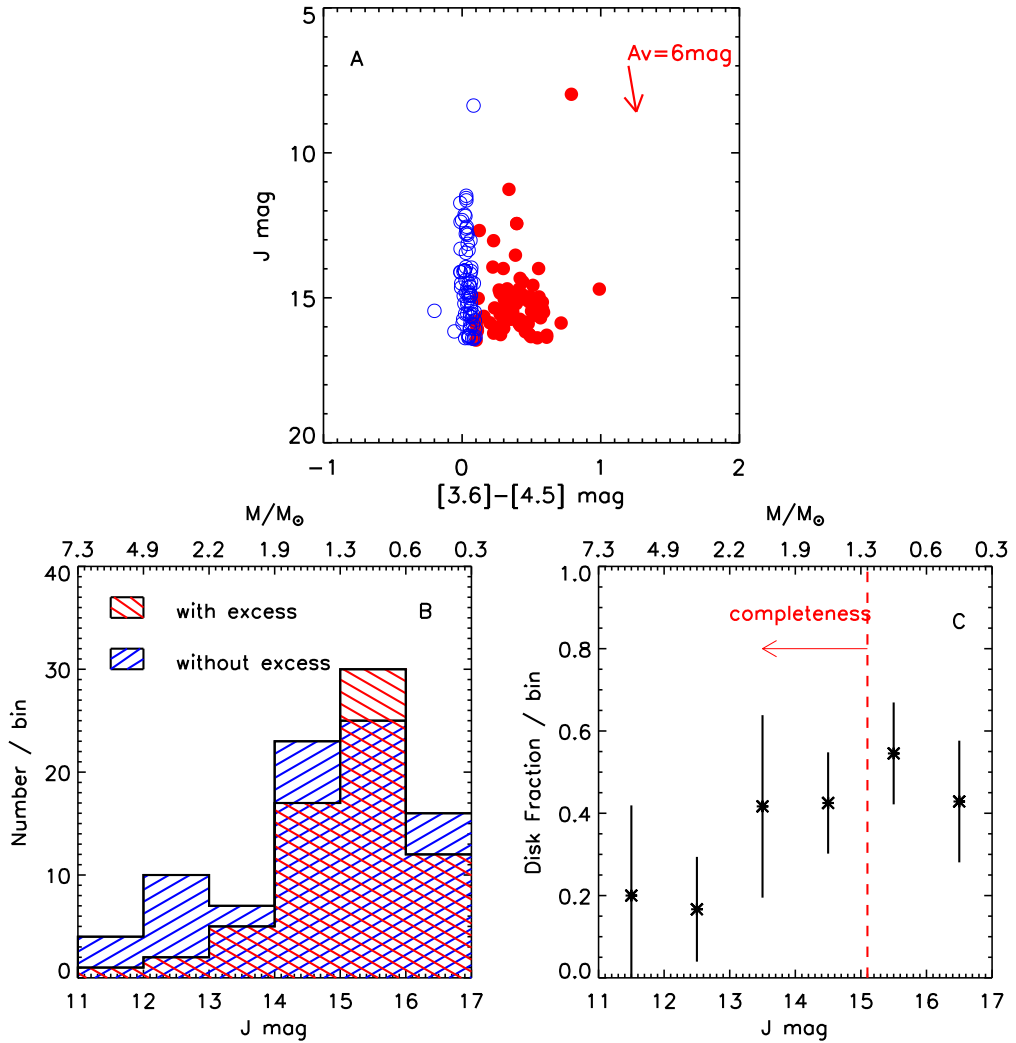


Fig. 10.— *A*:  $J - [3.6]-[4.5]$  CMD. The arrow represents an extinction  $A_V = 6$  mag. Filled circles represent sources with excess (i.e. with  $[3.6]-[4.5] > 0.2$ ), and empty circles represent sources without excess. *B*: Number of sources with and without excess per bin of  $J=1$  mag. *C*: Disk fraction computed as ratio of the sources with excess per  $J$  mag bin and the total number of sources per bin. The corresponding masses are computed using the 4 Myr isochrone.

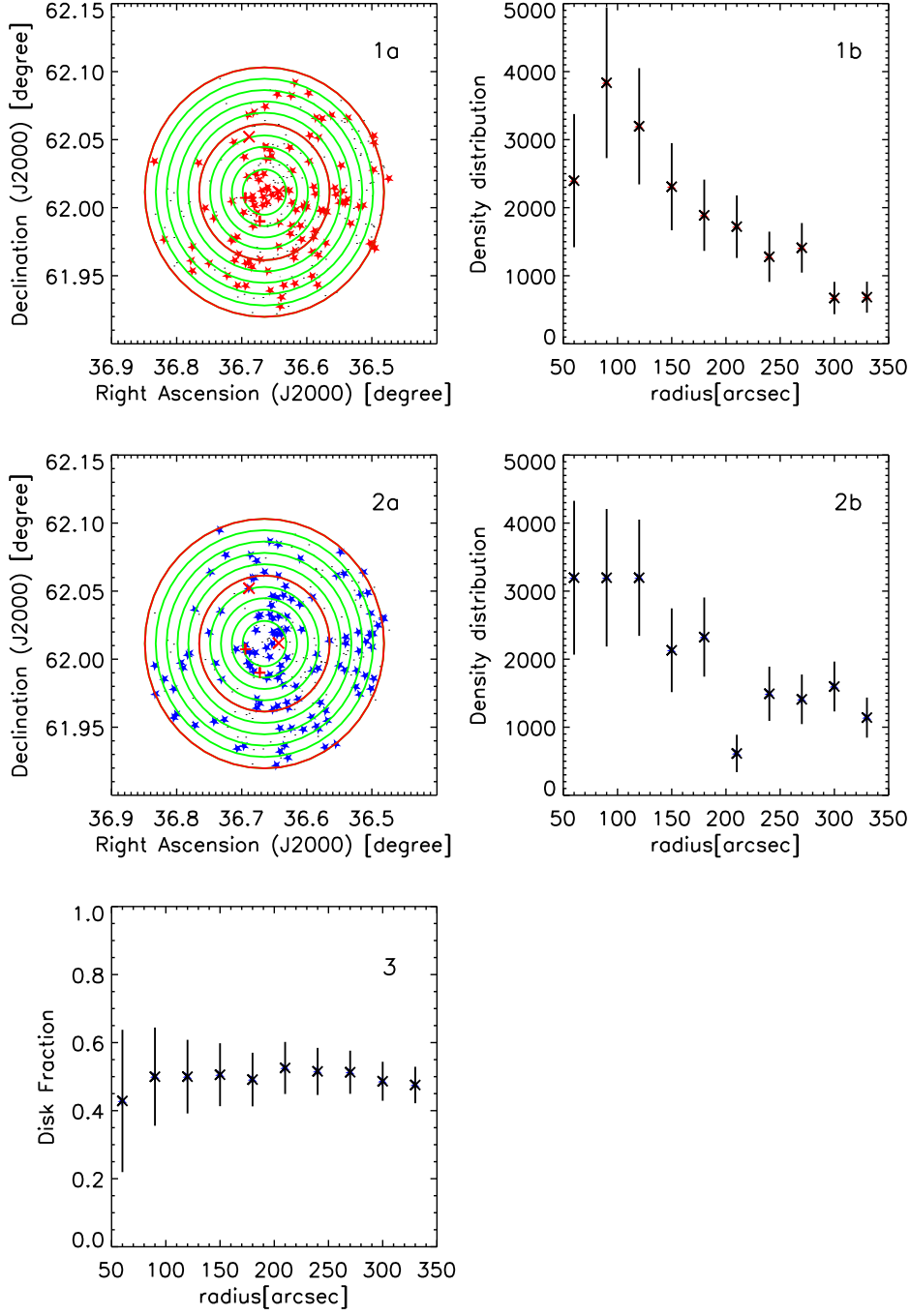


Fig. 11.— Spatial distribution (1a & 2a) and spatial density distribution (1b & 2b) of the sources with (1a & 1b) and without (2a & 2b) infrared excess. The excess has been selected with  $[3.6-4.5] > 0.2$  from the panel B of Fig. 4. The circle are as in Fig. 5. The 'x' and '+' symbols represent the positions of the O and B stars in the cluster. In panel 3 the disk fraction is computed as a function of the distance from the center of the cluster.

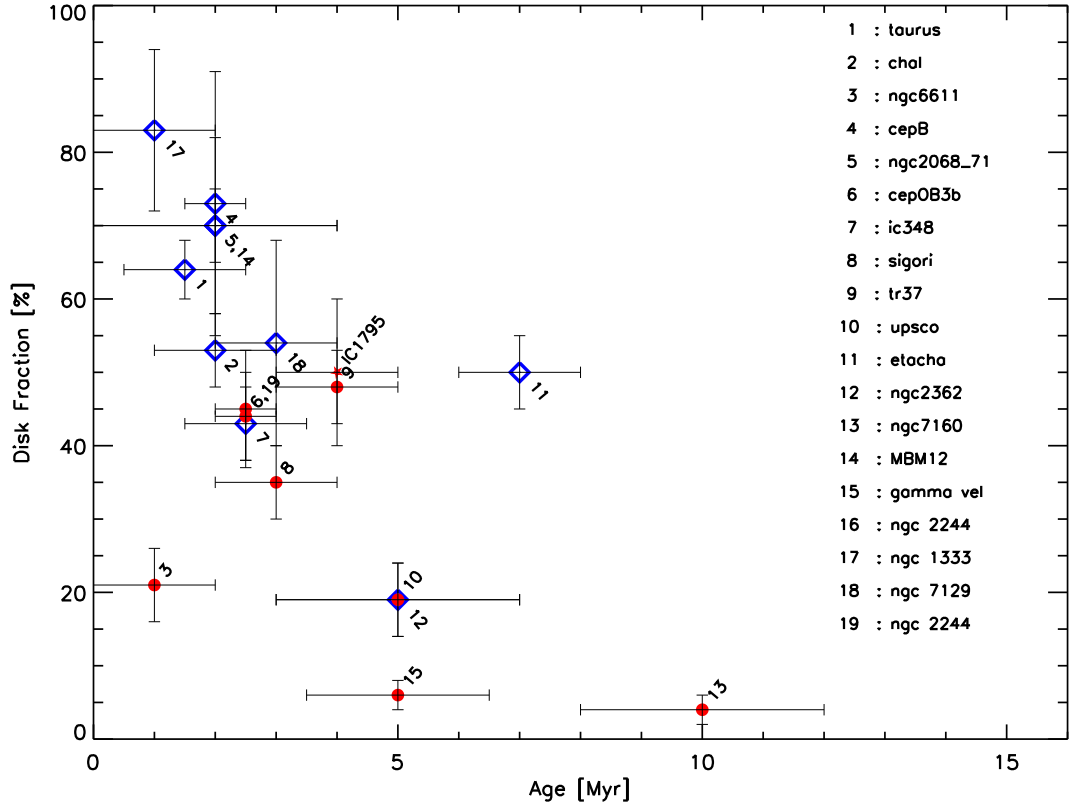


Fig. 12.— Disk fractions computed in the IRAC colors, as a function of the age of the cluster. The filled dots represent the OB associations, while the empty diamonds represent the low-mass star-forming regions.

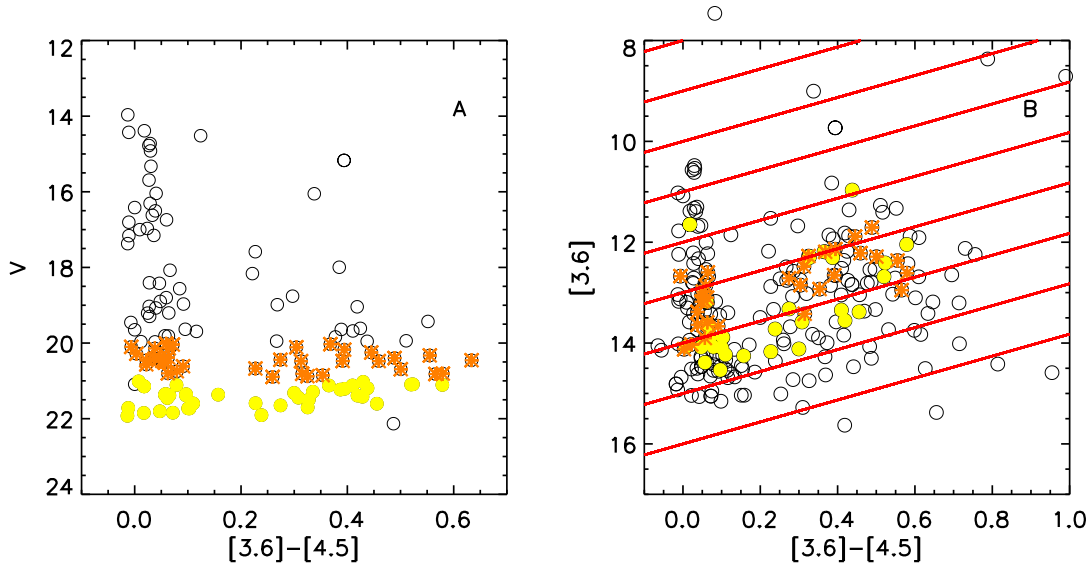


Fig. 13.— A:  $[[3.6]-[4.5], V]$  CMD. Highlighted with different symbols are the stars in 2 consecutive horizontal slices with  $V$  between 20 and 21 and with  $V$  between 21 and 22. B:  $[[3.6]-[4.5],[3.6]]$  CMD. Highlighted are the same sources as in panel A. The derived lines used to compute the disk fraction are overplotted.

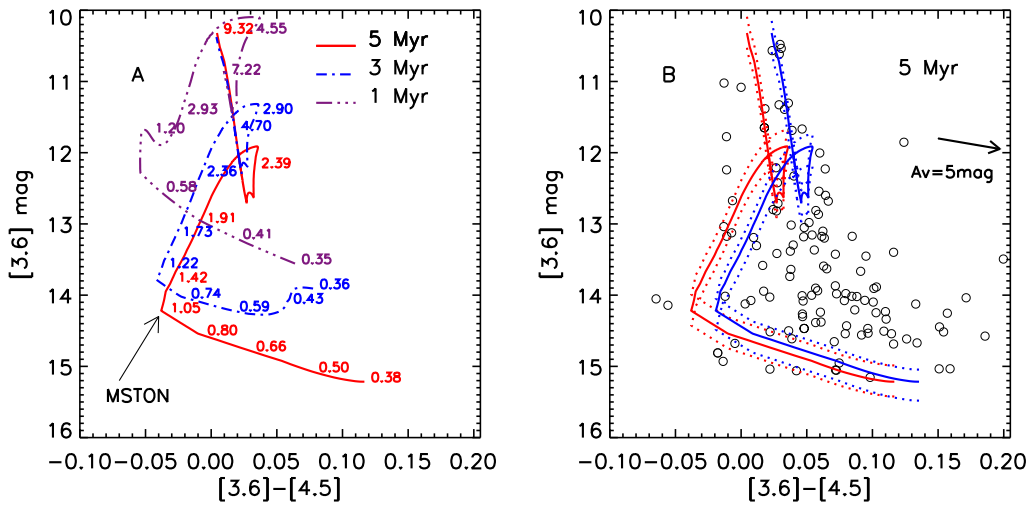


Fig. 14.— *A*: 1 Myr, 3 Myr and 5 Myr isochrones computed in the IRAC magnitudes, assuming a cluster distance of 2 kpc and  $A_V = 2$  mag. Overplotted are the position of the different masses over each isochrone. The arrow shows the position of the MSTON (Main Sequence Turn-On) for the 5 Myr isochrone. *B*: The circles represent the data (as in Fig. 6B) and overplotted is the 5 Myr isochrone reddened by  $A_V = 2$  mag and  $A_V = 4$  mag. The dotted lines represent the 5 Myr isochrones but shifted at a maximum and minimum distance of 2.2 and 1.8 kpc (as in Fig. 6B).

TABLE 1

TOTAL NUMBER OF *Spitzer* AND *Chandra* SOURCES DETECTED WITHIN 330 $''$  FROM THE CENTRE OF THE CLUSTER.

	Number of	sources
<i>Spitzer observations:</i>		
ch1	924	
ch2	845	
ch3	309	
ch4	248	
ch1+ch2	841	
with excess	367	
without excess	474	
ch1+ch2+ch3+ch4	145	
Class I	12	
Class I/II	57	
Class II	54	
Class III/phot	13	
not class.	9	
<i>Chandra + Spitzer obs.:</i>		
X-ray	413	
X-ray + IR <sup>a</sup>	277	
X-ray +ch1+ch2	244	
with excess	116	
without excess	128	
X-ray + ch1+ch2+ch3+ch4	54	
Class I	1	
Class I/II	6	
Class II	41	
Class III/phot	4	
not class.	2	
X-ray without IR	124	
IR without X-ray	665	
ch1+ch2 without X-ray	593	
with excess	248	
without excess	345	

<sup>a</sup>9 X-ray sources have multiple infrared counterparts and they were counted as a single source.

TABLE 2  
DISK FRACTION OF SOLAR TYPE STARS.

Cluster	Age [Myr]	Distance [pc]	Disk fraction SpT<K6	Disk fraction Total	Notes on the completeness	Ref. disk fraction
NGC 1333	1±1	280	...	83%±11% (87/72)	>0.08 M <sub>⊙</sub>	Gutermuth et al. (2008)
Taurus	1.5±1.5	140	80%±15% (33/41)	64%±5% (226/352)	K0 - M8	Luhman et al. (2010)
Cep B(embedded)	1.5±0.5	725	80%±25% (12/15)	73%±18% (22/30)	>0.5 M <sub>⊙</sub>	Getman et al. (2009)
NGC 6611 <sup>b</sup>	1±1	1750	...	21%±5% <sup>c</sup>	0.3-3 M <sub>⊙</sub>	Guarcello et al. (2007, 2009)
Cha I	2±1	165	74%±12% (14/19)	53%±7% (107/202)	K0 - M8	Luhman et al. (2008)
NGC 2068/71	2±1.5	400	...	79%±12% (54/69)	G6 - M6	Flaherty & Muzerolle (2008)
NGC 7129	2±1	1000	...	54%±14% (27/50)	>0.08 M <sub>⊙</sub>	Gutermuth et al. (2004)
MBM 12	2±2	275	...	70%±12% (7/12)	K3 - M5	Meeus et al. (2009)
IC 348	2.5±1	320	20%±8% (7/35)	43%±6% (128/294)	K0 - M8	Luhman et al. (2010)
Cep OB3b <sup>a</sup>	2.5±0.5	725	42%±14% (21/50)	45%±8% (63/140)	>0.5 M <sub>⊙</sub>	Getman et al. (2009)
NGC 2244 <sup>b</sup>	2.5±0.5	1500	...	44%±6% (164/374)	Not defined	Balog et al. (2007)
σ Ori <sup>a</sup>	3±1	350	...	35%±5% (117/336)	K4 - M5	Hernández et al. (2007)
NGC 7129	3±1	1000	...	54%±14% (27/50)	>0.2 M <sub>⊙</sub>	Gutermuth et al. (2004)
Tr 37 <sup>a</sup>	4±1	900	67%±% (33/49)	48% (62/129)	K0 - M2	Sicilia-Aguilar et al. (2006)
Upper Sco <sup>a</sup>	5±1	145	...	19%±5% (24/127)	K0 - M4	Carpenter et al. (2006)
NGC 2362	5±1	1480	...	19%±5% (38/195)	K1 - M4	Dahm & Hillenbrand (2007)
γ Vel <sup>a</sup>	5±1.5	350	...	6%±2% (29/579)	K5	Hernández et al. (2008)
η Cha	7±1	97	...	50%±5% (8/15)	K4 - M4	Sicilia-Aguilar et al. (2009)
NGC 7160 <sup>a</sup>	10±2	900	...	4%±2% (2/55)	K0 - M1	Sicilia-Aguilar et al. (2006)

<sup>a</sup>High mass cluster hosting 1/2 OB stars.

<sup>b</sup>High mass cluster hosting >5 OB stars.

<sup>c</sup>see section 6.3 for the disk fraction

TABLE 3  
SPITZER/IRAC SOURCES WITH CHANDRA COUNTERPARTS.

ID IRAC-	RA <sub>J2000</sub> [deg]	RA error $10^{-4}$ [deg]	DEC <sub>J2000</sub> [deg]	DEC error $10^{-4}$ [deg]	Infrared excess	Disk classification
02255380+6201164	36.474186	1.13	62.021217	1.17	✓	
02255585+6201477	36.482689	2.54	62.029911	2.38	-	
02255585+6201477	36.482689	2.54	62.029911	2.38	-	
02255717+6159399 <sup>a</sup>	36.488209	4.14	61.994419	4.24	✓	
02255780+6201287	36.490833	2.72	62.024651	2.44	~	
02255891+6158121	36.495461	0.48	61.970020	0.50	✓	ClassII
02255931+6202527	36.497120	1.88	62.047962	1.84	✓	
02255900+6203133	36.495831	4.03	62.053684	4.17	✓	
02255940+6159089	36.497513	1.54	61.985809	1.62	-	
02255945+6201413	36.497692	1.00	62.028152	1.03	✓	
02255960+6159159 <sup>a</sup>	36.498352	4.76	61.987751	4.92	✓	
02255940+6201087	36.497509	0.88	62.019093	0.99	-	
02255971+6158221	36.498806	0.27	61.972805	0.26	✓	Class I
02255988+6200312	36.499516	1.76	62.008663	1.96	~	
02255991+6159175 <sup>a</sup>	36.499619	4.54	61.988201	4.93	✓	
02260077+6201047	36.503204	3.00	62.017971	3.35	-	
02260021+6158427	36.500893	3.94	61.978523	3.55	~	
02260047+6202012	36.501976	2.39	62.033657	2.45	-	
02260057+6158256	36.502361	0.64	61.973778	0.63	✓	
02260077+6201047	36.503204	3.00	62.017971	3.35	-	
02260153+6202546	36.506386	0.49	62.048496	0.61	~	
02260186+6202185 <sup>a</sup>	36.507736	2.46	62.038483	2.64	✓	
02260207+6200478	36.508621	2.13	62.013279	2.34	-	
02260242+6159163	36.510101	2.24	61.987873	2.22	-	
02260312+6203492	36.512981	2.74	62.063671	3.01	~	ClassI,II
02260301+6200057	36.512524	1.84	62.001591	1.93	✓	
02260419+6202228 <sup>a</sup>	36.517479	2.23	62.039669	2.53	✓	
02260415+6202510	36.517303	1.50	62.047504	1.55	-	
02260463+6202152	36.519287	3.30	62.037567	3.39	✓	
02260452+6158267	36.518814	0.36	61.974087	0.37	-	phot. or ClassIII
02260466+6200027	36.519428	0.94	62.000759	0.99	✓	
02260469+6200216	36.519550	1.57	62.006008	1.55	~	
02260527+6201098	36.521946	2.70	62.019398	2.79	~	
02260410+6203266 <sup>a</sup>	36.517082	6.88	62.057377	5.38	✓	
02260556+6159299	36.523186	1.15	61.991642	1.16	-	
02260544+6158244 <sup>b</sup>	36.522663	0.96	61.973446	0.99	not	defined
02260587+6158465	36.524475	0.34	61.979580	0.34	-	
02260590+6202276	36.524574	7.70	62.040997	7.71	✓	
02260676+6203019	36.528187	9.55	62.050526	9.04	✓	
02260683+6159578	36.528469	1.37	61.999382	1.32	✓	
02260745+6203265 <sup>a</sup>	36.531025	5.58	62.057350	5.60	✓	
02260787+6159179	36.532776	0.60	61.988308	0.60	✓	ClassII
02260849+6203544	36.535381	4.76	62.065098	4.93	✓	ClassI,II
02260906+6202019	36.537758	1.69	62.006084	1.81	✓	
02260959+6200581	36.539974	0.51	62.016132	0.54	-	
02260960+6200414	36.540001	1.06	62.011494	1.02	-	
02260967+6200119	36.540306	0.80	62.003311	0.83	✓	ClassII
02261003+6159302	36.541798	2.66	61.991711	2.98	-	
02261007+6203454	36.541939	2.53	62.062611	2.63	-	
02261031+6200137	36.542953	8.10	62.003792	8.94	✓	
02261100+6200453	36.545849	1.34	62.012577	1.36	✓	ClassII
02261198+6203558	36.549911	8.38	62.065514	8.09	✓	
02261128+6201513	36.546993	1.49	62.030914	1.59	✓	
02261153+6204432	36.548027	2.31	62.078663	2.46	~	
02261196+6200129	36.549847	0.58	62.003578	0.58	✓	ClassII
02261207+6159439	36.550289	1.29	61.995518	1.25	~	
02261296+6203414	36.553982	1.82	62.061489	1.86	-	
02261320+6200346	36.554993	0.71	62.009617	0.73	✓	

TABLE 3—Continued

ID IRAC-	RA <sub>J2000</sub> [deg]	RA error $10^{-4}$ [deg]	DEC <sub>J2000</sub> [deg]	DEC error $10^{-4}$ [deg]	Infrared excess	Disk classification
02261320+6156152	36.554985	2.51	61.937565	2.64	-	
02261391+6200532	36.557976	0.45	62.014771	0.46	✓	ClassII
02261491+6204046	36.562115	1.08	62.067936	1.19	✓	
02261565+6200482	36.565212	1.39	62.013386	1.42	-	
02261645+6157174	36.568535	1.17	61.954838	1.18	-	
02261671+6159485 <sup>d</sup>	36.569630	0.55	61.996803	0.56	✓	ClassII
02261699+6158262	36.570793	0.74	61.973946	0.73	✓	
02261717+6157438	36.571529	2.47	61.962166	2.88	-	
02261727+6156069	36.571945	0.68	61.935253	0.71	-	
02261739+6159512	36.572475	0.86	61.997562	0.88	✓	
02261769+6202141	36.573708	5.24	62.037254	5.40	✓	
02261849+6203556 <sup>d</sup>	36.577049	0.76	62.065437	0.78	✓	
02261881+6159528	36.578392	0.20	61.998013	0.21	✓	ClassII
02261765+6203431 <sup>a</sup>	36.573559	7.33	62.061977	7.98	✓	
02261881+6159528	36.578392	0.20	61.998013	0.21	✓	ClassII
02261888+6158048	36.578659	1.82	61.968006	2.03	-	
02261959+6203058	36.581619	0.58	62.051609	0.60	✓	ClassII
02261970+6156554	36.582077	1.78	61.948715	1.93	-	
02261967+6157541	36.581944	1.98	61.965038	1.79	✓	
02261990+6159357	36.582928	1.10	61.993240	1.14	~	
02262010+6156358	36.583740	1.28	61.943279	1.35	✓	
02262029+6200119	36.584538	0.80	62.003304	0.83	-	
02262044+6157024	36.585178	0.91	61.950657	0.93	-	
02262048+6203521	36.585316	7.86	62.064484	8.74	✓	
02262048+6203521	36.585316	7.86	62.064484	8.74	✓	
02262082+6200365	36.586731	0.63	62.010132	0.63	✓	ClassII
02262048+6203521	36.585316	7.86	62.064484	8.74	✓	
02262112+6158582	36.587986	0.47	61.982826	0.47	✓	ClassII
02262148+6158419	36.589508	0.45	61.978298	0.47	✓	ClassII
02262140+6200551	36.589153	2.18	62.015308	2.31	✓	
02262132+6204362 <sup>a</sup>	36.588825	2.09	62.076733	2.08	✓	
02262191+6202438	36.591286	1.51	62.045509	1.58	-	
02262195+6158031	36.591454	0.68	61.967529	0.67	✓	
02262199+6159297	36.591637	1.87	61.9911596	1.91	-	
02262219+6156592	36.592449	2.76	61.949768	2.36	✓	
02262231+6157267	36.592960	1.57	61.957405	1.62	-	
02262227+6202403 <sup>a</sup>	36.592781	1.80	62.044525	1.68	✓	
02262273+6203109	36.594688	0.71	62.053017	0.77	✓	ClassII
02262318+6202023	36.596569	2.02	62.033985	1.99	✓	
02262328+6205020	36.597015	0.67	62.083889	0.71	✓	
02262411+6200012	36.600445	0.57	62.000320	0.57	✓	ClassII
02262440+6200090	36.601673	2.95	62.002487	2.92	✓	
02262447+6159106 <sup>a</sup>	36.601963	1.76	61.986271	1.80	✓	
02262488+6159265	36.603672	1.14	61.990704	1.26	✓	
02262527+6156538	36.605293	2.31	61.948265	2.37	~	
02262536+6200034	36.605682	0.49	62.000954	0.49	✓	ClassII
02262586+6201186	36.607735	3.72	62.021832	4.28	-	
02262587+6158354	36.607773	0.78	61.976490	0.76	✓	
02262637+6159124	36.609894	0.62	61.986782	0.79	✓	
02262646+6202241	36.610245	1.13	62.040028	1.19	-	
02262649+6204256	36.610363	2.30	62.073792	2.43	~	
02262724+6158142	36.613483	0.42	61.970612	0.44	-	photosphere or ClassIII
02262794+6159538	36.616409	0.70	61.998287	0.71	✓	
02262802+6158482	36.616756	1.46	61.980049	1.43	-	
02262817+6158218 <sup>a</sup>	36.617367	1.06	61.972721	1.10	✓	
02262836+6205306	36.618172	1.13	62.091839	1.15	✓	
02262839+6156388	36.618271	1.17	61.944122	1.18	✓	
02262860+6158055	36.619156	0.45	61.968185	0.45	✓	ClassII

TABLE 3—Continued

ID IRAC-	RA <sub>J2000</sub> [deg]	RA error $10^{-4}$ [deg]	DEC <sub>J2000</sub> [deg]	DEC error $10^{-4}$ [deg]	Infrared excess	Disk classification
02262879+6157481	36.619976	1.00	61.963371	1.01	✓	
02262938+6200135 <sup>a</sup>	36.622417	1.23	62.003757	1.26	✓	
02262940+6201375	36.622494	0.76	62.027077	0.79	✓	
02262962+6159126	36.623405	0.46	61.986824	0.47	✓	ClassII
02262966+6156575	36.623592	2.98	61.949306	3.08	-	
02262969+6202382	36.623714	2.30	62.043957	2.17	-	
02262966+6204566	36.623600	1.32	62.082382	1.40	✓	
02262989+6201223 <sup>a</sup>	36.624561	3.42	62.022858	3.56	✓	
02263007+6158506	36.625282	0.77	61.980713	0.85	✓	
02263023+6202383	36.625965	2.52	62.043983	2.48	✓	
02263046+6200453	36.626926	0.80	62.012596	0.85	✓	
02263091+6157504	36.628803	1.56	61.963989	1.62	-	
02263094+6155383	36.628910	2.71	61.927319	2.85	-	
02263131+6200037	36.630466	0.74	62.001019	0.74	-	
02263135+6158054	36.630630	1.80	61.968163	1.85	-	
02263140+6201527	36.630852	1.87	62.031300	1.83	-	
02263150+6201191	36.631229	2.60	62.021965	2.67	-	
02263167+6200439	36.631962	2.00	62.012192	2.11	✓	
02263184+6203125	36.632648	2.62	62.053486	2.93	~	ClassII
02263206+6156121	36.633568	0.64	61.936691	0.64	✓	
02263248+6156347	36.635338	0.56	61.942982	0.56	✓	
02263240+6202523	36.634998	2.21	62.047848	2.28	-	
02263230+6158525	36.634563	2.58	61.981243	2.35	~	ClassII
02263287+6201220	36.636955	1.63	62.022789	1.65	✓	
02263323+6201062	36.638443	1.11	62.018394	1.17	-	
02263332+6156030	36.638844	0.49	61.934166	0.59	✓	ClassII
02263328+6156045 <sup>b</sup>	36.638683	1.18	61.934570	1.30	not	
02263343+6159250	36.639301	1.48	61.990269	1.45	-	
02263362+6159431	36.640087	1.73	61.995312	1.73	-	
02263371+6155387	36.640465	0.91	61.927418	0.97	✓	
02263386+6155555	36.641064	0.87	61.932095	0.85	-	
02263394+6156573	36.641430	0.68	61.949242	0.66	-	
02263415+6201192 <sup>d</sup>	36.642292	0.39	62.022011	0.42	-	
02263422+6159201	36.642582	0.58	61.988918	0.60	✓	
02263431+6200252	36.642952	1.05	62.006989	1.12	✓	
02263433+6201527	36.643028	0.57	62.031307	0.59	-	
02263443+6200419 <sup>e</sup>	36.643478	0.40	62.011650	0.55	✓	ClassII
02263441+6205037	36.643356	2.74	62.084373	2.79	-	
02263455+6158169	36.643944	0.45	61.971359	0.45	✓	ClassII
02263455+6203404	36.643944	2.09	62.061234	2.01	~	
02263463+6159107 <sup>d</sup>	36.644291	0.46	61.986301	0.47	-	
02263480+6201053	36.645012	0.80	62.018150	0.85	-	
02263530+6204558	36.647102	7.39	62.082172	7.58	✓	
02263489+6157559 <sup>d</sup>	36.645367	0.53	61.965519	0.54	-	
02263495+6202427	36.645634	1.59	62.045185	1.71	~	
02263541+6155197	36.647522	2.93	61.922138	2.52	-	
02263585+6201062	36.649387	1.18	62.018379	1.22	-	
02263646+6201120	36.651913	0.39	62.020000	0.41	-	
02263648+6157462	36.651993	0.98	61.962841	1.00	-	
02263658+6201471	36.652416	1.34	62.029751	1.44	-	
02263667+6200416	36.652798	0.44	62.011562	0.45	-	
02263670+6202470	36.652905	0.47	62.046394	0.46	-	
02263693+6200345	36.653885	0.80	62.009590	0.83	✓	
02263709+6202222	36.654526	2.27	62.039505	2.30	-	
02263713+6202147	36.654709	1.14	62.037426	1.16	✓	
02263743+6202322	36.655949	0.84	62.042286	0.89	✓	
02263750+6156207	36.656258	0.76	61.939095	0.83	✓	ClassII
02263755+6201557	36.656471	1.53	62.032146	1.63	-	

TABLE 3—Continued

ID IRAC-	RA <sub>J2000</sub> [deg]	RA error $10^{-4}$ [deg]	DEC <sub>J2000</sub> [deg]	DEC error $10^{-4}$ [deg]	Infrared excess	Disk classification
02263768+6159187	36.656998	0.93	61.988541	0.91	-	
02263768+6200054	36.657005	0.83	62.001492	0.92	-	
02263755+6205115	36.656475	1.46	62.086525	1.55	~	
02263928+6201034 <sup>b</sup>	36.663658	9.63	62.017616	9.50	not	defined
02263847+6157126	36.660275	3.05	61.953499	2.79	✓	
02263851+6200490	36.660465	0.53	62.013611	0.54	✓	
02263862+6200142	36.660904	0.83	62.003944	0.88	✓	
02263865+6200533	36.661022	0.48	62.014793	0.52	✓	ClassII
02263865+6159135	36.661049	2.37	61.987080	2.61	✓	
02263868+6159094	36.661156	1.06	61.985931	1.10	-	
02263885+6200303	36.661873	0.52	62.008419	0.50	-	
02263882+6202112	36.661732	0.84	62.036434	0.86	✓	
02263954+6202400 <sup>b</sup>	36.664753	3.18	62.044449	3.40	✓	ClassII
02263958+6204263	36.664906	4.40	62.073975	4.71	✓	
02263953+6202401	36.664722	0.80	62.044468	0.81	✓	
02263962+6203506	36.665073	0.90	62.064049	0.97	~	ClassI <sub>II</sub>
02263987+6201292	36.666126	1.22	62.024773	1.25	✓	
02263999+6200279	36.666618	0.52	62.007748	0.51	✓	ClassII
02264011+6200068	36.667145	0.72	62.001896	0.70	✓	ClassI <sub>II</sub>
02263983+6156038 <sup>a</sup>	36.665943	6.51	61.934395	6.27	✓	
02264061+6200448	36.669224	1.25	62.012436	1.27	✓	
02264113+6157424	36.671383	0.94	61.961773	0.93	✓	
02264126+6201566 <sup>d</sup>	36.671932	0.63	62.032402	0.66	-	
02264140+6158026	36.672482	1.08	61.967381	1.04	-	
02264157+6201129	36.673222	0.61	62.020248	0.64	✓	
02264193+6201516	36.674725	0.90	62.031013	0.96	-	
02264238+6159456	36.676575	1.14	61.995995	1.29	✓	
02264247+6157511	36.676975	2.19	61.964203	2.19	-	
02264279+6204237	36.678291	3.30	62.073254	3.36	~	
02264240+6158162	36.676651	2.14	61.971180	1.95	-	
02264279+6201156	36.678280	2.13	62.020992	2.17	-	
02264290+6201282 <sup>d</sup>	36.678761	0.43	62.024494	0.46	✓	ClassII
02264297+6200166	36.679024	0.94	62.004616	1.00	-	
02264334+6200044	36.680576	0.64	62.001228	0.59	✓	
02264342+6203347	36.680908	0.99	62.059635	0.98	-	
02264353+6159270	36.681362	1.05	61.990829	1.20	-	
02264359+6204115	36.681625	0.79	62.069874	0.83	✓	ClassII
02264438+6155548 <sup>a</sup>	36.684906	8.17	61.931881	8.42	✓	
02264376+6159113	36.682331	0.67	61.986485	0.75	✓	
02264391+6200191	36.682941	1.05	62.005299	1.05	✓	
02264413+6200305	36.683865	0.50	62.008461	0.49	✓	ClassII
02264423+6203348	36.684284	0.95	62.059669	1.00	-	
02264425+6155223 <sup>a</sup>	36.684391	2.92	61.922852	2.83	✓	
02264421+6157229	36.684216	0.89	61.956352	0.91	✓	ClassII
02264480+6159395	36.686676	1.69	61.994293	1.95	-	
02264490+6204378	36.687080	3.92	62.077160	3.64	~	ClassI <sub>II</sub>
02264497+6200170	36.687363	0.79	62.004730	0.81	-	
02264527+6203075	36.688641	0.69	62.052090	0.60	-	photosphere or ClassIII
02264562+6157382	36.690098	2.44	61.960613	2.76	✓	
02264571+6159505	36.690472	0.55	61.997360	0.60	-	
02264592+6204019	36.691319	1.95	62.067184	1.97	✓	ClassI <sub>II</sub>
02264606+6201220 <sup>b</sup>	36.691906	2.27	62.022778	2.40	✓	ClassII
02264607+6157332	36.691956	1.99	61.959213	2.01	✓	
02264649+6200196 <sup>d</sup>	36.693714	0.97	62.005455	1.00	-	
02264651+6156331	36.693771	1.27	61.942516	1.36	✓	
02264674+6200367	36.694752	0.89	62.010181	0.96	-	
02264702+6202144	36.695930	0.79	62.037327	0.83	✓	ClassII
02264720+6156102	36.696674	2.43	61.936153	2.61	~	

TABLE 3—Continued

ID IRAC-	RA <sub>J2000</sub> [deg]	RA error $10^{-4}$ [deg]	DEC <sub>J2000</sub> [deg]	DEC error $10^{-4}$ [deg]	Infrared excess	Disk classification
02264736+6159478 <sup>d</sup>	36.697319	0.81	61.996601	0.91	✓	
02264898+6157567	36.704075	1.01	61.965763	1.03	✓	ClassII
02264970+6156338	36.707085	1.15	61.942734	1.29	✓	
02264963+6156035	36.706783	1.06	61.934315	1.07	-	
02264974+6158419	36.707260	1.42	61.978306	1.43	✓	
02265007+6200263	36.708637	0.71	62.007298	0.74	-	
02265061+6157404	36.710880	0.71	61.961216	0.77	✓	ClassII
02265084+6202534	36.711823	0.57	62.048153	0.59	✓	ClassII
02265100+6158384	36.712509	0.70	61.977337	0.72	✓	ClassII
02265167+6200166	36.715282	1.68	62.004604	1.62	✓	
02265171+6158335	36.715439	0.74	61.975979	0.78	✓	ClassII
02265339+6157007	36.722443	0.58	61.950188	0.58	✓	ClassII
02265387+6204355	36.724449	0.90	62.076534	0.91	-	
02265444+6157204	36.726822	1.16	61.955658	1.18	-	
02265534+6159075	36.730579	0.53	61.985413	0.56	-	
02265574+6202069	36.732258	1.31	62.035236	1.38	-	
02265607+6205409	36.733643	0.85	62.094688	0.86	-	
02265761+6159490	36.740036	1.99	61.996937	2.08	~	
02265809+6157155	36.742058	3.01	61.954308	2.72	~	
02265816+6159319	36.742332	0.59	61.992203	0.61	✓	
02265948+6203506	36.747852	1.78	62.064056	1.81	-	
02270002+6201106	36.750099	1.63	62.019604	1.83	-	
02270024+6157320	36.751011	2.75	61.958893	2.40	✓	
02270155+6159589	36.756439	0.81	61.999706	0.85	✓	
02270392+6201588	36.766327	0.68	62.032990	0.69	✓	
02270523+6157048	36.771774	1.19	61.951324	1.22	-	
02270536+6202109	36.772339	2.41	62.036358	2.47	-	
02270613+6158166	36.775528	0.62	61.971279	0.62	✓	ClassII
02270616+6157127	36.775681	2.07	61.953529	2.00	✓	
02270608+6157387	36.775322	3.38	61.960743	3.22	✓	
02270756+6200131	36.781513	0.74	62.003643	0.73	-	
02270756+6200131	36.781513	0.74	62.003643	0.73	-	
02270964+6159369	36.790161	3.11	61.993595	2.95	-	
02271047+6159501	36.793606	1.77	61.997246	1.83	-	
02271197+6157347	36.799881	3.91	61.959637	3.72	-	
02271295+6157250	36.803951	2.89	61.956944	2.67	-	
02271296+6158407	36.803982	2.08	61.977985	1.97	-	
02271410+6200456	36.808746	6.27	62.012680	6.23	✓	
02271452+6200193	36.810486	8.57	62.005371	9.03	✓	
02271660+6200520	36.819168	9.19	62.014439	9.46	✓	
02271627+6159086	36.817772	2.68	61.985733	2.82	~	
02271656+6158358	36.818981	1.67	61.976612	1.73	✓	
02271981+6158281	36.832546	1.74	61.974464	1.75	-	
02271999+6159435	36.833271	1.75	61.995407	1.65	-	
02272024+6202025	36.834324	0.26	62.034016	0.28	✓	ClassII

NOTE.—Notation for the Infrared Excess: ‘✓’=[3.6]-[4.5]>0.2mag; ‘-’=[3.6]-[4.5]<0.1mag; ‘~’=0.1<[3.6]-[4.5]<0.2mag.

<sup>a</sup>Source position in IRAC/channel 2.

<sup>b</sup>Source position in IRAC/channel 3.

<sup>c</sup>The counterparts at different wavelengths were found using a different matching procedure.

<sup>d</sup>IRAC source with 2 X-ray counterparts ('X binary').

<sup>e</sup>IRAC source with 3 X-ray counterparts.

TABLE 4  
OPTICAL, NEAR-INFRARED AND IRAC/SPITZER FLUXES OF THE IRAC/SPITZER SOURCES WITH X-RAY COUNTERPART.

ID IRAC-	$F_V$ [mJy]	$F_I$ [mJy]	$F_J$ [mJy]	$F_H$ [mJy]	$F_K$ [mJy]	$F_{3.6\mu m}$ [mJy]	$F_{4.5\mu m}$ [mJy]	$F_{5.8\mu m}$ [mJy]	$F_{8.0\mu m}$ [mJy]
02255380+6201164	....	....	....	....	....	1.3026± 0.0073	1.3182± 0.0088	....	....
02255585+6201477	....	....	....	....	....	0.4586± 0.0048	0.3066± 0.0055	....	....
02255585+6201477	....	....	....	....	....	0.4586± 0.0048	0.3066± 0.0055	....	....
02255717+6159399	0.0073	0.0707	....	....	....	0.1901± 0.0033	....	....	....
02255780+6201287	....	....	....	....	....	0.4427± 0.0048	0.3130± 0.0054	....	....
02255891+6158121	0.0616	0.7341	4.0410	7.8397	8.2401	8.2684± 0.0247	8.7915± 0.0271	9.0294± 0.2101	9.3836± 0.0890
02255931+6202527	....	....	....	....	....	0.7768± 0.0065	0.6863± 0.0088	2.1174± 0.0455	....
02255900+6203133	....	....	....	....	....	0.4109± 0.0073	0.6331± 0.0088	....	....
02255940+6159089	0.0582	0.4375	1.0532	1.5357	1.1693	0.7298± 0.0054	0.3884± 0.0039	1.7319± 0.0251	2.0907± 0.0523
02255945+6201413	....	....	....	....	....	2.3144± 0.0117	2.4546± 0.0133	2.5519± 0.0399	....
02255960+6159159	....	....	....	....	....	....	0.1395± 0.0030	1.7319± 0.0251	2.0907± 0.0523
02255940+6201087	0.2143	1.3407	4.1542	5.3740	4.5283	2.3800± 0.0116	1.6186± 0.0094	....	....
02255971+6158221	....	....	2.1013	9.0012	31.3278	92.1254± 0.2143	146.6403± 0.3530	239.5303± 0.5788	289.0532± 0.8720
02255988+6200312	0.0074	0.1328	0.6831	1.2311	1.1167	0.6453± 0.0055	0.4529± 0.0049	....	....
02255991+6159175	....	....	....	....	....	....	0.1447± 0.0028	....	2.0907± 0.0523
02260077+6201047	....	....	....	....	....	0.3343± 0.0049	0.2104± 0.0046	....	....
02260021+6158427	....	....	....	....	....	0.2721± 0.0039	0.2000± 0.0039	....	....
02260047+6202012	0.0131	0.1769	0.9430	1.8294	1.6290	0.6576± 0.0071	0.4523± 0.0074	....	....
02260057+6158256	0.0099	0.1442	....	....	....	5.0000± 0.0175	4.7460± 0.0179	....	13.1657± 0.1163
02260077+6201047	....	....	....	....	....	0.3343± 0.0049	0.2104± 0.0046	....	....
02260153+6202546	5.6794	10.7285	13.5048	12.7732	10.0909	5.0970± 0.0159	3.6551± 0.0160	2.3376± 0.0394	....
02260186+6202185	....	....	....	....	....	....	0.8064± 0.0091	2.3934± 0.0281	4.7682± 0.1050
02260207+6200478	0.0102	0.0959	....	....	....	0.4585± 0.0047	0.3205± 0.0045	....	....
02260242+6159163	0.0183	0.2481	....	....	....	0.4286± 0.0041	0.2950± 0.0034	....	....
02260312+6203492	....	....	....	....	....	0.3805± 0.0046	0.2754± 0.0060	1.2573± 0.0352	7.4349± 0.1988
02260301+6200057	....	....	....	....	....	0.5342± 0.0047	0.5353± 0.0044	....	....
02260419+6202228	....	....	....	....	....	....	0.6206± 0.0065	....	4.7682± 0.1050
02260415+6202510	....	....	0.5476	1.1976	1.1374	0.6190± 0.0045	0.3762± 0.0057	....	....
02260463+6202152	....	....	....	....	....	0.2958± 0.0043	....	....	4.7682± 0.1050
02260452+6158267	0.5931	5.2935	21.4037	32.3817	29.6436	16.6699± 0.0443	10.8992± 0.0316	8.1086± 0.0425	5.3639± 0.0766
02260466+6200027	....	....	0.4472	1.0723	1.2704	1.7228± 0.0082	1.8162± 0.0077	....	....
02260469+6200216	....	....	0.4154	1.0624	1.1586	0.7696± 0.0059	0.5404± 0.0046	....	....
02260527+6201098	....	....	....	....	....	0.4385± 0.0050	0.3233± 0.0054	....	....
02260410+6203266	....	....	....	....	....	....	0.3165± 0.0089	1.1409± 0.0308	4.6667± 0.1059
02260556+6159299	0.0889	0.5714	1.8814	2.5722	2.1475	1.2096± 0.0066	0.7935± 0.0047	....	....
02260544+6158244	0.0503	0.7207	....	....	....	....	....	14.1683± 0.0583	14.1716± 0.0996
02260587+6158465	3.9219	17.4639	40.7838	42.6874	35.3127	18.0509± 0.0457	11.8676± 0.0324	7.7691± 0.0390	....
02260590+6202276	....	....	....	....	....	0.1318± 0.0041	....	1.6879± 0.0364	11.4398± 0.1975
02260676+6203019	....	....	....	....	....	0.0844± 0.0031	....	1.3532± 0.0290	....
02260683+6159578	....	....	1.1028	1.8806	1.6902	1.0098± 0.0062	....	....	....
02260745+6203265	....	....	....	....	....	....	0.1902± 0.0043	1.5196± 0.0297	....
02260787+6159179	0.0521	0.4117	1.6691	2.9262	3.6302	3.7698± 0.0126	3.5652± 0.0121	3.4941± 0.0298	4.7396± 0.0584
02260849+6203544	....	....	....	....	....	0.1986± 0.0039	0.2324± 0.0052	1.0900± 0.0332	3.8531± 0.0957
02260906+6200219	0.0159	0.1262	....	....	....	0.7450± 0.0060	0.6052± 0.0049	....	3.2949± 0.0710

TABLE 4—Continued

ID IRAC-	$F_V$ [mJy]	$F_I$ [mJy]	$F_J$ [mJy]	$F_H$ [mJy]	$F_K$ [mJy]	$F_{3.6\mu m}$ [mJy]	$F_{4.5\mu m}$ [mJy]	$F_{5.8\mu m}$ [mJy]	$F_{8.0\mu m}$ [mJy]
02260959+6200581	6.1645	13.2843	17.8028	16.5310	11.8013	5.4760± 0.0174	3.4674± 0.0126	...	...
02260960+6200414	0.1369	0.7240	2.5263	3.0924	2.7538	1.5103± 0.0078	1.0445± 0.0060	...	...
02260967+6200119	0.0173	0.2061	1.1233	1.8463	1.9766	2.5289± 0.0107	2.7589± 0.0101	3.2730± 0.0316	4.9645± 0.0618
02261003+6159302	....	....	....	....	....	0.2655± 0.0034	0.1766± 0.0032	...	1.8659± 0.0490
02261007+6203454	....	....	....	....	....	0.4013± 0.0045	0.2660± 0.0048	1.0900± 0.0332	...
02261031+6200137	....	....	....	....	....	1.2635± 0.0452	1.2451± 0.0064	...	...
02261100+6200453	....	....	....	....	....	1.0392± 0.0064	0.9574± 0.0058	1.9951± 0.0271	2.6391± 0.0587
02261198+6203558	....	....	....	....	....	0.1196± 0.0041	...	1.0900± 0.0332	...
02261128+6201513	0.0108	0.1213	0.6060	0.8134	0.9907	0.6335± 0.0046	0.5342± 0.0046	1.0832± 0.0226	...
02261153+6204432	....	....	....	....	....	0.6820± 0.0074	0.5109± 0.0093	1.5851± 0.0414	...
02261196+6200129	0.0354	0.3546	1.6387	3.1210	3.2503	3.7277± 0.0126	3.3468± 0.0110	3.4648± 0.0308	3.9014± 0.0568
02261207+6159439	0.0074	0.0931	0.7490	1.4266	1.4857	0.7841± 0.0045	0.5516± 0.0039	...	1.8659± 0.0490
02261296+6203414	0.0281	0.2283	0.7022	1.2656	1.0184	0.6300± 0.0053	0.4041± 0.0053	0.9759± 0.0306	...
02261320+6200346	....	....	1.4012	2.3458	2.2281	2.7003± 0.0103	2.6966± 0.0093	3.0861± 0.0303	...
02261320+6156152	0.0103	0.1450	0.6173	1.0240	0.8393	0.4949± 0.0055	0.3336± 0.0037	...	...
02261391+6200532	....	....	1.0339	2.7688	4.8745	7.6964± 0.0224	7.9229± 0.0214	6.9452± 0.0384	5.4349± 0.0609
02261491+6204046	....	....	....	....	....	1.4946± 0.0083	1.7342± 0.0095	2.0313± 0.0378	...
02261565+6200482	0.0105	0.1716	0.8760	1.2425	1.3675	0.7470± 0.0049	0.5042± 0.0038	...	...
02261645+6157174	0.0174	0.2678	1.7002	2.9806	2.7035	1.6131± 0.0089	1.0929± 0.0072	...	...
02261671+6159485	0.0133	0.1724	0.9172	1.7470	2.1278	2.3732± 0.0076	2.4506± 0.0079	2.5969± 0.0201	3.3826± 0.0975
02261699+6158262	0.0926	0.5767	....	....	....	2.2164± 0.0087	1.8152± 0.0091	...	...
02261717+6157438	....	....	....	....	....	0.3781± 0.0046	0.2408± 0.0047	...	...
02261727+6156069	0.0758	0.8244	3.7195	6.1702	5.4945	3.6082± 0.0144	2.4486± 0.0086	...	...
02261739+6159512	0.0096	0.1196	0.7421	1.3624	1.2358	1.0372± 0.0045	0.8811± 0.0043	...	3.3826± 0.0975
02261769+6202141	....	....	....	....	....	0.2175± 0.0047	...	0.9204± 0.0310	...
02261849+6203556	....	....	....	....	....	2.6170± 0.0107	2.1788± 0.0120	1.7622± 0.0323	...
02261881+6159528	3.1124	8.8990	16.8457	20.8113	28.5713	35.9941± 0.0794	33.0929± 0.0736	28.1996± 0.0736	19.7041± 0.0763
02261765+6203431	....	....	....	....	....	...	0.1631± 0.0054	1.4315± 0.0338	...
02261881+6159528	3.1124	8.8990	16.8457	20.8113	28.5713	35.9941± 0.0794	33.0929± 0.0736	28.1996± 0.0736	19.7041± 0.0763
02261888+6158048	....	....	0.4770	0.8837	0.9726	0.5528± 0.0050	0.3692± 0.0048	...	...
02261959+6203058	....	....	1.0058	2.8728	5.0111	4.9716± 0.0172	5.4634± 0.0197	5.5616± 0.0405	5.8156± 0.0979
02261970+6156554	0.0069	0.0827	0.4597	0.9085	0.9461	0.6540± 0.0058	0.4370± 0.0043	...	...
02261967+6157541	0.0084	0.0952	0.5182	0.9779	0.8471	0.6031± 0.0049	0.4757± 0.0051	...	...
02261990+6159357	0.0084	0.1122	0.5950	1.0922	0.9907	0.5702± 0.0030	0.4037± 0.0032	...	...
02262010+6156358	0.0083	0.0765	0.5426	1.1866	1.2244	1.2468± 0.0077	1.2134± 0.0061	...	...
02262029+6200119	0.0433	0.4411	1.7478	2.9262	2.5818	1.4760± 0.0061	1.0010± 0.0041	...	...
02262044+6157024	0.0434	0.4977	2.2829	3.9292	3.7319	2.1077± 0.0100	1.4210± 0.0074	...	...
02262048+6203521	....	....	....	....	....	0.1110± 0.0039	10.5435± 0.0341	11.1644± 0.0564	7.5089± 0.1310
02262048+6203521	....	....	....	....	....	0.1110± 0.0039	...	...	7.5089± 0.1310
02262082+6200365	0.0489	0.4940	2.1013	3.4222	3.4668	2.7640± 0.0097	2.5800± 0.0079	2.8239± 0.0225	3.3343± 0.0365
02262048+6203521	....	....	....	....	....	0.1110± 0.0039	...	1.7701± 0.0287	7.5089± 0.1310
02262112+6158582	0.0162	0.3043	2.1207	4.0022	3.8720	3.4545± 0.0101	2.9812± 0.0105	2.7241± 0.0194	1.8166± 0.0446
02262148+6158419	0.0131	0.2141	1.3883	2.8728	3.7664	4.2733± 0.0126	4.6581± 0.0149	5.9031± 0.0271	8.7761± 0.0600
02262140+6200551	....	....	....	....	....	0.3941± 0.0038	0.3541± 0.0033	...	...

TABLE 4—Continued

ID- IRAC-	$F_V$ [mJy]	$F_I$ [mJy]	$F_J$ [mJy]	$F_H$ [mJy]	$F_K$ [mJy]	$F_{3.6\mu m}$ [mJy]	$F_{4.5\mu m}$ [mJy]	$F_{5.8\mu m}$ [mJy]	$F_{8.0\mu m}$ [mJy]
02262132+6204362	....	....	....	....	....	....	0.6992± 0.0064	0.9339± 0.0282	3.5138± 0.0972
02262191+6202438	0.0203	0.2609	....	....	....	1.0970± 0.0077	0.2386± 0.0051	....	....
02262195+6158031	0.0234	0.3010	1.4537	3.0082	3.4350	2.8531± 0.0106	2.4348± 0.0102	2.6262± 0.0251	....
02262199+6159297	0.0062	0.0896	....	....	....	0.2997± 0.0025	0.1893± 0.0026	....	....
02262219+6156592	....	....	....	....	....	0.4430± 0.0045	0.5047± 0.0042	....	....
02262231+6157267	....	....	0.6831	1.4666	1.2940	0.7198± 0.0055	0.4955± 0.0047	....	....
02262227+6202403	....	....	0.9005	1.5216	1.7058	....	1.0089± 0.0079	....	....
02262273+6203109	0.0269	0.3288	1.6387	3.0641	3.3108	3.1841± 0.0128	3.3963± 0.0151	4.2446± 0.0380	6.5168± 0.1083
02262318+6202023	....	....	....	....	....	0.9024± 0.0081	0.9420± 0.0075	....	....
02262328+6205020	0.0034	0.0127	....	....	....	3.5602± 0.0137	4.5682± 0.0220	5.8689± 0.0456	....
02262411+6200012	0.0235	0.2092	1.3258	2.3895	2.6542	2.4358± 0.0080	2.2342± 0.0073	2.3161± 0.0171	3.1943± 0.0930
02262440+6200090	....	....	....	....	....	0.2177± 0.0028	0.1853± 0.0026	....	3.1943± 0.0930
02262447+6159106	....	....	....	....	....	0.5632± 0.0045	....	7.5838± 0.1242	....
02262488+6159265	0.0100	0.1270	0.6060	0.9339	1.0963	0.7803± 0.0044	....	1.0460± 0.0182	2.4428± 0.0506
02262527+6156538	....	....	....	....	....	0.3750± 0.0040	0.2670± 0.0030	....	....
02262536+6200034	0.0117	0.2515	1.6691	3.3289	3.4668	3.3614± 0.0103	3.0712± 0.0094	2.7515± 0.0178	3.1943± 0.0930
02262586+6201186	0.0239	0.1478	....	....	....	0.2711± 0.0046	0.1770± 0.0037	....	....
02262587+6158354	0.0051	0.0892	0.4903	0.9870	1.1586	2.1528± 0.0089	2.1561± 0.0082	2.1409± 0.0224	....
02262637+6159124	0.0242	0.3870	1.8471	3.2681	3.0474	2.3066± 0.0085	1.8992± 0.0078	2.0538± 0.0193	....
02262646+6202241	0.1003	0.6927	2.5263	3.6838	3.1618	1.6905± 0.0099	1.1304± 0.0080	....	....
02262649+6204256	....	....	....	....	....	0.4154± 0.0043	0.3153± 0.0055	....	....
02262724+6158142	0.5011	3.7544	12.4305	17.3101	15.5572	8.4515± 0.0238	5.5889± 0.0164	3.9824± 0.0282	1.7791± 0.0511
02262794+6159538	....	....	0.7353	1.5499	2.1475	1.7052± 0.0065	1.6611± 0.0067	1.4931± 0.0172	....
02262802+6158482	0.0067	0.1532	0.8600	1.5216	1.3550	0.7961± 0.0056	0.5441± 0.0042	....	....
02262817+6158218	0.0060	0.0824	....	....	....	....	1.0039± 0.0053	....	....
02262836+6205306	0.0172	0.2201	1.1442	1.8980	2.0508	1.2018± 0.0064	1.0277± 0.0090	....	....
02262839+6156388	....	....	1.1547	2.3458	2.8309	1.3046± 0.0072	1.0356± 0.0046	....	....
02262860+6158055	0.0385	0.4387	2.3686	4.6377	6.5453	8.7307± 0.0252	8.9387± 0.0243	9.0890± 0.0430	9.8422± 0.0711
02262879+6157481	0.0130	0.1685	0.7022	1.4135	1.4320	1.2889± 0.0064	1.2026± 0.0056	....	....
02262938+6200135	....	....	....	....	....	0.6970± 0.0409	0.8615± 0.0049	....	....
02262940+6201375	0.0310	0.2944	1.6538	3.2681	3.8720	3.9207± 0.0166	3.6057± 0.0137	3.0411± 0.0357	....
02262962+6159126	0.0252	0.2928	1.6538	3.6838	5.2472	5.8257± 0.0177	5.8458± 0.0181	5.8718± 0.0330	6.5099± 0.0639
02262966+6156575	....	....	....	....	....	0.2673± 0.0035	0.1828± 0.0024	....	....
02262969+6202382	....	....	....	....	....	0.6724± 0.0066	0.4052± 0.0059	....	....
02262966+6204566	....	....	....	....	....	0.6962± 0.0045	0.5665± 0.0048	....	....
02262989+6201223	0.0108	0.0886	....	....	....	....	0.2633± 0.0040	....	....
02263007+6158506	0.0381	0.4271	2.0440	3.6166	4.0173	2.8374± 0.0120	2.3211± 0.0096	1.7916± 0.0268	....
02263023+6202383	....	....	....	....	....	0.5083± 0.0058	0.4052± 0.0059	....	....
02263046+6200453	....	....	1.7159	2.9262	2.9644	2.2390± 0.0098	1.8933± 0.0078	....	....
02263091+6157504	0.0075	0.1373	....	....	....	0.6954± 0.0051	0.4399± 0.0037	....	....
02263094+6155383	....	....	....	....	....	0.4451± 0.0057	0.2944± 0.0038	....	....
02263131+6200037	0.0359	0.5182	2.2620	3.9655	3.7319	2.0059± 0.0081	1.3547± 0.0069	....	....
02263135+6158054	....	....	....	....	....	0.5834± 0.0049	0.4041± 0.0039	....	....
02263140+6201527	0.0226	0.2168	0.9694	1.5933	1.5415	0.7723± 0.0064	0.5206± 0.0053	....	....

TABLE 4—Continued

ID IRAC-	$F_V$ [mJy]	$F_I$ [mJy]	$F_J$ [mJy]	$F_H$ [mJy]	$F_K$ [mJy]	$F_{3.6\mu m}$ [mJy]	$F_{4.5\mu m}$ [mJy]	$F_{5.8\mu m}$ [mJy]	$F_{8.0\mu m}$ [mJy]
02263150+6201191	....	....	0.4431	0.8676	0.7378	0.4391± 0.0052	0.2867± 0.0040	....	....
02263167+6200439	....	....	....	....	....	0.5492± 0.0051	0.4928± 0.0043	....	....
02263184+6203125	....	....	....	....	....	0.3865± 0.0044	0.2639± 0.0051	1.8542± 0.0286	4.6085± 0.0894
02263206+6156121	0.6910	3.2579	7.5594	8.3618	7.1110	3.5671± 0.0128	2.2589± 0.0077	....	....
02263248+6156347	....	....	0.4858	1.3011	2.2905	4.8413± 0.0163	5.4338± 0.0141	5.5039± 0.0331	6.5651± 0.0469
02263240+6202523	....	....	....	....	....	0.4981± 0.0051	0.3371± 0.0051	....	....
02263230+6158525	....	....	0.5578	0.8517	0.9203	0.5176± 0.0054	0.3666± 0.0044	3.2701± 0.0381	3.6499± 0.0749
02263287+6201220	....	....	0.9874	1.6379	1.4994	0.8331± 0.0064	....	....	....
02263323+6201062	0.0249	0.3114	1.4272	2.4791	2.2905	1.2458± 0.0071	0.8250± 0.0050	....	....
02263332+6156030	0.0141	0.3950	....	....	....	8.0323± 0.0257	7.6334± 0.0199	6.6761± 0.0338	6.6351± 0.0487
02263328+6156045	0.0133	0.3720	....	....	....	....	....	6.6761± 0.0338	6.6351± 0.0487
02263343+6159250	0.0319	0.3575	1.2779	2.0811	1.8877	0.9843± 0.0067	0.6521± 0.0056	....	....
02263362+6159431	0.0143	0.2025	0.8063	1.4135	1.1801	0.6586± 0.0052	0.4242± 0.0054	1.1292± 0.0233	....
02263371+6155387	....	....	0.7022	1.5499	1.9406	2.1068± 0.0102	2.0909± 0.0084	....	....
02263386+6155555	0.0320	0.4972	2.6454	4.7676	4.6551	2.5651± 0.0114	1.7411± 0.0068	....	....
02263394+6156573	4.4741	9.6859	12.2036	11.2279	8.0897	3.6641± 0.0133	2.4022± 0.0072	1.8014± 0.0239	....
02263415+6201192	4.6936	16.9723	37.8868	40.7662	33.1078	15.9256± 0.0438	10.4644± 0.0278	6.9814± 0.0413	....
02263422+6159201	0.1141	1.0369	4.0410	6.5811	6.5453	5.9951± 0.0207	5.0415± 0.0182	4.1879± 0.0331	....
02263431+6200252	0.0239	0.2375	....	....	....	1.2116± 0.0067	1.3893± 0.0527	....	....
02263433+6201527	6.4077	14.1690	22.4124	21.5924	17.2159	7.8609± 0.0268	5.1136± 0.0170	3.4814± 0.0342	....
02263443+6200419	....	....	1024.4441	836.1803	602.4631	126.5426± 0.4112	167.2925± 0.3872	130.3327± 0.3150	97.2387± 0.2737
02263441+6205037	....	....	....	....	....	0.2437± 0.0030	0.1707± 0.0032	....	....
02263455+6158169	0.2307	1.7625	6.1729	10.0531	12.2442	13.1244± 0.0384	11.9664± 0.0328	10.4599± 0.0510	8.4359± 0.0703
02263455+6203404	....	....	....	....	....	0.4005± 0.0037	0.2878± 0.0048	....	....
02263463+6159107	2.6984	13.4320	35.1956	41.5241	34.6681	17.1499± 0.0517	11.2846± 0.0340	8.1037± 0.0462	....
02263480+6201053	0.0755	0.6423	2.7957	4.5113	3.9804	2.1342± 0.0094	1.3963± 0.0066	....	....
02263530+6204558	....	....	....	....	....	0.0655± 0.0021	0.1707± 0.0032	....	2.2613± 0.0534
02263489+6157559	0.1558	1.7512	7.2860	12.0865	11.1668	6.0500± 0.0193	4.0395± 0.0124	....	....
02263495+6202427	....	....	....	....	....	0.6289± 0.0049	0.4547± 0.0049	....	....
02263541+6155197	....	....	....	....	....	0.7046± 0.0085	0.4736± 0.0040	....	....
02263585+6201062	0.0350	0.3377	....	....	....	1.1978± 0.0069	0.8187± 0.0050	....	....
02263646+6201120	9.4515	22.5393	32.3958	32.3817	23.7646	10.9598± 0.0306	6.9279± 0.0192	4.8630± 0.0318	....
02263648+6157462	0.0375	0.4602	2.2003	3.7870	3.1618	1.7463± 0.0085	1.1571± 0.0054	....	....
02263658+6201471	....	....	0.9605	1.6838	1.5133	0.8986± 0.0058	0.5949± 0.0046	....	....
02263667+6200416	0.8187	4.8949	15.2226	18.9802	16.1410	7.8002± 0.0227	5.1443± 0.0164	3.3170± 0.0270	....
02263670+6202470	1.0922	5.4568	14.4042	18.6337	15.9930	8.2723± 0.0242	5.4348± 0.0177	3.8660± 0.0289	....
02263693+6200345	0.0328	0.3097	1.5083	2.7183	2.7793	2.0323± 0.0087	1.7204± 0.0082	....	....
02263709+6202222	0.0105	0.1011	0.4640	0.7912	0.7942	0.4315± 0.0043	0.3018± 0.0042	....	....
02263713+6202147	0.0101	0.1180	0.6584	1.0335	1.1911	1.0637± 0.0062	1.0010± 0.0060	....	....
02263743+6202322	0.0171	0.1913	0.8443	1.7960	2.3547	1.8570± 0.0081	2.0000± 0.0089	2.3571± 0.0259	....
02263750+6156207	....	....	....	....	....	3.0078± 0.0123	3.2885± 0.0103	3.3875± 0.0300	3.5306± 0.0466
02263755+6201557	....	....	0.5950	1.0527	1.2704	0.6596± 0.0050	0.4602± 0.0044	....	....
02263768+6159187	0.1580	1.3333	4.2314	6.7035	5.7535	3.0206± 0.0137	1.9822± 0.0101	....	....
02263768+6200054	0.0236	0.3953	1.8988	3.2681	3.0756	1.8041± 0.0079	1.2105± 0.0070	....	....

TABLE 4—Continued

ID- IRAC-	$F_V$ [mJy]	$F_I$ [mJy]	$F_J$ [mJy]	$F_H$ [mJy]	$F_K$ [mJy]	$F_{3.6\mu m}$ [mJy]	$F_{4.5\mu m}$ [mJy]	$F_{5.8\mu m}$ [mJy]	$F_{8.0\mu m}$ [mJy]
02263755+6205115	....	....	....	....	....	0.5622± 0.0040	0.3954± 0.0039	....	....
02263928+6201034	....	....	....	....	....	....	....	0.5198± 0.0171	5.0335± 0.0596
02263847+6157126	....	....	....	....	....	0.3548± 0.0047	0.3065± 0.0030	....	....
02263851+6200490	0.0508	0.4977	....	....	....	4.7355± 0.0153	4.3330± 0.0142	....	5.0335± 0.0596
02263862+6200142	....	....	0.6645	1.1228	1.8194	1.6513± 0.0074	1.3715± 0.0071	....	....
02263865+6200533	0.0423	0.4102	....	....	....	5.0764± 0.0157	4.5978± 0.0146	3.7603± 0.0292	5.0335± 0.0596
02263865+6159135	0.0132	0.1858	0.7286	1.2891	1.0091	0.5273± 0.0060	....	....	....
02263868+6159094	0.0697	0.7772	....	....	....	2.3105± 0.0121	1.5168± 0.0091	....	....
02263885+6200303	0.9110	4.0601	11.7622	13.8771	11.6931	5.9422± 0.0180	3.9397± 0.0136	2.7006± 0.0254	....
02263882+6202112	0.0196	0.3091	....	....	....	1.9824± 0.0086	1.5632± 0.0070	....	....
02263954+6202400	....	....	....	....	....	2.0549± 0.0086	1.9664± 0.0086	2.0519± 0.0251	2.6854± 0.1303
02263958+6204263	....	....	....	....	....	0.1574± 0.0028	0.1480± 0.0037	1.1800± 0.0200	....
02263953+6202401	0.0380	0.3069	1.7478	2.9532	3.4989	2.0549± 0.0086	1.9664± 0.0086	2.0519± 0.0251	....
02263962+6203506	0.0483	0.3612	1.5649	2.4116	2.3117	1.2282± 0.0059	0.8744± 0.0059	1.2867± 0.0172	3.0335± 0.0497
02263987+6201292	0.0111	0.1689	....	....	....	0.8273± 0.0048	0.7207± 0.0042	....	....
02263999+6200279	0.0289	0.2890	1.5363	3.0082	3.9078	4.9402± 0.0152	4.7619± 0.0158	5.6742± 0.0297	6.8067± 0.0623
02264011+6200068	0.0119	0.1549	....	....	....	2.4182± 0.0097	2.2253± 0.0098	1.6389± 0.0237	4.7998± 0.0644
02263983+6156038	....	....	....	....	....	....	0.1332± 0.0034	....	2.4231± 0.0595
02264061+6200448	....	....	0.5041	0.9513	1.0374	0.6620± 0.0040	0.6607± 0.0047	....	....
02264113+6157424	....	....	0.4555	1.0053	1.0278	2.3653± 0.0115	2.6532± 0.0098	2.6752± 0.0349	....
02264126+6201566	0.1100	0.8259	3.4236	5.7319	5.0111	2.7042± 0.0096	1.8271± 0.0075	....	....
02264140+6158026	0.0332	0.5274	2.5263	4.4699	4.2455	2.3947± 0.0123	1.5227± 0.0076	....	....
02264157+6201129	0.0166	0.1713	0.8063	1.6229	1.8532	1.8903± 0.0067	1.6749± 0.0063	....	....
02264193+6201516	0.0856	0.5303	1.8814	3.0641	2.7035	1.3497± 0.0062	0.8956± 0.0048	....	....
02264238+6159456	0.0080	0.1942	0.9430	1.6229	1.8027	1.3173± 0.0074	1.0850± 0.0071	....	....
02264247+6157511	....	....	0.4431	1.1649	1.2132	0.7006± 0.0068	0.4678± 0.0043	....	2.1519± 0.0602
02264279+6204237	....	....	....	....	....	0.2723± 0.0037	0.2017± 0.0042	1.0773± 0.0221	....
02264240+6158162	0.0066	0.1279	....	....	....	0.7427± 0.0066	0.4827± 0.0047	....	....
02264279+6201156	....	....	....	....	....	0.2682± 0.0026	0.1833± 0.0025	....	....
02264290+6201282	0.0880	0.6300	2.9545	4.9923	5.7007	5.2625± 0.0151	4.9496± 0.0137	5.0147± 0.0266	5.7396± 0.0426
02264297+6200166	0.0509	0.4193	....	....	....	1.1685± 0.0056	0.8159± 0.0056	....	....
02264334+6200044	0.0130	0.2612	1.0244	2.2819	2.6787	3.7483± 0.0129	3.3567± 0.0138	2.9462± 0.0260	....
02264342+6203347	0.0095	0.1832	1.1547	2.3030	2.3117	1.5093± 0.0074	1.0217± 0.0054	....	....
02264353+6159270	0.0253	0.3899	1.7318	2.9532	2.5115	1.5005± 0.0083	1.0030± 0.0068	....	....
02264359+6204115	....	....	0.7771	1.1437	1.4188	1.6983± 0.0072	1.5840± 0.0080	2.0186± 0.0227	2.8955± 0.0738
02264438+6155548	....	....	....	....	....	....	0.1055± 0.0037	....	5.1055± 0.0934
02264376+6159113	0.1977	1.4687	4.2314	6.5811	5.7535	3.7767± 0.0154	2.9625± 0.0131	2.5607± 0.0311	....
02264391+6200191	....	....	....	....	....	0.8262± 0.0044	0.9313± 0.0060	....	....
02264413+6200305	0.0192	0.2094	1.0435	2.2197	3.0756	3.4172± 0.0106	3.4664± 0.0116	3.5274± 0.0198	4.6913± 0.0445
02264423+6203348	0.0377	0.3814	1.7002	2.7945	2.5115	1.3389± 0.0067	0.8658± 0.0051	....	....
02264425+6155223	0.0316	0.2861	0.8063	1.1023	0.9907	....	0.3237± 0.0039	....	....
02264421+6157229	0.0076	0.1851	1.2204	2.5252	2.9372	3.3369± 0.0151	2.8804± 0.0100	2.8063± 0.0384	3.2091± 0.0582
02264480+6159395	....	....	0.7087	0.9870	0.9998	0.5660± 0.0047	0.3828± 0.0047	....	....
02264490+6204378	....	....	....	....	....	0.2263± 0.0035	0.1168± 0.0040	1.5293± 0.0238	4.7258± 0.0768

TABLE 4—Continued

ID IRAC-	F <sub>V</sub> [mJy]	F <sub>I</sub> [mJy]	F <sub>J</sub> [mJy]	F <sub>H</sub> [mJy]	F <sub>K</sub> [mJy]	F <sub>3.6μm</sub> [mJy]	F <sub>4.5μm</sub> [mJy]	F <sub>5.8μm</sub> [mJy]	F <sub>8.0μm</sub> [mJy]
02264497+6200170	0.0601	0.5116	2.2003	3.4858	3.1041	1.5798± 0.0065	1.0039± 0.0063	...	...
02264527+6203075	...	...	715.3001	867.5608	831.6306	291.0872± 0.8387	200.8893± 0.6110	215.4599± 0.4909	115.3846± 0.3012
02264562+6157382	...	...	...	...	...	0.4807± 0.0058	0.6510± 0.0044	...	...
02264571+6159505	0.7323	3.5887	9.8739	10.0531	8.7082	4.4349± 0.0150	2.9980± 0.0121	1.9941± 0.0210	...
02264592+6204019	...	...	...	...	...	0.7097± 0.0059	0.6400± 0.0053	1.5656± 0.0322	9.9310± 0.1698
02264606+6201220	...	...	...	...	...	1.6131± 0.0055	1.7954± 0.0062	1.8337± 0.0159	1.7643± 0.0806
02264607+6157332	...	...	...	...	...	0.8157± 0.0070	0.7654± 0.0048	...	2.7209± 0.0606
02264649+6200196	...	...	1.3258	2.0811	2.0508	1.0362± 0.0050	0.6730± 0.0051	...	...
02264651+6156331	...	...	...	...	...	2.0206± 0.0131	1.8370± 0.0092	...	3.0858± 0.0813
02264674+6200367	0.0207	0.2435	1.0150	1.8463	1.5846	0.9603± 0.0044	0.6681± 0.0045	...	...
02264702+6202144	...	...	0.7153	1.2311	1.2704	1.4691± 0.0062	1.8142± 0.0066	2.1438± 0.0225	3.0148± 0.0929
02264720+6156102	...	...	0.7219	1.5933	1.5701	1.1254± 0.0122	0.8653± 0.0068	...	...
02264736+6159478	...	...	0.9783	2.0244	2.0508	1.7424± 0.0079	1.4961± 0.0074	...	...
02264898+6157567	...	...	...	...	...	2.4535± 0.0122	2.9773± 0.0103	4.7730± 0.0452	3.5246± 0.0613
02264970+6156338	...	...	0.4640	1.1649	1.4994	2.7228± 0.0169	2.7520± 0.0125	2.5411± 0.0469	...
02264963+6156035	0.9870	7.2801	18.8143	23.2434	19.4058	10.3722± 0.0570	6.6354± 0.0226	4.7926± 0.0663	...
02264974+6158419	...	...	0.4949	1.1866	1.1586	0.9502± 0.0063	0.7849± 0.0052	...	...
02265007+6200263	0.0238	0.3184	1.5794	2.7688	2.6542	1.5358± 0.0059	1.0326± 0.0055	...	...
02265061+6157404	...	...	...	...	...	3.9765± 0.0163	4.9832± 0.0150	4.7593± 0.0448	4.7120± 0.0588
02265084+6202534	0.3369	2.4737	9.7834	12.3112	11.6931	6.8825± 0.0234	5.4259± 0.0179	3.9990± 0.0367	3.9063± 0.0633
02265100+6158384	...	...	0.8063	2.3030	3.2804	3.1959± 0.0125	2.9990± 0.0107	3.1546± 0.0315	3.8797± 0.0575
02265167+6200166	...	...	...	...	...	0.4579± 0.0033	0.4397± 0.0039	...	...
02265171+6158335	0.0133	0.2497	1.4537	3.1210	3.4668	3.0470± 0.0121	3.1561± 0.0104	2.9677± 0.0309	3.8797± 0.0575
02265339+6157007	0.0121	0.3246	2.6454	6.6420	10.5665	11.5377± 0.0406	11.0474± 0.0308	11.0176± 0.0650	16.5582± 0.1019
02265387+6204355	1.9262	4.6402	6.6449	6.2273	4.5701	2.0960± 0.0094	1.3745± 0.0082	...	...
02265444+6157204	...	...	0.5895	1.6379	1.8532	1.2654± 0.0074	0.8522± 0.0050	...	...
02265534+6159075	1.3941	4.5724	8.8407	8.7559	6.8538	3.2938± 0.0109	2.1868± 0.0078	...	...
02265574+6202069	...	...	0.4513	1.0922	1.0862	0.6931± 0.0043	0.4809± 0.0032	...	...
02265607+6205409	0.5764	1.9113	3.6854	3.8931	3.2503	1.4858± 0.0066	0.9589± 0.0070	...	...
02265761+6159490	...	...	...	...	...	0.4680± 0.0043	0.3441± 0.0034	...	...
02265809+6157155	...	...	...	...	...	0.4284± 0.0048	0.3045± 0.0032	...	...
02265816+6159319	0.0091	0.1435	0.8289	1.7470	2.4885	3.4329± 0.0120	2.9694± 0.0098	...	...
02265948+6203506	...	...	0.4390	1.0430	1.3060	0.7178± 0.0061	0.4910± 0.0050	...	...
02270002+6201106	...	...	0.4814	0.9779	0.8393	0.5347± 0.0042	0.3571± 0.0039	...	...
02270024+6157320	...	...	...	...	...	0.3620± 0.0039	0.3010± 0.0030	...	...
02270155+6159589	...	...	...	...	...	2.2194± 0.0095	2.1028± 0.0086	...	...
02270392+6201588	...	...	0.6288	1.6379	2.1083	2.2821± 0.0085	1.8399± 0.0078	...	...
02270523+6157048	0.4099	1.8119	3.6182	4.6377	3.6302	1.7121± 0.0101	1.0820± 0.0052	...	...
02270536+6202109	...	...	...	...	...	0.2934± 0.0033	0.2011± 0.0031	...	...
02270613+6158166	0.0235	0.3054	1.6087	3.0641	3.3723	3.6474± 0.0126	3.5613± 0.0101	3.4481± 0.0291	3.6647± 0.0452
02270616+6157127	...	...	...	...	...	0.8901± 0.0078	0.9881± 0.0050	...	...
02270608+6157387	...	...	...	...	...	0.2784± 0.0039	0.2249± 0.0025	...	...
02270756+6200131	0.0127	0.3679	3.7887	9.0012	9.9984	6.1469± 0.0243	3.9970± 0.0171	2.4041± 0.0473	...
02270756+6200131	0.0127	0.3679	3.7887	9.0012	9.9984	6.1469± 0.0243	3.9970± 0.0171	2.4041± 0.0473	...

TABLE 4—*Continued*

ID IRAC-	$F_V$ [mJy]	$F_I$ [mJy]	$F_J$ [mJy]	$F_H$ [mJy]	$F_K$ [mJy]	$F_{3.6\mu m}$ [mJy]	$F_{4.5\mu m}$ [mJy]	$F_{5.8\mu m}$ [mJy]	$F_{8.0\mu m}$ [mJy]
02270964+6159369	....	....	....	....	....	$0.4745 \pm 0.0061$	$0.3269 \pm 0.0046$	....	....
02271047+6159501	0.0102	0.2050	1.1233	1.7470	1.7862	$0.9922 \pm 0.0082$	$0.6740 \pm 0.0060$	....	....
02271197+6157347	0.0942	0.3849	0.7771	1.0053	0.9288	$0.4215 \pm 0.0064$	$0.2934 \pm 0.0036$	....	....
02271295+6157250	....	....	0.4310	1.0240	1.0091	$0.6950 \pm 0.0089$	$0.4805 \pm 0.0045$	....	....
02271296+6158407	0.0216	0.2321	0.9605	1.5216	1.3929	$0.6880 \pm 0.0065$	$0.4491 \pm 0.0040$	....	....
02271410+6200456	....	....	....	....	....	$0.2598 \pm 0.0069$	....	$2.0117 \pm 0.0485$	$5.1065 \pm 0.1374$
02271452+6200193	0.1127	0.8491	2.7195	3.8575	3.5639	$1.7522 \pm 0.0639$	....	....	....
02271660+6200520	....	....	....	....	....	$1.5926 \pm 0.0649$	....	$1.7456 \pm 0.0482$	....
02271627+6159086	0.0104	0.1777	0.8841	1.3253	1.3426	$0.5586 \pm 0.0070$	$0.4129 \pm 0.0042$	....	....
02271656+6158358	0.0063	0.1038	0.5630	1.0822	1.0374	$0.9119 \pm 0.0071$	$0.7267 \pm 0.0049$	....	....
02271981+6158281	0.0256	0.2700	1.3630	2.2197	1.9585	$1.0274 \pm 0.0082$	$0.6964 \pm 0.0049$	....	....
02271999+6159435	0.4979	1.8388	3.5850	4.4699	3.2503	$1.5113 \pm 0.0114$	$0.9571 \pm 0.0068$	....	$4.6479 \pm 0.0940$
02272024+6202025	1.3813	10.6400	49.9446	71.4990	79.4201	$70.2547 \pm 0.1635$	$61.3439 \pm 0.1532$	$53.6399 \pm 0.1421$	$40.4043 \pm 0.1594$

NOTE.—The near-infrared fluxes are from the 2MASS catalog Skrutskie et al. (2006), selecting only sources flagged ‘AAA’. The optical fluxes are from José et al. in preparation. The IRAC flux errors refer to the covariance matrix calculated from the “best-fit” of the PRF to the data and do not include calibration uncertainty ( $\sim 10\%$  of the flux).

TABLE 5

CLUSTER MEMBER CANDIDATES: DESIGNATION AND POSITIONS OF IRAC SOURCES WITH EXCESS WITHOUT X-RAY COUNTERPART.

ID IRAC-	RA <sub>J2000</sub> [deg]	RA error $10^{-4}$ [deg]	DEC <sub>J2000</sub> [deg]	DEC error $10^{-4}$ [deg]
02270033+6205291	36.751377	1.09	62.091415	1.12
02271605+6200506	36.816875	0.43	62.014042	0.44
02271147+6201578	36.797775	0.57	62.032722	0.60
02271512+6200152	36.813011	0.45	62.004215	0.46
02271175+6158265	36.798965	0.65	61.974022	0.67
02270991+6158521	36.791275	1.63	61.981152	1.73
02264351+6205302	36.681278	3.98	62.091713	3.92
02264566+6204469	36.690266	0.60	62.079685	0.60
02270243+6200092	36.760136	1.02	62.002544	1.05
02263985+6205356	36.666031	5.19	62.093216	5.15
02264926+6203131	36.705231	1.63	62.053650	1.71
02265258+6202179	36.719074	2.50	62.038315	2.40
02271166+6157119	36.798573	1.27	61.953308	1.74
02265704+6200587	36.737675	2.37	62.016312	2.66
02265770+6200430	36.740398	0.95	62.011936	0.92
02264230+6204412	36.676254	2.29	62.078098	2.46
02263648+6206069	36.652004	1.45	62.101921	1.60
02265787+6200283	36.741112	1.13	62.007870	1.08
02264396+6204054	36.683167	5.15	62.068153	5.35
02270190+6159131	36.757904	7.53	61.986961	8.26
02264299+6204100	36.679127	4.42	62.069454	4.61
02270071+6159226	36.752964	0.38	61.989597	0.40
02264101+6204364	36.670876	2.35	62.076767	2.41
02270217+6158583	36.759029	2.45	61.982857	2.49
02265433+6200584	36.726395	1.50	62.016228	1.58
02265824+6159566	36.742676	2.14	61.999046	2.32
02270838+6157024	36.784935	1.46	61.950680	1.32
02265430+6200448	36.726261	2.01	62.012451	2.27
02265398+6200396	36.724911	0.50	62.010986	0.50
02270091+6158478	36.753777	0.83	61.979946	0.87
02265046+6201324	36.710236	1.51	62.025658	1.60
02263797+6204378	36.658195	6.49	62.077168	6.77
02270433+6157363	36.768024	1.67	61.960075	1.73
02264423+6202464	36.684288	0.89	62.046223	0.88
02265682+6159142	36.736732	2.36	61.987274	2.36
02264970+6200588	36.707077	0.91	62.016335	0.95
02265782+6158377	36.740898	2.64	61.977142	2.76
02264197+6202428	36.674873	1.04	62.045235	1.09
02264781+6201123	36.699203	0.92	62.020096	1.02
02262952+6205518	36.623009	0.86	62.097713	0.87
02264605+6201221	36.691887	0.59	62.022797	0.62
02264800+6200576	36.700001	1.96	62.016006	1.93
02270253+6157046	36.760521	1.12	61.951283	1.02
02264766+6200592	36.698593	1.67	62.016449	1.71
02265560+6158517	36.731667	1.41	61.981014	1.38
02264441+6201480	36.685043	1.40	62.030003	1.47
02264808+6200490	36.700348	1.44	62.013607	1.56
02264515+6201320	36.688110	2.02	62.025558	2.04
02264675+6201026	36.694805	1.56	62.017384	1.57
02262986+6205201	36.624416	2.08	62.088928	2.11
02265324+6159124	36.721840	1.76	61.986790	1.65
02265657+6158167	36.735699	1.53	61.971313	1.58
02264334+6201432	36.680584	1.64	62.028675	1.65
02265922+6157289	36.746742	2.32	61.958027	2.60
02263045+6204552	36.626877	1.53	62.081989	1.57
02265139+6159252	36.714127	1.92	61.990337	2.05
02264472+6201039	36.686325	1.61	62.017742	1.60
02264531+6200544	36.688805	1.36	62.015099	1.42

TABLE 5—Continued

ID IRAC-	RA <sub>J2000</sub> [deg]	RA error $10^{-4}$ [deg]	DEC <sub>J2000</sub> [deg]	DEC error $10^{-4}$ [deg]
02264994+6159423	36.708065	0.64	61.995083	0.70
02263066+6204411	36.627762	6.30	62.078075	6.63
02264856+6159576	36.702320	2.02	61.999344	2.03
02265062+6159144	36.710911	2.52	61.987347	2.56
02264573+6200251	36.690525	0.75	62.006966	0.73
02262962+6204414	36.623398	1.58	62.078167	1.63
02264771+6159550	36.698799	2.01	61.998615	2.02
02263241+6203518	36.635040	3.08	62.064396	3.05
02265343+6158188	36.722610	2.31	61.971893	2.33
02264572+6200131	36.690487	1.06	62.003635	1.12
02262883+6204365	36.620129	0.95	62.076797	1.02
02264107+6201211	36.671124	1.73	62.022541	1.85
02263081+6203502	36.628380	1.64	62.063934	1.68
02263152+6203331	36.631325	1.96	62.059208	2.16
02263839+6201459	36.659939	0.76	62.029404	0.83
02264099+6201076	36.670776	2.30	62.018787	2.38
02264433+6200027	36.684719	0.83	62.000736	0.86
02264710+6159238	36.696262	0.96	61.989952	0.99
02263903+6201298	36.662609	1.50	62.024940	1.65
02264000+6200545	36.666649	0.65	62.015137	0.66
02263131+6203075	36.630451	3.48	62.052086	3.44
02265124+6157513	36.713505	1.87	61.964245	1.86
02265582+6156379	36.732563	1.11	61.943851	1.12
02265210+6157362	36.717083	1.41	61.960068	1.39
02263059+6203152	36.627441	3.69	62.054234	3.90
02265019+6157577	36.709145	1.87	61.966015	1.77
02264340+6159382	36.680817	0.73	61.993931	0.83
02263700+6201129	36.654163	6.04	62.020256	5.51
02264755+6158192	36.698109	0.95	61.972008	0.96
02263974+6200109	36.665581	0.72	62.003033	0.70
02263447+6201342	36.643616	0.79	62.026169	0.78
02263626+6200559	36.651093	1.18	62.015522	1.16
02264177+6159402	36.674049	1.28	61.994495	1.31
02262984+6202441	36.624340	1.77	62.045589	1.52
02262016+6205106	36.583988	2.51	62.086273	2.33
02264207+6159243	36.675278	2.06	61.990089	1.85
02262754+6203108	36.614742	3.30	62.053005	3.17
02262015+6205106	36.583969	2.90	62.086277	2.88
02263487+6201107	36.645279	1.39	62.019642	1.43
02263911+6200006	36.662975	1.08	62.000172	1.08
02263613+6200468	36.650528	1.92	62.013004	1.94
02264007+6159453	36.666950	1.66	61.995907	1.69
02262284+6204130	36.595158	2.46	62.070282	2.57
02264298+6158535	36.679089	1.58	61.981522	1.65
02262198+6204219	36.591591	1.54	62.072754	1.65
02263826+6159587	36.659424	1.31	61.999649	1.42
02263546+6200378	36.647755	1.99	62.010502	2.06
02264176+6158503	36.674004	0.62	61.980648	0.59
02262208+6204082	36.592018	4.33	62.068935	4.68
02263629+6200228	36.651199	3.34	62.006340	3.27
02261795+6204595	36.574806	0.43	62.083206	0.42
02263238+6201144	36.634914	2.44	62.020657	2.31
02263867+6159406	36.661110	1.95	61.994610	2.00
02264479+6157563	36.686630	2.25	61.965633	2.08
02264892+6156541	36.703846	1.88	61.948353	2.01
02263509+6200286	36.646210	1.78	62.007942	1.76
02262053+6203573	36.585541	0.56	62.065926	0.59
02262221+6203481	36.592525	1.07	62.063354	1.09

TABLE 5—Continued

ID IRAC-	RA <sub>J2000</sub> [deg]	RA error $10^{-4}$ [deg]	DEC <sub>J2000</sub> [deg]	DEC error $10^{-4}$ [deg]
02262064+6204068	36.585991	0.75	62.068542	0.78
02262156+6203522	36.589840	0.92	62.064491	0.94
02262923+6201481	36.621777	0.40	62.030014	0.40
02263887+6159212	36.661957	1.25	61.989231	1.24
02262002+6203388	36.583420	0.27	62.060768	0.28
02264367+6157567	36.681976	1.02	61.965744	1.02
02264451+6157367	36.685448	2.66	61.960186	2.33
02264288+6157568	36.678658	1.90	61.965778	1.90
02263081+6201025	36.628357	1.92	62.017365	1.84
02263648+6159324	36.652008	2.23	61.992340	2.44
02263111+6200553	36.629620	1.99	62.015350	2.09
02262779+6201395	36.615810	1.60	62.027645	1.79
02263351+6200061	36.639633	1.80	62.001694	1.89
02264716+6156281	36.696507	2.23	61.941135	2.16
02262460+6202206	36.602512	1.52	62.039051	1.74
02264094+6157557	36.670597	1.35	61.965462	1.50
02264327+6157180	36.680298	1.04	61.955002	1.05
02264186+6157374	36.674408	2.20	61.960377	2.26
02263532+6159162	36.647175	1.53	61.987839	1.60
02263634+6159002	36.651421	3.04	61.983398	2.88
02261768+6203533	36.573673	3.44	62.064819	3.63
02264374+6157020	36.682247	1.75	61.950546	1.98
02261312+6204548	36.554668	3.02	62.081898	2.91
02263089+6200123	36.628719	2.08	62.003429	2.06
02263265+6159390	36.636040	4.43	61.994171	3.12
02263645+6158422	36.651855	2.04	61.978397	2.27
02262824+6200461	36.617680	1.31	62.012794	1.33
02263265+6159390	36.636051	2.22	61.994171	2.41
02263695+6158253	36.653969	0.89	61.973694	0.99
02262584+6201141	36.607647	1.97	62.020576	1.97
02263477+6158522	36.644855	1.29	61.981155	1.31
02263597+6158349	36.649887	2.12	61.976360	2.20
02264017+6157233	36.667385	0.66	61.956478	0.68
02263977+6157249	36.665695	0.66	61.956909	0.67
02262906+6200162	36.621078	1.39	62.004505	1.41
02262962+6200067	36.623421	1.56	62.001865	1.59
02263204+6159304	36.633484	2.83	61.991768	3.03
02261582+6203423	36.565907	7.35	62.061756	7.45
02263313+6158556	36.638035	0.72	61.982124	0.78
02262453+6201150	36.602200	1.52	62.020844	1.58
02263072+6159361	36.628014	1.18	61.993362	1.27
02263828+6157376	36.659508	1.02	61.960442	1.04
02262992+6159417	36.624687	5.48	61.994930	5.11
02262339+6201159	36.597473	6.28	62.021088	7.05
02263099+6159162	36.629112	3.54	61.987827	3.28
02262659+6200126	36.610809	1.13	62.003498	1.18
02262679+6200087	36.611645	1.28	62.002426	1.33
02260909+6204451	36.537888	6.82	62.079201	6.46
02262691+6200036	36.612110	1.90	62.001007	1.94
02263154+6158508	36.631401	2.36	61.980770	2.51
02261586+6202379	36.566078	6.78	62.043861	7.65
02262435+6200298	36.601448	2.38	62.008282	2.30
02261008+6203539	36.542019	5.68	62.064960	5.79
02261113+6203319	36.546360	3.74	62.058861	3.73
02263768+6156392	36.657013	1.31	61.944225	1.32
02261008+6203502	36.542004	6.24	62.063934	6.58
02263269+6157570	36.636223	1.69	61.965843	1.87
02261202+6203161	36.550064	1.05	62.054482	1.06

TABLE 5—Continued

ID IRAC-	RA <sub>J2000</sub> [deg]	RA error $10^{-4}$ [deg]	DEC <sub>J2000</sub> [deg]	DEC error $10^{-4}$ [deg]
02262838+6159025	36.618248	3.24	61.984032	3.05
02261734+6201385	36.572254	6.22	62.027363	6.84
02262752+6159097	36.614651	3.06	61.986019	3.06
02260861+6204033	36.535892	3.52	62.067593	3.62
02261013+6203366	36.542225	1.40	62.060158	1.39
02261052+6203303	36.543831	0.94	62.058414	0.96
02263236+6157458	36.634819	2.66	61.962730	2.49
02262696+6159079	36.612316	0.95	61.985519	0.96
02262234+6200137	36.593098	0.97	62.003815	1.05
02263130+6157478	36.630428	3.25	61.963284	3.16
02262853+6158187	36.618858	0.90	61.971859	0.89
02260643+6204078	36.526806	4.97	62.068821	4.84
02260732+6203433	36.530510	2.05	62.062019	2.11
02263175+6157306	36.632278	2.73	61.958488	2.91
02262478+6159141	36.603256	0.66	61.987259	0.68
02261626+6201284	36.567768	4.48	62.024544	4.87
02260836+6203245	36.534851	0.50	62.056801	0.51
02260536+6204052	36.522316	0.76	62.068115	0.78
02260671+6203259	36.527969	3.31	62.057201	3.42
02262166+6159323	36.590260	1.66	61.992294	1.79
02260728+6203143	36.530346	5.05	62.053967	4.99
02260783+6203009	36.532642	0.61	62.050243	0.62
02261314+6201390	36.554729	4.11	62.027500	4.35
02262034+6159450	36.584766	1.00	61.995838	1.02
02260516+6203287	36.521511	3.63	62.057972	3.74
02262796+6157322	36.616486	1.15	61.958935	1.18
02261792+6200067	36.574650	2.00	62.001865	2.13
02260364+6203428	36.515186	6.42	62.061882	6.07
02262088+6159068	36.586994	2.30	61.985210	2.31
02261410+6200439	36.558743	2.35	62.012188	2.34
02260273+6203383	36.511391	5.38	62.060650	5.29
02260720+6202266	36.529999	7.25	62.040718	7.14
02261544+6200211	36.564346	1.99	62.005852	2.00
02260332+6203289	36.513847	4.63	62.058022	4.66
02260500+6202511	36.520821	0.50	62.047527	0.51
02260158+6203460	36.506577	1.89	62.062775	1.89
02260688+6202186	36.528656	5.35	62.038502	5.21
02261971+6158561	36.582123	1.08	61.982254	1.10
02260720+6202110	36.530014	5.89	62.036377	6.23
02260222+6203283	36.509258	7.22	62.057858	7.61
02260251+6203171	36.510445	1.62	62.054737	1.75
02261717+6159237	36.571560	0.84	61.989914	0.81
02261771+6159155	36.573807	0.67	61.987633	0.69
02262246+6157547	36.593582	1.46	61.965191	1.35
02260424+6202377	36.517670	5.61	62.043819	5.81
02260672+6201592	36.528019	3.75	62.033119	3.85
02260051+6203191	36.502117	9.31	62.055294	9.85
02260099+6203083	36.504139	1.70	62.052303	1.80
02260121+6202243	36.505024	0.41	62.040092	0.43
02261161+6159551	36.548382	0.98	61.998638	1.00
02262195+6157068	36.591454	2.66	61.951885	2.60
02260240+6201596	36.510014	5.35	62.033211	6.10
02255814+6203025	36.492268	6.66	62.050694	6.61
02260196+6202040	36.508171	3.50	62.034431	3.84
02261251+6159187	36.552143	2.83	61.988541	2.72
02261109+6159382	36.546188	2.54	61.993958	2.45
02255901+6201599	36.495857	3.49	62.033318	3.51
02255913+6202366	36.496380	2.55	62.043491	2.55

TABLE 5—*Continued*

ID IRAC-	RA <sub>J2000</sub> [deg]	RA error $10^{-4}$ [deg]	DEC <sub>J2000</sub> [deg]	DEC error $10^{-4}$ [deg]
02260892+6159322	36.537155	1.05	61.992275	1.17
02255696+6202370	36.487343	7.45	62.043606	8.23
02261901+6156250	36.579205	2.06	61.940285	1.95
02255828+6201436	36.492817	4.57	62.028790	4.61
02255812+6201380	36.492149	7.19	62.027218	7.72
02260332+6200131	36.513851	1.17	62.003643	1.24
02260697+6159122	36.529022	2.11	61.986710	2.31
02261924+6155512	36.580158	1.03	61.930901	0.97
02260544+6158246	36.522675	0.35	61.973492	0.41
02260292+6158565	36.512161	0.60	61.982368	0.60
02260237+6158308	36.509884	0.49	61.975220	0.52
02260187+6158348	36.507786	0.64	61.976341	0.65
02260760+6156491	36.531658	1.15	61.946983	1.16
02260445+6157348	36.518532	4.54	61.959667	5.16
02255760+6158528	36.490013	4.85	61.981339	5.00
02262573+6203558	36.607193	0.31	62.065487	0.32

TABLE 6  
CLUSTER MEMBER CANDIDATES: IRAC SOURCES WITH EXCESS WITHOUT X-RAY COUNTERPART.

ID IRAC-	$F_V$ [mJy]	$F_I$ [mJy]	$F_J$ [mJy]	$F_H$ [mJy]	$F_K$ [mJy]	$F_{3.6\mu m}$ [mJy]	$F_{4.5\mu m}$ [mJy]	$F_{5.8\mu m}$ [mJy]	$F_{8.0\mu m}$ [mJy]
02270033+6205291	...	...	...	...	...	1.1322± 0.0061	2.5148± 0.0115	3.2495± 0.0278	...
02271605+6200506	1.0782	14.5794	208.2036	371.7919	619.3419	114.7894± 0.3332	120.9486± 0.3271	115.4599± 0.3373	73.2051± 0.3046
02271147+6201578	0.0135	0.1829	0.9088	1.6684	2.2487	3.1107± 0.0106	3.0494± 0.0110	2.9472± 0.0231	...
02271512+6200152	4.7239	24.0846	65.8398	68.9128	60.2463	32.1743± 0.0982	25.1779± 0.0725	17.0157± 0.0942	13.6489± 0.1281
02271175+6158265	...	...	...	...	...	5.8413± 0.0213	4.9457± 0.0146	3.6184± 0.0390	...
02270991+6158521	...	...	...	...	...	0.9234± 0.0072	0.7527± 0.0044	...	...
02264351+6205302	...	...	...	...	...	0.2417± 0.0040	0.6026± 0.0054	...	...
02264566+6204469	...	...	...	...	...	2.9971± 0.0102	3.9269± 0.0142	5.7818± 0.0314	9.6677± 0.0823
02270243+6200092	...	...	...	...	...	1.4936± 0.0078	1.6670± 0.0078	...	...
02263985+6205356	...	...	...	...	...	0.2056± 0.0044	0.1769± 0.0040	1.1781± 0.0321	4.1815± 0.0902
02264926+6203131	...	...	...	...	...	0.7340± 0.0056	0.7211± 0.0055	...	...
02265258+6202179	...	...	...	...	...	0.3259± 0.0034	0.2680± 0.0028	...	...
02271166+6157119	...	...	0.7219	2.4791	4.1680	4.4564± 0.0301	4.2144± 0.0144	4.7192± 0.0632	7.7456± 0.0921
02265704+6200587	0.0638	0.6603	...	...	...	0.3038± 0.0032	1.8281± 0.0080	...	...
02265770+6200430	...	...	0.5182	0.9870	1.4452	1.3448± 0.0062	1.3567± 0.0068	...	...
02264230+6204412	0.1519	0.5831	1.1028	1.1332	1.0862	0.3573± 0.0037	0.2871± 0.0045	...	...
02263648+6206069	...	...	0.4116	1.0922	1.3675	0.9180± 0.0064	0.7264± 0.0097	...	...
02265787+6200283	...	...	...	...	...	1.0901± 0.0057	1.0188± 0.0056	...	...
02264396+6204054	...	...	0.7771	1.1437	1.4188	0.1594± 0.0036	1.5840± 0.0080	2.0186± 0.0227	5.0414± 0.1463
02270190+6159131	0.0070	0.0562	1.4945	4.3883	7.0458	0.0913± 0.0030	0.1015± 0.0023	0.7040± 0.0215	10.3649± 0.0671
02264299+6204100	...	...	0.7771	1.1437	1.4188	0.1747± 0.0034	1.5840± 0.0080	2.0186± 0.0227	...
02270071+6159226	0.0055	0.1466	1.4945	4.3883	7.0458	12.9481± 0.0356	12.8656± 0.0319	11.3601± 0.0516	10.3649± 0.0671
02264101+6204364	...	...	...	...	...	0.3751± 0.0038	0.2986± 0.0046	...	...
02270217+6158583	...	...	...	...	...	0.3629± 0.0037	0.3519± 0.0028	...	...
02265433+6200584	...	...	...	...	...	0.4440± 0.0031	0.5713± 0.0038	...	...
02265824+6159566	...	...	...	...	...	0.4176± 0.0042	0.3879± 0.0037	...	...
02270838+6157024	...	...	1.0827	2.3243	3.4350	2.9657± 0.0202	2.5692± 0.0099	5.4853± 0.0739	10.7988± 0.1144
02265430+6200448	...	...	...	...	...	0.2902± 0.0027	0.2594± 0.0032	...	...
02265398+6200396	0.0069	0.1223	1.0532	2.1994	2.7538	2.9922± 0.0091	2.8251± 0.0097	2.6693± 0.0187	...
02270091+6158478	...	...	...	...	...	1.6611± 0.0073	1.4743± 0.0053	1.8180± 0.0259	2.5138± 0.0433
02265046+6201324	...	...	...	...	...	0.3612± 0.0026	0.3203± 0.0025	...	...
02263797+6204378	...	...	...	...	...	0.0850± 0.0024	0.1037± 0.0033	1.1155± 0.0174	3.2505± 0.0565
02270433+6157363	...	...	...	...	...	0.6679± 0.0050	0.5297± 0.0032	...	...
02264423+6202464	0.0083	0.0955	0.5682	1.0430	1.4452	1.5279± 0.0067	1.5049± 0.0067	...	...
02265682+6159142	...	...	...	...	...	0.3152± 0.0033	0.3390± 0.0030	...	...
02264970+6200588	...	...	...	...	...	0.7750± 0.0035	0.7667± 0.0041	...	...
02265782+6158377	...	...	...	...	...	0.2599± 0.0030	0.2043± 0.0023	...	...
02264197+6202428	0.0329	0.2440	0.9605	1.4398	1.3550	0.9778± 0.0052	0.7951± 0.0049	...	...
02264781+6201123	0.0430	0.2420	0.8289	1.3877	1.1586	0.6609± 0.0030	0.5686± 0.0034	...	...
02262952+6205518	...	...	...	...	...	1.5544± 0.0070	1.2223± 0.0111	...	...
02264605+6201221	...	...	0.5278	0.9001	1.2472	1.6131± 0.0055	1.7954± 0.0062	1.8337± 0.0159	...
02264800+6200576	...	...	...	...	...	0.2545± 0.0022	0.2810± 0.0028	...	...
02270253+6157046	...	...	...	...	...	2.3996± 0.0129	2.6206± 0.0094	2.9853± 0.0333	...
02264766+6200592	...	...	...	...	...	0.2986± 0.0023	0.2810± 0.0028	...	...

TABLE 6—Continued

ID IRAC-	$F_V$ [mJy]	$F_I$ [mJy]	$F_J$ [mJy]	$F_H$ [mJy]	$F_K$ [mJy]	$F_{3.6\mu m}$ [mJy]	$F_{4.5\mu m}$ [mJy]	$F_{5.8\mu m}$ [mJy]	$F_{8.0\mu m}$ [mJy]
02265560+6158517	...	...	...	...	...	$0.7130 \pm 0.0047$	$0.7645 \pm 0.0042$	...	...
02264441+6201480	...	...	...	...	...	$0.5392 \pm 0.0035$	$0.5130 \pm 0.0031$	...	...
02264808+6200490	...	...	...	...	...	$0.3853 \pm 0.0027$	$0.3869 \pm 0.0033$	...	...
02264515+6201320	...	...	...	...	...	$0.2945 \pm 0.0027$	$0.3002 \pm 0.0027$	...	...
02264675+6201026	...	...	...	...	...	$0.3209 \pm 0.0023$	$0.2966 \pm 0.0029$	...	...
02262986+6205201	...	...	...	...	...	$0.4352 \pm 0.0040$	$0.3355 \pm 0.0055$	...	...
02265324+6159124	...	...	...	...	...	$0.5591 \pm 0.0043$	$0.5709 \pm 0.0043$	...	...
02265657+6158167	...	...	...	...	...	$0.6259 \pm 0.0045$	$0.7301 \pm 0.0036$	...	...
02264334+6201432	...	...	...	...	...	$0.4581 \pm 0.0034$	$0.4789 \pm 0.0032$	...	...
02265922+6157289	...	...	...	...	...	$0.3819 \pm 0.0043$	$0.3769 \pm 0.0033$	...	...
02263045+6204552	...	...	...	...	...	$0.5832 \pm 0.0042$	$0.6505 \pm 0.0051$	...	...
02265139+6159252	...	...	...	...	...	$0.4157 \pm 0.0038$	$0.3686 \pm 0.0038$	...	...
02264472+6201039	0.0082	0.0888	0.7700	1.4006	1.4320	$0.3808 \pm 0.0026$	$0.6646 \pm 0.0039$	...	...
02264531+6200544	...	...	...	...	...	$0.4492 \pm 0.0028$	$0.3880 \pm 0.0033$	...	...
02264994+6159423	0.0187	0.1846	0.9517	1.7151	2.5347	$2.6454 \pm 0.0099$	$2.6729 \pm 0.0102$	$2.5890 \pm 0.0241$	...
02263066+6204411	...	...	...	...	...	$0.1317 \pm 0.0035$	$0.5479 \pm 0.0055$	$0.8783 \pm 0.0238$	$2.9487 \pm 0.0738$
02264856+6159576	...	...	...	...	...	$0.4194 \pm 0.0037$	$0.4477 \pm 0.0042$	...	...
02265062+6159144	...	...	...	...	...	$0.3730 \pm 0.0042$	$0.4472 \pm 0.0045$	...	...
02264573+6200251	...	...	...	...	...	$1.6670 \pm 0.0065$	$1.7589 \pm 0.0081$	...	...
02262962+6204414	...	...	...	...	...	$0.6951 \pm 0.0052$	$0.5479 \pm 0.0055$	$1.0059 \pm 0.0232$	$2.6124 \pm 0.0742$
02264771+6159550	...	...	...	...	...	$0.4285 \pm 0.0038$	$0.4243 \pm 0.0041$	...	...
02263241+6203518	...	...	...	...	...	$0.2816 \pm 0.0037$	$0.2276 \pm 0.0052$	...	...
02265343+6158188	...	...	...	...	...	$0.4346 \pm 0.0044$	$0.4339 \pm 0.0034$	$1.5626 \pm 0.0285$	$4.7288 \pm 0.1079$
02264572+6200131	...	...	0.4597	0.9513	1.1270	$0.9096 \pm 0.0049$	$0.8315 \pm 0.0055$	...	...
02262883+6204365	...	...	...	...	...	$1.3879 \pm 0.0069$	$1.2490 \pm 0.0078$	$0.8842 \pm 0.0240$	$2.8353 \pm 0.0777$
02264107+6201211	...	...	0.4193	0.7768	0.8316	$0.3998 \pm 0.0032$	$0.3525 \pm 0.0030$	...	...
02263081+6203502	...	...	...	...	...	$0.5500 \pm 0.0042$	$0.5242 \pm 0.0061$	...	...
02263152+6203331	...	...	...	...	...	$0.4891 \pm 0.0044$	$0.6510 \pm 0.0066$	$1.1556 \pm 0.0232$	$3.3895 \pm 0.0750$
02263839+6201459	0.0112	0.0955	0.8600	1.5787	1.7536	$1.9403 \pm 0.0081$	$2.0079 \pm 0.0080$	$2.1839 \pm 0.0240$	...
02264099+6201076	...	...	...	...	...	$0.2686 \pm 0.0027$	$0.2307 \pm 0.0028$	$0.5198 \pm 0.0171$	...
02264433+6200027	0.0053	0.0871	...	...	...	$1.7493 \pm 0.0078$	$1.7628 \pm 0.0093$	$1.8581 \pm 0.0220$	...
02264710+6159238	...	...	0.4903	0.9339	1.0566	$1.5201 \pm 0.0074$	$1.3953 \pm 0.0075$	...	...
02263903+6201298	...	...	...	...	...	$0.5909 \pm 0.0042$	$0.5682 \pm 0.0038$	...	...
02264000+6200545	0.0469	0.3990	1.5649	2.6934	2.8050	$2.0901 \pm 0.0075$	$1.6640 \pm 0.0071$	$1.4413 \pm 0.0179$	...
02263131+6203075	...	...	...	...	...	$0.3385 \pm 0.0047$	$0.2731 \pm 0.0052$	$1.8542 \pm 0.0286$	$4.6085 \pm 0.0894$
02265124+6157513	...	...	...	...	...	$0.5511 \pm 0.0046$	$1.0128 \pm 0.0048$	$2.2065 \pm 0.0297$	...
02265582+6156379	...	...	0.9874	2.7945	4.0173	$3.8364 \pm 0.0216$	$3.6225 \pm 0.0145$	$3.4824 \pm 0.0455$	...
02265210+6157362	...	...	...	...	...	$1.0676 \pm 0.0069$	$1.1947 \pm 0.0059$	...	...
02263059+6203152	...	...	...	...	...	$0.2461 \pm 0.0039$	$0.2731 \pm 0.0052$	...	$4.6085 \pm 0.0894$
02265019+6157577	...	...	...	...	...	$0.7673 \pm 0.0058$	$2.4466 \pm 0.0086$	$3.6252 \pm 0.0400$	$6.3521 \pm 0.1318$
02264340+6159382	0.0105	0.1963	1.1233	2.4339	3.2804	$2.9853 \pm 0.0130$	$2.6206 \pm 0.0117$	$2.4119 \pm 0.0272$	...
02263700+6201129	9.4515	22.5393	32.3958	32.3817	23.7646	$0.1898 \pm 0.0044$	$6.9279 \pm 0.0192$	$4.8630 \pm 0.0318$	...
02264755+6158192	...	...	...	...	...	$2.5710 \pm 0.0122$	$2.6324 \pm 0.0101$	$2.5284 \pm 0.0346$	...
02263974+6200109	...	...	...	...	...	$2.5308 \pm 0.0098$	$3.1690 \pm 0.0124$	$3.9149 \pm 0.0285$	$4.7998 \pm 0.0644$

TABLE 6—Continued

ID IRAC-	F <sub>V</sub> [mJy]	F <sub>I</sub> [mJy]	F <sub>J</sub> [mJy]	F <sub>H</sub> [mJy]	F <sub>K</sub> [mJy]	F <sub>3.6μm</sub> [mJy]	F <sub>4.5μm</sub> [mJy]	F <sub>5.8μm</sub> [mJy]	F <sub>8.0μm</sub> [mJy]
02263447+6201342	0.0277	0.1945	0.8841	2.0059	2.7538	3.1606± 0.0126	3.1403± 0.0114	2.5245± 0.0296	...
02263626+6200559	...	...	0.9172	1.5642	1.5415	1.1841± 0.0066	1.2925± 0.0064	1.7397± 0.0252	...
02264177+6159402	...	...	...	...	...	1.1450± 0.0071	1.1868± 0.0076	...	...
02262984+6202441	...	...	...	...	...	1.1626± 0.0084	1.0860± 0.0081	...	...
02262016+6205106	...	...	...	...	...	0.5034± 0.0054	0.7308± 0.0097	...	...
02264207+6159243	...	...	...	...	...	0.6869± 0.0058	0.6581± 0.0058	...	...
02262754+6203108	...	...	...	...	...	0.3134± 0.0043	0.3335± 0.0052	...	...
02262015+6205106	...	...	...	...	...	0.4433± 0.0054	0.7308± 0.0097	...	...
02263487+6201107	...	...	...	...	...	0.9331± 0.0061	1.1611± 0.0058	...	...
02263911+6200006	...	...	0.7153	1.6379	1.8532	1.3457± 0.0071	1.0751± 0.0073	...	...
02263613+6204048	...	...	...	...	...	0.5578± 0.0047	0.5769± 0.0047	...	...
02264007+6159453	...	...	...	...	...	0.7049± 0.0056	0.6423± 0.0059	...	...
02262284+6204130	...	...	...	...	...	0.3974± 0.0043	1.0860± 0.0080	0.9339± 0.0282	...
02264298+6158535	...	...	...	...	...	1.2439± 0.0093	0.9733± 0.0087	...	...
02262198+6204219	...	...	...	...	...	0.8247± 0.0062	1.6472± 0.0099	3.1194± 0.0345	4.3314± 0.0893
02263826+6159587	...	...	...	...	...	0.8560± 0.0057	0.8832± 0.0067	...	...
02263546+6200378	...	...	...	...	...	0.5604± 0.0051	1.3893± 0.0527	...	...
02264176+6158503	0.3250	3.2340	14.9447	20.0586	20.3203	11.8413± 0.0409	9.6443± 0.0325	6.1742± 0.0533	5.1923± 0.0950
02262208+6204082	...	...	...	...	...	0.1953± 0.0037	1.0860± 0.0080	1.3278± 0.0269	...
02263629+6200228	...	...	...	...	...	0.2659± 0.0038	0.2134± 0.0037	...	...
02261795+6204595	...	...	0.4683	2.7688	9.0351	23.8100± 0.0691	27.5791± 0.0982	30.0783± 0.1176	39.9704± 0.2739
02263238+6201144	...	...	...	...	...	0.4419± 0.0047	0.5836± 0.0044	...	...
02263867+6159406	...	...	...	...	...	0.5894± 0.0052	0.5249± 0.0054	...	...
02264479+6157563	...	...	...	...	...	0.7060± 0.0064	0.5890± 0.0045	...	...
02264892+6156541	...	...	...	...	...	0.8183± 0.0072	0.8240± 0.0055	...	...
02263509+6200286	...	...	...	...	...	0.6055± 0.0049	1.3893± 0.0527	...	...
02262053+6203573	...	...	...	...	...	4.9667± 0.0167	10.5435± 0.0341	11.1644± 0.0564	7.5089± 0.1310
02262221+6203481	...	...	...	...	...	1.2977± 0.0069	1.6779± 0.0103	1.9198± 0.0308	...
02262064+6204068	...	...	...	...	...	2.2615± 0.0094	2.2984± 0.0123	3.8170± 0.0344	5.3205± 0.0860
02262156+6203522	...	...	...	...	...	1.8208± 0.0085	2.2895± 0.0131	1.7701± 0.0287	6.1874± 0.0949
02262923+6201481	2.2861	7.2400	14.2721	15.9331	18.3624	28.9716± 0.0806	33.0731± 0.0845	40.2055± 0.1310	70.2564± 0.2307
02263887+6159212	0.0084	0.1920	0.8679	1.3253	1.2021	1.5005± 0.0092	1.1848± 0.0078	...	...
02262002+6203388	...	...	2.3905	27.6885	72.4320	78.6876± 0.1837	61.2945± 0.1576	56.3894± 0.1576	30.7101± 0.1904
02264367+6157567	...	...	...	...	...	2.5847± 0.0130	2.6986± 0.0103	...	...
02264451+6157367	...	...	...	...	...	0.5834± 0.0058	0.5939± 0.0042	...	2.1519± 0.0602
02264288+6157568	...	...	...	...	...	0.8964± 0.0078	0.9654± 0.0059	...	...
02263081+6201025	...	...	...	...	...	0.6617± 0.0056	0.6288± 0.0047	...	...
02263648+6159324	...	...	...	...	...	0.4306± 0.0044	0.3951± 0.0050	...	...
02263111+6200553	...	...	...	...	...	0.5164± 0.0046	0.4298± 0.0039	...	...
02262779+6201395	0.0084	0.0779	0.5230	0.8517	0.9816	0.9453± 0.0075	1.0405± 0.0071	...	...
02263351+6200061	...	...	...	...	...	0.5266± 0.0042	0.4467± 0.0046	...	...
02264716+6156281	...	...	...	...	...	1.0911± 0.0106	0.9472± 0.0072	...	...
02262460+6202206	...	...	0.4597	0.8919	0.9288	1.1577± 0.0089	1.2945± 0.0089	...	...
02264094+6157557	0.0059	0.0812	0.5787	1.1228	1.3550	1.2351± 0.0083	1.3034± 0.0068	...	...

TABLE 6—Continued

ID IRAC-	$F_V$ [mJy]	$F_I$ [mJy]	$F_J$ [mJy]	$F_H$ [mJy]	$F_K$ [mJy]	$F_{3.6\mu m}$ [mJy]	$F_{4.5\mu m}$ [mJy]	$F_{5.8\mu m}$ [mJy]	$F_{8.0\mu m}$ [mJy]
02264327+6157180	...	...	0.4949	1.2311	2.2077	$2.4789 \pm 0.0125$	$2.4308 \pm 0.0091$	...	$3.2091 \pm 0.0582$
02264186+6157374	...	...	...	...	...	$0.7139 \pm 0.0069$	$0.8873 \pm 0.0052$	$1.0538 \pm 0.0330$	...
02263532+6159162	0.0099	0.1269	0.5182	0.9601	0.9816	$0.9567 \pm 0.0070$	$0.8593 \pm 0.0067$	...	...
02263634+6159002	...	...	...	...	...	$0.3999 \pm 0.0053$	$0.3927 \pm 0.0051$	...	...
02261768+6203533	...	...	...	...	...	$0.2805 \pm 0.0043$	$0.2406 \pm 0.0054$	$1.7622 \pm 0.0323$	...
02264374+6157020	...	...	...	...	...	$0.7585 \pm 0.0065$	$0.8179 \pm 0.0050$	...	...
02261312+6204548	...	...	...	...	...	$0.5705 \pm 0.0072$	$0.4693 \pm 0.0129$	...	...
02263089+6200123	...	...	...	...	...	$0.4307 \pm 0.0039$	$0.4393 \pm 0.0042$	...	...
02263265+6159390	...	...	...	...	...	$0.3687 \pm 0.0071$	$0.3932 \pm 0.0046$	$1.1292 \pm 0.0233$	...
02263645+6158422	...	...	...	...	...	$0.6141 \pm 0.0061$	$0.5518 \pm 0.0055$	...	...
02262824+6200461	...	...	0.9088	1.4006	1.4721	$1.0333 \pm 0.0065$	$0.8698 \pm 0.0048$	...	...
02263265+6159390	...	...	...	...	...	$0.3789 \pm 0.0040$	$0.3932 \pm 0.0046$	$1.1292 \pm 0.0233$	...
02263695+6158253	0.0236	0.2621	0.8213	1.5499	1.6902	$2.4104 \pm 0.0117$	$3.1383 \pm 0.0124$	$4.2613 \pm 0.0395$	$5.8038 \pm 0.0695$
02262584+6201141	0.0491	0.1124	...	...	...	$0.6725 \pm 0.0063$	$0.6281 \pm 0.0047$	...	...
02263477+6158522	0.0317	0.2947	1.0058	1.7310	1.8027	$1.4153 \pm 0.0088$	$1.2273 \pm 0.0072$	...	...
02263597+6158349	...	...	...	...	...	$0.6059 \pm 0.0060$	$0.5084 \pm 0.0051$	...	...
02264017+6157233	0.0094	0.2460	...	...	...	$5.9696 \pm 0.0226$	$6.7352 \pm 0.0186$	$6.1761 \pm 0.0499$	$8.6252 \pm 0.0673$
02263977+6157249	...	...	...	...	...	$6.1626 \pm 0.0233$	$6.3498 \pm 0.0178$	$6.1761 \pm 0.0499$	$7.9043 \pm 0.1243$
02262906+6200162	...	...	...	...	...	$0.8212 \pm 0.0054$	$0.9126 \pm 0.0050$	...	...
02262962+6200067	...	...	...	...	...	$0.5599 \pm 0.0041$	$0.4798 \pm 0.0039$	...	...
02263204+6159304	...	...	...	...	...	$0.3158 \pm 0.0040$	$0.2678 \pm 0.0041$	...	...
02261582+6203423	...	...	...	...	...	$0.1230 \pm 0.0038$	$0.1631 \pm 0.0054$	$1.1693 \pm 0.0319$	...
02263313+6158556	...	...	0.7843	1.6994	2.3765	$3.2899 \pm 0.0143$	$3.0583 \pm 0.0123$	$3.2701 \pm 0.0381$	$3.6499 \pm 0.0749$
02262453+6201150	...	...	...	...	...	$0.8418 \pm 0.0062$	$0.8180 \pm 0.0053$	...	$2.2564 \pm 0.0576$
02263072+6159361	...	...	...	...	...	$0.8587 \pm 0.0051$	$0.8599 \pm 0.0058$	...	...
02263828+6157376	...	...	...	...	...	$1.7982 \pm 0.0090$	$1.9536 \pm 0.0073$	...	...
02262992+6159417	...	...	...	...	...	$0.1168 \pm 0.0026$	$0.8599 \pm 0.0058$	...	...
02262339+6201159	...	...	...	...	...	$0.1532 \pm 0.0042$	$0.8180 \pm 0.0053$	...	$2.2564 \pm 0.0576$
02263099+6159162	...	...	...	...	...	$0.2826 \pm 0.0035$	$0.2911 \pm 0.0039$	...	...
02262659+6200126	...	...	0.4472	0.8209	0.9726	$0.7265 \pm 0.0042$	$0.6790 \pm 0.0040$	...	$3.1943 \pm 0.0930$
02262679+6200087	...	...	...	...	...	$0.6584 \pm 0.0041$	$0.6758 \pm 0.0040$	...	$3.1943 \pm 0.0930$
02260909+6204451	6.2503	12.8629	16.8457	15.0765	11.0645	$0.1951 \pm 0.0054$	$0.1966 \pm 0.0081$	$1.3239 \pm 0.0405$	...
02262691+6200036	...	...	...	...	...	$0.3681 \pm 0.0032$	$0.2883 \pm 0.0031$	...	$3.1943 \pm 0.0930$
02263154+6158508	...	...	...	...	...	$0.4468 \pm 0.0048$	$0.3908 \pm 0.0042$	...	...
02261586+6202379	0.2881	0.8809	1.6691	1.6838	1.2940	$0.1532 \pm 0.0047$	$0.4096 \pm 0.0053$	$1.5166 \pm 0.0325$	$4.5562 \pm 0.1020$
02262435+6200298	...	...	...	...	...	$0.3720 \pm 0.0038$	$0.3320 \pm 0.0029$	$0.6375 \pm 0.0187$	...
02261008+6203539	...	...	...	...	...	$0.1660 \pm 0.0039$	$0.1618 \pm 0.0045$	$1.0900 \pm 0.0332$	$3.8531 \pm 0.0957$
02261113+6203319	...	...	...	...	...	$0.2360 \pm 0.0036$	$1.7134 \pm 0.0089$	$2.3748 \pm 0.0414$	$4.4231 \pm 0.1010$
02263768+6156392	...	...	...	...	...	$0.9853 \pm 0.0061$	$1.1660 \pm 0.0050$	...	...
02261008+6203502	...	...	...	...	...	$0.1482 \pm 0.0039$	$0.2660 \pm 0.0048$	$1.0900 \pm 0.0332$	$3.8531 \pm 0.0957$
02263269+6157570	...	...	...	...	...	$0.5458 \pm 0.0045$	$0.5785 \pm 0.0040$	...	...
02261202+6203161	0.0058	0.0976	0.5787	1.3499	1.3180	$1.2772 \pm 0.0063$	$1.0702 \pm 0.0071$	$1.6976 \pm 0.0301$	$3.9290 \pm 0.1058$
02262838+6159025	...	...	...	...	...	$0.2540 \pm 0.0035$	$0.2435 \pm 0.0036$	...	...
02261734+6201385	...	...	...	...	...	$0.1603 \pm 0.0045$	$0.1610 \pm 0.0041$	$1.3914 \pm 0.0325$	$2.7830 \pm 0.0803$

TABLE 6—Continued

ID IRAC-	F <sub>V</sub> [mJy]	F <sub>I</sub> [mJy]	F <sub>J</sub> [mJy]	F <sub>H</sub> [mJy]	F <sub>K</sub> [mJy]	F <sub>3.6μm</sub> [mJy]	F <sub>4.5μm</sub> [mJy]	F <sub>5.8μm</sub> [mJy]	F <sub>8.0μm</sub> [mJy]
02262752+6159097	...	...	...	...	...	0.2403± 0.0032	1.1729± 0.0061	...	...
02260861+6204033	...	...	...	...	...	0.2620± 0.0039	0.2324± 0.0052	1.0900± 0.0332	3.8531± 0.0957
02261013+6203366	...	...	...	...	...	0.7799± 0.0051	0.7655± 0.0059	2.3748± 0.0414	4.4231± 0.1010
02261052+6203303	...	...	...	...	...	1.5524± 0.0071	1.7134± 0.0089	2.3748± 0.0414	4.4231± 0.1010
02263236+6157458	...	...	...	...	...	0.3491± 0.0040	0.2948± 0.0030	...	...
02262696+6159079	...	...	...	...	...	1.2155± 0.0059	1.1729± 0.0061	...	...
02262234+6200137	0.0141	0.1927	0.9343	1.6229	1.6290	1.0402± 0.0051	0.8892± 0.0040	...	...
02263130+6157478	0.0075	0.1373	...	...	...	0.2864± 0.0039	0.4399± 0.0037	...	...
02262853+6158187	...	...	0.7421	1.4006	1.7216	1.6876± 0.0077	1.5267± 0.0067	...	1.7791± 0.0511
02260643+6204078	0.0292	0.1870	...	...	...	0.1897± 0.0037	0.2321± 0.0053	1.0411± 0.0345	...
02260732+6203433	...	...	...	...	...	0.4693± 0.0043	0.5050± 0.0050	1.3748± 0.0319	3.0375± 0.0885
02263175+6157306	...	...	...	...	...	0.2886± 0.0036	0.2438± 0.0027	...	...
02262478+6159141	0.0130	0.2121	0.9343	1.8980	2.1278	2.3056± 0.0084	2.4457± 0.0093	2.7329± 0.0234	7.5838± 0.1242
02261626+6201284	...	...	...	...	...	0.2272± 0.0042	0.1772± 0.0039	1.3914± 0.0325	2.7830± 0.0803
02260836+6203245	...	...	...	...	...	4.0627± 0.0125	7.1245± 0.0217	10.2446± 0.0486	11.4201± 0.1098
02260536+6204052	...	...	...	...	...	2.1136± 0.0085	2.2984± 0.0121	2.9198± 0.0385	...
02260671+6203259	...	...	...	...	...	0.2355± 0.0033	0.1902± 0.0043	1.5196± 0.0297	6.7071± 0.1692
02262166+6159323	0.0062	0.0896	...	...	...	0.3410± 0.0027	0.3445± 0.0030	...	...
02260728+6203143	...	...	...	...	...	0.1602± 0.0034	0.1506± 0.0045	1.3532± 0.0290	...
02260783+6203009	...	...	...	...	...	2.2547± 0.0077	1.7539± 0.0085	1.4824± 0.0253	...
02261314+6201390	0.0079	0.0386	...	...	...	0.1908± 0.0034	0.1821± 0.0035	1.0832± 0.0226	...
02262034+6159450	...	...	0.4472	0.8676	1.0566	0.7596± 0.0037	0.7010± 0.0038	0.9912± 0.0141	...
02260516+6203287	...	...	...	...	...	0.2416± 0.0038	0.3165± 0.0089	1.5264± 0.0331	4.6667± 0.1059
02262796+6157322	...	...	...	...	...	0.9770± 0.0055	0.9757± 0.0049	...	...
02261792+6200067	...	...	...	...	...	0.3457± 0.0031	0.3507± 0.0028	...	1.6233± 0.0387
02260364+6203428	...	...	...	...	...	0.1755± 0.0045	0.1827± 0.0052	1.2573± 0.0352	7.4349± 0.1988
02262088+6159068	...	...	...	...	...	0.2691± 0.0027	0.2393± 0.0033	...	1.8166± 0.0446
02261410+6200439	...	...	...	...	...	0.4253± 0.0041	0.4601± 0.0040	...	4.3284± 0.1255
02260273+6203383	0.0055	0.0337	...	...	...	0.2077± 0.0046	0.1827± 0.0052	1.2573± 0.0352	7.4349± 0.1988
02260720+6202266	...	...	...	...	...	0.1196± 0.0034	0.1428± 0.0046	0.8767± 0.0295	11.4398± 0.1975
02261544+6200211	...	...	...	...	...	0.3785± 0.0034	0.4213± 0.0034	...	...
02260332+6203289	0.0055	0.0337	2.4802	2.5960	2.0698	0.2163± 0.0042	0.4454± 0.0061	1.1409± 0.0308	...
02260500+6202511	...	...	0.4310	1.8126	3.5639	3.3301± 0.0104	2.8004± 0.0121	2.0401± 0.0286	...
02260158+6203460	...	...	...	...	...	0.7639± 0.0065	0.6268± 0.0081	1.2035± 0.0397	...
02260688+6202186	...	...	...	...	...	0.1737± 0.0038	0.1428± 0.0046	0.8767± 0.0295	9.0404± 0.2089
02261971+6158561	...	...	...	...	...	0.7591± 0.0039	0.8145± 0.0052	...	1.8166± 0.0446
02260720+6202110	...	...	...	...	...	0.1508± 0.0037	0.1428± 0.0046	1.5108± 0.0288	9.0404± 0.2089
02260222+6203283	0.0055	0.0337	...	...	...	0.1444± 0.0043	0.2402± 0.0059	...	7.4349± 0.1988
02260251+6203171	...	...	...	...	...	0.8066± 0.0060	1.1166± 0.0082	...	...
02261717+6159237	...	...	...	...	...	1.0960± 0.0046	1.2796± 0.0056	1.3239± 0.0158	...
02261771+6159155	0.0144	0.1716	0.8600	1.5077	1.5846	1.5514± 0.0056	1.4802± 0.0062	1.7260± 0.0165	...
02262246+6157547	...	...	...	...	...	0.8648± 0.0055	0.7801± 0.0059	...	...
02260424+6202377	0.6019	1.6253	2.5497	2.6934	2.0134	0.1175± 0.0028	0.4738± 0.0055	...	...
02260672+6201592	0.0053	0.0203	...	...	...	0.2476± 0.0039	0.2143± 0.0046	...	...

TABLE 6—Continued

ID IRAC-	F <sub>V</sub> [mJy]	F <sub>I</sub> [mJy]	F <sub>J</sub> [mJy]	F <sub>H</sub> [mJy]	F <sub>K</sub> [mJy]	F <sub>3.6μm</sub> [mJy]	F <sub>4.5μm</sub> [mJy]	F <sub>5.8μm</sub> [mJy]	F <sub>8.0μm</sub> [mJy]
02260051+6203191	...	...	...	...	...	0.1288± 0.0052	0.2402± 0.0059	1.5577± 0.0449	7.6657± 0.1742
02260099+6203083	...	...	...	...	...	0.8496± 0.0064	0.8986± 0.0083	1.5577± 0.0449	...
02260121+6202243	...	...	...	...	...	9.0333± 0.0257	12.7470± 0.0413	10.6556± 0.0493	9.5227± 0.1033
02261161+6159551	...	...	...	...	...	1.2027± 0.0059	1.2767± 0.0058	1.1918± 0.0225	...
02262195+6157068	...	...	...	...	...	0.3738± 0.0043	0.3264± 0.0041	...	...
02260240+6201596	...	...	...	...	...	0.2106± 0.0050	0.3572± 0.0069	1.2955± 0.0406	...
02255814+6203025	...	...	...	...	...	0.2292± 0.0065	0.6331± 0.0088	2.1174± 0.0455	10.8974± 0.3045
02260196+6202040	...	...	...	...	...	0.3138± 0.0050	0.3572± 0.0069	1.2955± 0.0406	...
02261251+6159187	...	...	...	...	...	0.2380± 0.0029	0.2439± 0.0037	...	...
02261109+6159382	...	...	...	...	...	0.3016± 0.0033	0.2442± 0.0034	...	1.8659± 0.0490
02255901+6201599	...	...	...	...	...	0.4942± 0.0073	0.3879± 0.0075	...	11.3708± 0.2751
02255913+6202366	...	...	...	...	...	0.4211± 0.0047	3.8310± 0.0186	...	...
02260892+6159322	...	...	...	...	...	1.0353± 0.0055	0.9047± 0.0049	...	1.9645± 0.0529
02255696+6202370	0.0159	0.0876	...	...	...	0.1494± 0.0050	0.2666± 0.0071	1.9266± 0.0496	5.4014± 0.1621
02261901+6156250	...	...	...	...	...	0.5683± 0.0051	0.5864± 0.0040	...	...
02255828+6201436	...	...	...	...	...	0.2863± 0.0054	0.2670± 0.0060	...	...
02255812+6201380	...	...	...	...	...	0.1580± 0.0047	0.3130± 0.0054	2.5519± 0.0399	...
02260332+6200131	...	...	0.6230	1.5077	1.4721	1.2292± 0.0074	1.0504± 0.0061	...	...
02260697+6159122	...	...	...	...	...	0.3683± 0.0037	0.3210± 0.0038	...	...
02261924+6155512	0.0108	0.1588	0.8760	1.7151	2.0890	2.0353± 0.0101	1.8241± 0.0076	...	...
02260544+6158246	0.0503	0.7207	4.7697	10.5269	13.9293	15.0539± 0.0405	14.7727± 0.0407	14.1683± 0.0583	14.1716± 0.0996
02260292+6158565	0.0180	0.2583	1.5794	3.1791	3.9439	3.7649± 0.0128	3.6443± 0.0126	2.7984± 0.0284	...
02260237+6158308	0.0157	0.1800	1.1028	2.9262	3.8720	5.1391± 0.0161	4.9951± 0.0166	4.9207± 0.0335	4.6055± 0.0676
02260187+6158348	0.0158	0.2048	1.2204	2.8203	3.1618	3.0490± 0.0109	3.1087± 0.0118	3.2221± 0.0283	4.6055± 0.0676
02260760+6156491	...	...	0.4350	0.7556	1.0374	1.4878± 0.0084	1.4773± 0.0083	...	...
02260445+6157348	0.0183	0.1484	0.7771	0.9085	0.9035	0.2560± 0.0053	0.2295± 0.0044	...	...
02255760+6158528	0.4024	1.7384	3.6516	3.8575	3.0195	0.1809± 0.0038	0.9473± 0.0063	...	...
02262573+6203558	...	...	56.8183	485.6237	1354.9724	1536.7286± 3.6076	2204.5454± 5.3316	2234.8337± 5.0596	1363.9052± 3.4499

NOTE.—The IRAC flux errors refer to the covariance matrix calculated from the “best-fit” of the PRF to the data and do not include calibration uncertainty (~10% of the flux).

## REFERENCES

- Adams, F. C., Hollenbach, D., Laughlin, G., & Gorti, U. 2004, *ApJ*, 611, 360
- Allen, L. E., et al. 2004, *ApJS*, 154, 363
- Asplund, M., Grevesse, N., & Sauval, A. J. 2005, in *ASP Conf. Ser.* 336: Cosmic Abundances as Records of Stellar Evolution and Nucleosynthesis, ed. T. G. Barnes, III & F. N. Bash, 25
- Bally, J., Sutherland, R. S., Devine, D., & Johnstone, D. 1998, *AJ*, 116, 293
- Balog, Z., Muzerolle, J., Rieke, G. H., Su, K. Y. L., Young, E. T., & Megeath, S. T. 2007, *ApJ*, 660, 1532
- Binney, J., & Tremaine, S. 1987, Galactic dynamics, ed. S. Binney, J. & Tremaine
- Bonatto, C., Santos, Jr., J. F. C., & Bica, E. 2006, *A&A*, 445, 567
- Bouwman, J., Lawson, W. A., Dominik, C., Feigelson, E. D., Henning, T., Tielens, A. G. G. M., & Waters, L. B. F. M. 2006, *ApJ*, 653, L57
- Broos, P. S., Feigelson, E. D., Townsley, L. K., Getman, K. V., Wang, J., Garmire, G. P., Jiang, Z., & Tsuboi, Y. 2007, *ApJS*, 169, 353
- Broos, P. S., Townsley, L. K., Feigelson, E. D., Getman, K. V., Bauer, F. E., & Garmire, G. P. 2010, *ApJS*, submitted
- Brott, I., & Hauschildt, P. H. 2005, in *ESA Special Publication*, Vol. 576, The Three-Dimensional Universe with Gaia, ed. C. Turon, K. S. O'Flaherty, & M. A. C. Perryman, 565
- Cardelli, J. A., Clayton, G. C., & Mathis, J. S. 1989, *ApJ*, 345, 245
- Carpenter, J. M., Mamajek, E. E., Hillenbrand, L. A., & Meyer, M. R. 2006, *ApJ*, 651, L49
- Castelli, F., & Kurucz, R. L. 2003, in *IAU Symposium*, Vol. 210, Modelling of Stellar Atmospheres, ed. N. Piskunov, W. W. Weiss, & D. F. Gray, 20
- Chieffi, A., & Straniero, O. 1989, *ApJS*, 71, 47
- Clarke, C. J. 2007, *MNRAS*, 376, 1350
- Currie, T., et al. 2007, *ApJ*, 659, 599
- Dahm, S. E., & Hillenbrand, L. A. 2007, *AJ*, 133, 2072
- Damiani, F., Prisinzano, L., Micela, G., & Sciortino, S. 2006, *A&A*, 459, 477
- Degl'Innocenti, S., Prada Moroni, P. G., Marconi, M., & Ruoppo, A. 2008, *Ap&SS*, 316, 25
- Eisner, J. A., Plambeck, R. L., Carpenter, J. M., Corder, S. A., Qi, C., & Wilner, D. 2008, *ApJ*, 683, 304
- Evans, N. J., et al. 2009, *ApJS*, 181, 321
- Fang, M., van Boekel, R., Wang, W., Carmona, A., Sicilia-Aguilar, A., & Henning, T. 2009, *A&A*, 504, 461
- Fazio, G. G., et al. 2004, *ApJS*, 154, 10
- Fedele, D., van den Ancker, M. E., Henning, T., Jayawardhana, R., & Oliveira, J. M. 2010, *A&A*, 510, A72+
- Feigelson, E., Townsley, L., Güdel, M., & Stassun, K. 2007, in *Protostars and Planets V*, ed. B. Reipurth, D. Jewitt, & K. Keil, 313–328
- Feigelson, E. D., Martin, A. L., McNeill, C. J., Broos, P. S., & Garmire, G. P. 2009, *AJ*, 138, 227
- Feigelson, E. D., & Townsley, L. K. 2008, *ApJ*, 673, 354
- Ferguson, J. W., Alexander, D. R., Allard, F., Barman, T., Bodnarik, J. G., Hauschildt, P. H., Heffner-Wong, A., & Tamanai, A. 2005, *ApJ*, 623, 585
- Flaherty, K. M., & Muzerolle, J. 2008, *AJ*, 135, 966
- Franceschini, A., et al. 2006, *A&A*, 453, 397
- Getman, K. V., Feigelson, E. D., Luhman, K. L., Sicilia-Aguilar, A., Wang, J., & Garmire, G. P. 2009, *ApJ*, 699, 1454
- Getman, K. V., Feigelson, E. D., Townsley, L., Broos, P., Garmire, G., & Tsujimoto, M. 2006, *ApJS*, 163, 306

- Gorti, U., Dullemond, C. P., & Hollenbach, D. 2009, *ApJ*, 705, 1237
- Guarcello, M. G., Micela, G., Damiani, F., Peres, G., Prisinzano, L., & Sciortino, S. 2009, *A&A*, 496, 453
- Guarcello, M. G., Prisinzano, L., Micela, G., Damiani, F., Peres, G., & Sciortino, S. 2007, *A&A*, 462, 245
- Gutermuth, R. A., Megeath, S. T., Muzeirole, J., Allen, L. E., Pipher, J. L., Myers, P. C., & Fazio, G. G. 2004, *ApJS*, 154, 374
- Gutermuth, R. A., Megeath, S. T., Myers, P. C., Allen, L. E., Pipher, J. L., & Fazio, G. G. 2009, *ApJS*, 184, 18
- Gutermuth, R. A., et al. 2008, *ApJ*, 674, 336
- Hachisuka, K., et al. 2006, *ApJ*, 645, 337
- Hartmann, L., Megeath, S. T., Allen, L., Luhman, K., Calvet, N., D'Alessio, P., Franco-Hernandez, R., & Fazio, G. 2005, *ApJ*, 629, 881
- Hatchell, J., Fuller, G. A., Richer, J. S., Harries, T. J., & Ladd, E. F. 2007, *A&A*, 468, 1009
- Henning, T., & Meeus, G. 2009, ArXiv e-prints
- Hernández, J., Hartmann, L., Calvet, N., Jeffries, R. D., Gutermuth, R., Muzeirole, J., & Stauffer, J. 2008, *ApJ*, 686, 1195
- Hernández, J., et al. 2007, *ApJ*, 662, 1067
- Hillenbrand, L. A. 1997, *AJ*, 113, 1733
- Hillenbrand, L. A., Strom, S. E., Calvet, N., Merrill, K. M., Gatley, I., Makidon, R. B., Meyer, M. R., & Skrutskie, M. F. 1998, *AJ*, 116, 1816
- Iglesias, C. A., & Rogers, F. J. 1996, *ApJ*, 464, 943
- Jeffries, R. D. 2007, *MNRAS*, 376, 1109
- Jeffries, R. D., Oliveira, J. M., Naylor, T., Mayne, N. J., & Littlefair, S. P. 2007, *MNRAS*, 376, 580
- Johnstone, D., Hollenbach, D., & Bally, J. 1998, *ApJ*, 499, 758
- Kennedy, G. M., & Kenyon, S. J. 2009, *ApJ*, 695, 1210
- Kroupa, P. 2002, *Science*, 295, 82
- Lada, C. J., et al. 2006, *AJ*, 131, 1574
- Luhman, K. L., Allen, P. R., Espaillat, C., Hartmann, L., & Calvet, N. 2010, *ApJS*, 186, 111
- Luhman, K. L., et al. 2008, *ApJ*, 675, 1375
- Lyo, A., Lawson, W. A., Mamajek, E. E., Feigelson, E. D., Sung, E., & Crause, L. A. 2003, *MNRAS*, 338, 616
- Mamajek, E. E., Meyer, M. R., Hinz, P. M., Hoffmann, W. F., Cohen, M., & Hora, J. L. 2004, *ApJ*, 612, 496
- Mann, R. K., & Williams, J. P. 2009, *ApJ*, 694, L36
- Mathys, G. 1989, *A&AS*, 81, 237
- McCullough, P. R., Fugate, R. Q., Christou, J. C., Ellerbroek, B. L., Higgins, C. H., Spinhirne, J. M., Cleis, R. A., & Moroney, J. F. 1995, *ApJ*, 438, 394
- Meeus, G., et al. 2009, *A&A*, 497, 379
- Megeath, S. T., et al. 2004, *ApJS*, 154, 367
- Mentuch, E., Brandeker, A., van Kerkwijk, M. H., Jayawardhana, R., & Hauschildt, P. H. 2008, *ApJ*, 689, 1127
- Mercer, E. P., Miller, J. M., Calvet, N., Hartmann, L., Hernandez, J., Sicilia-Aguilar, A., & Gutermuth, R. 2009, *AJ*, 138, 7
- O'dell, C. R., & Wong, K. 1996, *AJ*, 111, 846
- Oey, M. S., Watson, A. M., Kern, K., & Walth, G. L. 2005, *AJ*, 129, 393
- Olczak, C., Pfalzner, S., & Spurzem, R. 2006, *ApJ*, 642, 1140
- Oliveira, J. M., Jeffries, R. D., van Loon, J. T., Littlefair, S. P., & Naylor, T. 2005, *MNRAS*, 358, L21
- Oliveira, J. M., Jeffries, R. D., van Loon, J. T., & Rushton, M. T. 2006, *MNRAS*, 369, 272

- Pascucci, I., Apai, D., Luhman, K., Henning, T., Bouwman, J., Meyer, M. R., Lahuis, F., & Natta, A. 2009, *ApJ*, 696, 143
- R Development Core Team. 2009, R: A language and environment for statistical computing (Vienna, Austria: R Foundation for Statistical Computing), 409, ISBN 3-900051-07-0
- Reach, W. T., et al. 2005, *PASP*, 117, 978
- Richards, G. T., et al. 2009, *AJ*, 137, 3884
- Rogers, F. J., Swenson, F. J., & Iglesias, C. A. 1996, *ApJ*, 456, 902
- Ruch, G. T., Jones, T. J., Woodward, C. E., Polomski, E. F., Gehrz, R. D., & Megeath, S. T. 2007, *ApJ*, 654, 338
- Scally, A., & Clarke, C. 2001, *MNRAS*, 325, 449
- Sicilia-Aguilar, A., Hartmann, L. W., Hernández, J., Briceño, C., & Calvet, N. 2005, *AJ*, 130, 188
- Sicilia-Aguilar, A., Henning, T., & Hartmann, L. W. 2010, *ApJ*, 710, 597
- Sicilia-Aguilar, A., Henning, T., Juhász, A., Bouwman, J., Garmire, G., & Garmire, A. 2008, *ApJ*, 687, 1145
- Sicilia-Aguilar, A., et al. 2006, *ApJ*, 638, 897
- . 2009, *ApJ*, 701, 1188
- Siess, L., Dufour, E., & Forestini, M. 2000, *A&A*, 358, 593
- Skrutskie, M. F., et al. 2006, *AJ*, 131, 1163
- Stelzer, B., & Scholz, A. 2009, *A&A*, 507, 227
- Telleschi, A., Güdel, M., Briggs, K. R., Audard, M., & Palla, F. 2007, *A&A*, 468, 425
- Wang, J., Feigelson, E. D., Townsley, L. K., Román-Zúñiga, C. G., Lada, E., & Garmire, G. 2009, *ApJ*, 696, 47
- Wang, J., Townsley, L. K., Feigelson, E. D., Broos, P. S., Getman, K. V., Román-Zúñiga, C. G., & Lada, E. 2008, *ApJ*, 675, 464
- Weisskopf, M. C., Brinkman, B., Canizares, C., Garmire, G., Murray, S., & Van Speybroeck, L. P. 2002, *PASP*, 114, 1
- Werner, M. W., et al. 2004, *ApJS*, 154, 1
- Winston, E., et al. 2007, *ApJ*, 669, 493
- Xu, Y., Reid, M. J., Zheng, X. W., & Menten, K. M. 2006, *Science*, 311, 54